THE UNIVERSITY OF CHICAGO

POST-TRANSLATIONAL CONTROL OF BNIP3 AND MITOPHAGY BY ULK1 KINASE

A DISSERTATION SUBMITTED TO

THE FACULTY OF THE DIVISION OF THE BIOLOGICAL SCIENCES

AND THE PRITZKER SCHOOL OF MEDICINE

IN CANDIDACY FOR THE DEGREE OF

DOCTOR OF PHILOSOPHY

COMMITTEE ON CANCER BIOLOGY

BY

LOGAN PATRICK POOLE

CHICAGO, ILLINOIS

AUGUST 2021

DEDICATION

I dedicate this dissertation to my beloved grandmother, Lavon Hyberger, for being an endless source of motivation and support. Her continued battle against metastatic breast cancer inspired me to pursue a Ph.D. in cancer biology. I will forever be grateful for her comforting phone calls as I worked late nights in lab and her enduring curiosity as we discussed my research.

TABLE OF CONTENTS

LIST OF FIGURES

LIST OF TABLES

ABBREVIATIONS

Alb	Albumin
AMBRA1	Autophagy and Beclin regulator 1
AMPK	AMP activated protein kinase
ARIH1	Ariadne RBR E3 ubiquitin protein ligase 1
ATG	Autophagy-related gene
Bcl-2	B-cell lymphoma 2
Bcl-X_L	Bcl-2-like protein 1
BH3	Bcl-2 homology 3
BIM	Bcl-2-like protein 11
BNIP3	BCL2/adenovirus E1B 19 kDa interacting protein 3
BNIP3L	BCL2/adenovirus E1B 19 kDa interacting protein 3-like
CD	Conserved domain
CHX	Cyclohexamide
CK2	Casein kinase 2
CTD	C-terminal domain
DRP1	Dynamin-related protein 1
EAT	Early autophagy targeting/tethering
EMT	Epithelial-mesenchymal transition
ER	Endoplasmic reticulum
ES	Embryonic stem cell
ETC	Electron transport chain
EV	Empty vector

FIP200	FAK family-interacting protein of 200 kDa
FLAG	DYKDDDDK (tag)
FLP	Flippase recombinase
FoxO3	Forkhead Box O3
FRT	FLP recombinase-target
FUNDC1	FUN14 domain containing 1
GABARAP	Gamma-aminobutyric acid receptor-associated protein
GFP	Green fluorescent protein (tag)
GR	Glucocorticoid receptor
HA	Hemagglutinin (tag)
HCC	Hepatocellular carcinoma
HIF1α	Hypoxia-inducible factor-1 alpha
HRE	Hypoxia response element
IMS	Mitochondrial intermembrane space
KLHL20	Klech-like protein 20
LAMP1	Lysosomal associated membrane protein 1
LC3	Microtubule-associated protein 1A/1B-light chain 3
LIR	LC3 interaction region
MAMs	Mitochondria-associated membranes
MARCH5	Membrane associated ring-CH-type finger 5
MCK	Muscle creatine kinase
MCR	Mitochondrial cargo receptor
Mfn2	Mitofusin-2

MIM	MIT-interacting motif
MIT	Microtubule-interacting and transport
Mox2	Mesenchyme homeobox 2
mTORC1	Mammalian target of rapamycin complex 1
MUL1	Mitochondrial E3 ubiquitin ligase 1
NDP52	Calcium-binding and coiled-coil domain-containing protein 2
NEDD4L	NEDD4 like E3 ubiquitin protein ligase
NF-κB	Nuclear factor kappa-light-chain-enhancer of activated B cells
NIX	Nip-like protein X (BNIP3L)
NOXA	Phorbol-12-myristate-13-acetate-induced protein 1
OCR	Oxygen consumption rate
OMM	Outer mitochondrial membrane
Opa1	Dynamin-like 120 kDa protein, mitochondrial
OPTN	Optineurin
OXPHOS	Oxidative phosphorylation
PanIN	Pancreatic intraepithelial neoplasia
PDAC	Pancreatic ductal adenocarcinoma
Pdx1	Pancreatic and duodenal homeobox 1
PE	Phosphatidylethanolamine
PEST	Proline, glutamic acid, serine, and threonine rich
PGAM	Phosphoglycerate mutase 2
PI	Phosphatidylinositol
PI3KC3	Class-III phosphoinositide-3-kinase

PI3P	Phosphatidylinositol-3-phosphate
PINK	PTEN-induced putative kinase-1
PKA	Protein kinase A
PPARα	Peroxisome proliferator-activated receptor-alpha
PUMA	p53 upregulated modulator of apoptosis
Rb	Retinoblastoma protein
Rheb	Ras homolog enriched in brain
ROS	Reactive oxygen species
SNP	Single nucleotide polymorphism
Sqstm1	Sequestosome 1
SUMO	Small ubiquitin-like modifier
TA	Tail-anchored
TCGA	The Cancer Genome Atlas
TM	Transmembrane
TNBC	Triple negative breast cancer
TOMM20	Translocase of outer mitochondrial membrane 20
ULK1	UNC-51-like kinase 1
VDAC	Voltage-dependent anion channel-1
VPS34	Vacuolar protein sorting-associated protein 34
WIPI2	WD repeat domain, phosphoinositide interacting 2
WT	Wild-type
$\Delta\Psi_M$	Membrane depolarization

ACKNOWLEDGEMENTS

The success of my graduate school journey at the University of Chicago was the result of the unbelievable support of a number people. My research would not have been possible without the support of my advisor Dr. Kay Macleod, and the members of the Macleod lab. During my time in graduate school, Kay and the Macleod lab have mentored me to think critically and independently, and have shaped me into the scientist I am today. Throughout my time in the lab, I have had the opportunity to meet a number of incredible people and have made lifelong friends. When I joined the lab, the existing members, including Erin, Lauren, Aparajita, Marina, and Maya gave me valuable advice on how to succeed in graduate school and taught me important laboratory techniques. As I progressed through my program, additional students joined the lab, including Alex, Ivan, Andy, and Thea, which provided me with the opportunity to mentor and teach them as others had done for me. I'd also like to thank the postdocs in the lab, Damian and Georgi, for their mentorship and advice. They were always willing to take the time to listen to my problems, both experimental and personal, and help me to devise actionable steps to address them. Finally, I would like to thank Grazyna, our wonderful lab manager, who worked tirelessly to make sure the lab ran smoothly. Her frequent pep talks and life advice provided me with the support I needed in order to push through the inevitable stresses of graduate school.

Beyond the Macleod lab, there are many people at the University of Chicago that played a critical role in my graduate school experience. I am thankful for the mentorship of my thesis committee members Dr. Mark Lingen, Dr. Robert Keenan, and Dr. Steve Kron. My project underwent substantial changes multiple times throughout graduate

school. Their insightful comments and encouragement during my thesis committee meetings helped me to maintain focus and perform my best work. I would also like to thank the experts at the core facilities at the University of Chicago, including the DNA Sequencing Core, Biophysics Core, Light Microscopy Core, Transgenics/ES Cell Technology Mouse Core, and the Animal Resources Center. My success in graduate school would also not be possible without the support of the Committee on Cancer Biology cluster office, as well as those in the Ben May Department for Cancer Research, especially Pete Booker. Pete was an incredibly supportive presence in my life over the last several years, frequently checking in on my mental health and wellbeing. He was an endless source of positivity and never failed to offer life advice, support, and prayers. I must also thank those involved in the extracurricular activities that helped me to grow as an individual outside of the lab. Dr. Megan Mekinda and others at the University of Chicago Comprehensive Cancer Center gave me the opportunity to perform outreach to the community as well as mentor high school students interested in careers involving biomedical research. Additionally, members of the Polsky Center for Entrepreneurship and Innovation taught me how to utilize the critical thinking and scientific background that I developed during graduate school to drive innovation and produce actionable solutions at the intersection of science and business, which will prove crucial in my future career.

I would like to thank my friends for their constant support throughout my time in graduate school. When I first moved to Chicago, I did not know anyone in the city. Thankfully, my fellow classmates Alex, Anastasia, Kyle, Matt, Sriram, and I became fast friends and sources of support. Over time I began to develop additional friendships with

people outside of the University of Chicago ecosystem, including Eduardo, Alex and Felipe. I am also incredibly thankful for the friendships I have been able to maintain with people outside of the city of Chicago, including Esteban, Luis Diego, Megan, and my close friend of almost 15 years, Melissa. All of these friends helped me maintain my sanity during the ups and downs of graduate school, and provided me with support and advice when I needed to vent.

Finally, none of this would have been possible without the support of my family, which has acted as a pillar of strength during my graduate school experience. Throughout each step of my education, they have been there to encourage and support my progress. Graduate school has been the greatest challenge of my life thus far, and I hope they realize how critical they were to my perseverance and success. Whether it be weekly family Zoom calls, visits to Iowa, or phone calls with my mother singing the “just keep swimming” song from Finding Nemo, their endless support provided me with the strength I needed to get back up each time graduate school and life pushed me down. I must also thank my grandmother, Lavon Hyberger, for being an inspiration and a model of perseverance in the face of adversity. I’ve known my entire life that I wanted to be a scientist, but her ongoing battle with metastatic breast cancer inspired me to pursue a degree in cancer biology. She has been a mentor and positive role model throughout my life, and offered unbelievable support as I pursued my degree. Our late-night phone calls while I worked in the lab helped me maintain my sanity, and her endless curiosity gave me opportunities to practice explaining my research to non-scientists. I am excited to move on to the next major steps in my life and career, and can rest assured that I have the support network necessary to overcome anything that life throws at me.

ABSTRACT

BNIP3 is a mitochondrial cargo receptor that specifically targets mitochondria for degradation at the autolysosome through a specialized form of autophagy called mitophagy. BNIP3 is transcriptionally upregulated in response to a number of stressors, including hypoxia, where it functions to decrease mitochondrial mass, limit ROS, and promote the efficient use of limiting metabolites and oxygen. ULK1, the catalytic component of the autophagy initiation complex, is best known for its role in stimulating general autophagy, however recent work has demonstrated that ULK1 may also promote mitophagy. The mechanism through which ULK1 specifically promotes mitophagy remains poorly understood. Here we show that ULK1 phosphorylates BNIP3 on a critical serine residue (S17) adjacent to its amino terminal LIR motif to promote its interaction with LC3 and mitophagy. Similarly, we found that ULK1 phosphorylates the BNIP3 homolog, BNIP3L, on a homologous serine residue (S35), suggestive of an expanded role of ULK1 in the specific regulation of mitophagy.

Additionally, we determined that ULK1 interaction promotes the stability of BNIP3 protein by limiting its turnover at the proteasome independent of S17 phosphorylation. This stabilization of BNIP3 protein by ULK1 requires an intact BNIP3 “BH3” domain, and deletion of this domain increases BNIP3 protein levels and decreases BNIP3 turnover independent of ULK1. We found that this process of BNIP3 protein stabilization was critical to the increase in BNIP3 protein levels upon hypoxic stress, as inhibition of ULK1 blocked BNIP3 protein upregulation in response to hypoxia. Together, the work in this thesis expands our understanding of the mechanism through which ULK1 specifically regulates mitophagy through the stabilization and phosphorylation of BNIP3.

CHAPTER 1

INTRODUCTION

Autophagy in cellular stress response and homeostasis

Macroautophagy, hereby referred to as autophagy, is an evolutionarily conserved process involving the sequestration, lysosomal degradation, and recycling of intracellular components including damaged or dysfunctional organelles, protein aggregates, intracellular pathogens, and other cytoplasmic components (Figure 1.1).[1] As an adaptive process critical to maintaining cellular homeostasis, autophagy is upregulated in response to a number of cellular stressors including nutrient deprivation, growth factor depletion, oxidative stress, hypoxia, and pathogenic infection.[2] This process is performed by a tightly regulated group of autophagy-related genes (ATGs) which are essential for autophagosome formation and the delivery of autophagic cargo to the lysosome. These ATG proteins can be grouped into the following functional categories: initiation and phagophore nucleation, phagophore expansion, cargo sequestration, autophagosome maturation, and fusion with the lysosome.[2]

Autophagy initiation is tightly regulated by cellular energy conditions through the integration of upstream signals by ULK1 (UNC-51-like kinase 1). Under high-nutrient conditions, ULK1 is inactivated following phosphorylation by the master growth regulating kinase mTOR (mammalian target of rapamycin).[3] However, upon declining cellular energy levels, ULK1 activity is induced by AMPK (AMP-activated protein kinase) phosphorylation.[3,4] In response to cellular stressors, the ULK1 complex (composed of ULK1, ATG13, FIP200, and ATG101) is activated and recruited to a phosphatidylinositol-3-phosphate (PI3P)-rich initiation site.[5] PI3P-rich membrane

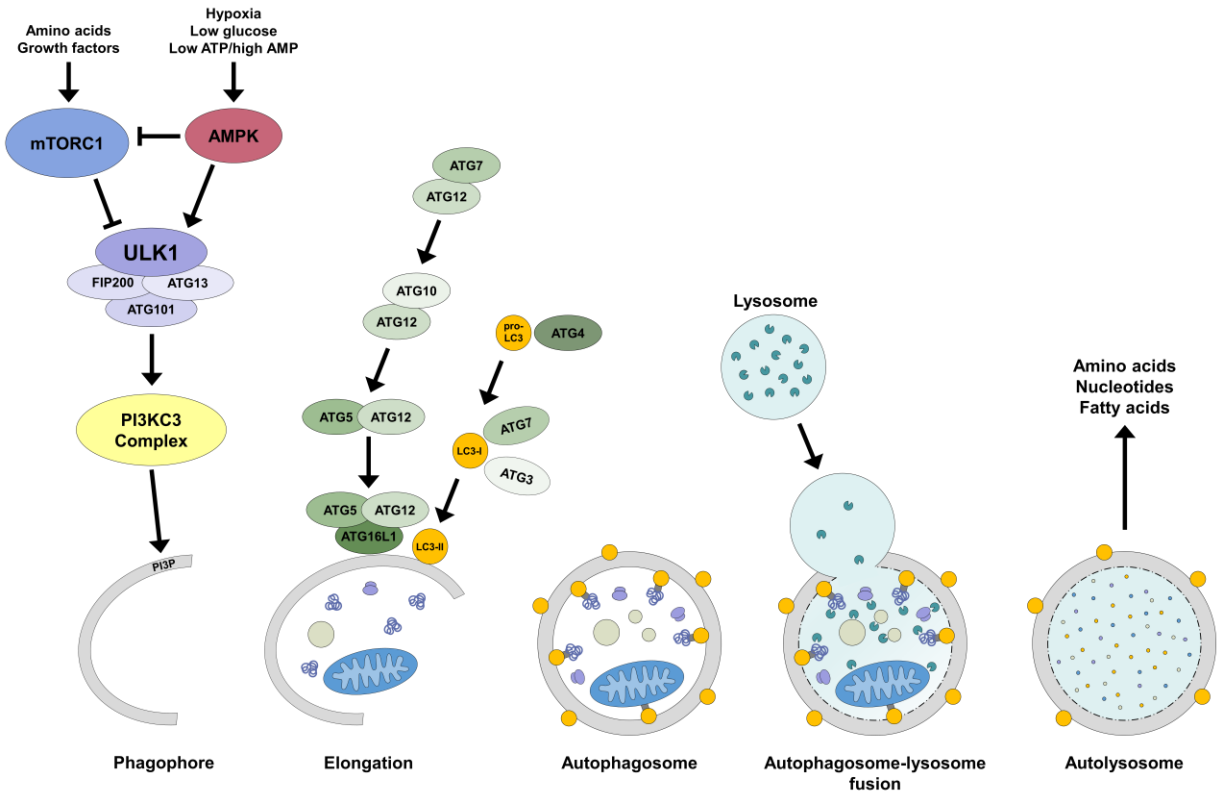

Figure 1.1: Overview of the autophagy process. Under high-nutrient conditions, ULK1 is inhibited by mTORC1. Under nutrient stress (depletion of amino acids or growth factors), hypoxia, or low glucose, AMPK is stimulated and both inhibits mTORC1 and activates ULK1. Activated ULK1 complex is recruited to a PI3P-rich ER-mitochondrial contact site where it activates the PI3KC3 complex, which generates PI3P which dictates the location of the phagophore isolation membrane. Phagophore elongation is mediated by two ubiquitin-like systems. The first involves the formation of the ATG5-ATG12-ATG16L1 complex, which acts as the E3 ligase in the second system. The second system involves the cleaving of pro-LC3 by ATG4 to yield LC3-I, followed by conjugation of LC3-I to PE by ATG7 and ATG3, forming LC3-II. LC3-II decorates the inner and outer surfaces of the phagophore membrane, aiding in autophagosome development and recruiting autophagic cargo. After the autophagosome is sealed, it fuses with the lysosome, forming the autolysosome, followed by degradation of the sequestered cargo by lysosomal hydrolases. The degraded cargo, including amino acids, nucleotides, and fatty acids, are then released into the cytoplasm for biosynthetic reactions or catabolized for energy production.

domains can be found in a number of subcellular localizations including the endoplasmic reticulum (ER), ER-mitochondria or ER-plasma membrane contact sites, or the Golgi complex.[6–9] However, considering the localization of ATG14 to ER-mitochondrial contact sites (also called mitochondria-associated membranes, or MAMs) following starvation, it is believed that autophagy initiation mainly occurs at MAMs.[9] Following activation, the ULK1 complex enhances the activity of the Class-III phosphoinositide-3-kinase (PI3KC3) complex (composed of VPS34, BECLIN-1, ATG14, and p115) by phosphorylating BECLIN-1 and ATG14L.[10,11] The catalytic component of the PI3KC3 complex, VPS34, is a class III PI3K that converts phosphatidylinositol (PI) to PI3P, which dictates the location of phagophore formation.[12] This, in turn, recruits the PI3P-binding protein WIPI2 to the phagophore, which is critical for the recruitment of ATGs required for phagophore elongation.[13]

Downstream of WIPI2 recruitment, there are two ubiquitin-like systems required for phagophore elongation. First, the E1 enzyme ATG7 and E2 enzyme ATG10 conjugate ATG12 to ATG5.[14] ATG16L1 then binds ATG5 and homodimerizes to form the heterohexamer ATG12-ATG5-ATG16L1 complex.[15] This complex acts as an E3 ligase in the second ubiquitin-like conjugation system critical for autophagy. Acting alongside the E1 ligase ATG7 and E2 ligase ATG3, the complex conjugates ATG8 family proteins to phosphatidylethanolamine (PE).[16] The ATG8 family of proteins includes eight members grouped into LC3 and GABARAP subfamilies.[16] Following cleavage by ATG4 and conjugation to PE, LC3 becomes LC3-II and is integrated into the inner and outer membrane of the elongating phagophore, aiding in autophagosome development and recruiting autophagic cargo.[17–19] The continued elongation of the

phagophore membrane is not fully characterized, although it is thought that the transmembrane protein ATG9 may act to deliver the necessary membrane material.[20] Following elongation, the phagophore is sealed to form a double-membrane vesicle through a poorly understood mechanism that may involve different ATG8 family proteins.[21] As the autophagosome matures, PE-conjugated ATG8 family proteins link the autophagosome to the microtubule-based kinesin motors responsible for delivering the autophagosome to the lysosome.[22] ATG4 then acts to remove ATG8 from the outer autophagosome membrane for recycling.[23] Finally, the autophagosome is fused with the lysosome through a syntaxin-17 SNARE-driven mechanism promoted by ATG14, and the sequestered cargo of the autolysosome is degraded by acidic lysosomal hydrolases.[2,24,25] The degraded byproducts are later released into the cytoplasm for reuse or catabolized for energy production.[2,8] Lysosomal acidification and fusion of autophagosomes with lysosomes can be experimentally inhibited by treatment with bafilomycin A_1, allowing the assessment of autophagic flux.[26]

Disturbance of autophagy has been implicated in aging and the progression of a number of diseases, including neurodegenerative disease, immune and inflammatory disease, and cancer.[2] The role of autophagy in cancer is strongly context-dependent, with both pro- and anti-tumoral roles at various stages of cancer progression. Autophagy is believed to play a tumor-suppressive role in tissues prior to the onset of tumorigenesis by protecting cells against metabolic and oxidative stress, and loss of autophagy has been associated with increased risk of cancer.[27] However, it is important to note that this cytoprotective function may also promote tumorigenesis by protecting premalignant cells from genotoxic and inflammatory stress. The catabolic recycling of

cellular components can also provide cancer cells with metabolic plasticity, promoting cell survival in suboptimal environments.[28] Autophagy has also been implicated in playing a context-dependent role in metastasis. Signals that trigger epithelial-mesenchymal transition (EMT), such as hypoxia, also activate autophagy.[29] Activation of autophagy has been shown to downregulate major EMT transcription factors thereby inhibiting EMT in many cancers.[30–32] Conversely, autophagy has been implicated in promoting resistance to anoikis through a poorly defined process, as well as promoting cell migration through focal adhesion turnover, both of which promote the metastatic process.[33–36] The induction of autophagy has also been noted as a side effect of many cancer therapies, leading to the proposal of co-treatment with pharmacological autophagy inhibitors as a strategy to enhance therapeutic efficacy and reduce resistance to treatment.[37–40] However, in some contexts, therapy-induced autophagy activation has been shown to induce immunogenic cell death.[41–43] Therefore, it is important to recognize the context-dependent role of autophagy when proposing the co-treatment of patients with cancer therapies and autophagy inhibitors.

ULK1 regulation, function, localization, and known roles at the mitochondria

ULK1 (UNC-51-like kinase 1), the mammalian homolog of Atg1 in yeast, is a critical upstream modulator of autophagy initiation in mammalian cells.[44] Atg1 was originally identified through genetic screens in yeast.[45–47] Cells with *atg1* mutations died at a faster rate under nutrient starvation and failed to accumulate autophagic bodies upon protease inhibition, which linked autophagy to cellular metabolism.[45] ULK1 (or Atg1 in yeast) acts as part of the autophagy initiation complex, sometimes referred to as the ULK1 complex (or Atg1 complex in yeast).[5]

The ULK1 complex is comprised of ULK1 and the noncatalytic subunits FIP200 (FAK family-interacting protein of 200 kDa), ATG13, and ATG101. FIP200 is a large coiled-coil scaffolding protein which may play a role in the scaffolding and spatial targeting of early autophagosomes.[48] In yeast, FIP200 is replaced by either Atg11 during selective autophagy, or Atg17 during bulk autophagy, both of which are scaffolding proteins.[49–51] Atg17 further co-assembles with Atg29 and Atg31, which are required for starvation-induced autophagy in yeast.[52] ATG13 and ATG101 heterodimerize with each other via their HORMA domains, and ATG13 associates with ULK1 via the C-terminal portion of its IDR (intrinsically disordered region).[53–56] In yeast, ATG13 is conserved (Atg13), but there is no yeast homolog to ATG101.

The ULK1 protein sequence contains three general domains: the N-terminal kinase domain, the S/P spacer, and the C-terminal domain (CTD) (Figure 1.2).[57,58] The N-terminal kinase domain (amino acids 1-278) is essential for the kinase activity of the protein, and contains a critical residue at lysine 46 (K46). Mutation of K46 to asparagine (N) ablates the kinase function of ULK1. Utilizing arrayed degenerate peptide libraries, recent studies have elucidated the optimal ULK1 phosphorylation consensus motif.[59] The ULK1 kinase domain strongly prefers serine as the phosphoacceptor residue over threonine. Additionally the presence of leucine or methionine at the -3 position, and aliphatic or aromatic hydrophobic residues at positions +1 and +2 enhance ULK1 binding.[59] This preference for hydrophobic residues is unusual, as many serine/threonine kinases are known to phosphorylate sites near proline or charged residues.[60,61] ULK1 is known to phosphorylate a number of protein targets essential for starvation-induced autophagy, some of which will be outlined later in this section.[62]

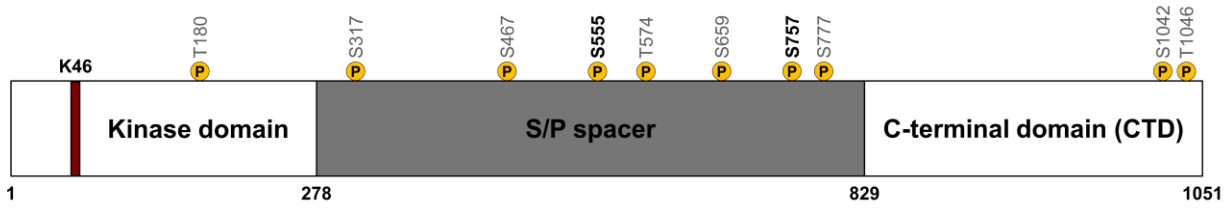

Figure 1.2: Schematic of ULK1 protein domains and known phosphorylation sites. The ULK1 protein sequence contains the following domains: the kinase domain, the S/P spacer, and the C-terminal domain (CTD). The kinase domain contains a critical residue at K47 that is required for ULK1 kinase function. The S/P spacer domain is the site for many post-translational modification events. The most notable phosphorylation sites (bolded) are S555 (AMPK) and S757 (mTOR), which promote and inhibit ULK1 activity respectively, and are used as markers of ULK1 activation/inhibition via western blot. The C-terminal domain is the site of the interaction of ULK1 with ATG13. Additionally, residues 1038-1044 are believed to contain a motif that is required for a dominant-negative autophagy inhibitory function via interaction with a yet unidentified autophagy-regulating protein.

Phosphorylation site	Modifying enzyme	Effect on ULK1 activity
S757	mTOR	Inhibits autophagy
S317, S467, S555, T574, S659, S777	AMPK	Promotes autophagy
T180	ULK1	Promotes autophagy
S1042, T1046	ULK1	Promotes degradation

Table 1.1: List of ULK1 phosphorylation sites. Over 30 phosphorylation events have been reported for ULK1, although the functional significance and responsible kinases for many of these events have not been experimentally verified. mTOR and AMPK are the primary regulators of ULK1 activity. The phosphorylation of S555 (AMPK) and S757 (mTOR) are used as markers of ULK1 activation/inhibition via western blot. ULK1 is also known to autophosphorylate, which has been shown to either promote the activity or degradation of ULK1.

The S/P spacer domain of ULK1 (amino acids 279-828), rich in serine and proline residues, is the site for many post-translational modification events (Table 1.1).[44,58] ULK1 is hyperphosphorylated under nutrient-rich conditions, and dephosphorylated upon starvation.[63] Over 30 phosphorylation events have been reported for ULK1, although the functional significance and responsible kinases for many of these events have not been experimentally verified.[44] Several of the more characterized ULK1 post-translational modifications will be outlined later in this section. ULK1 contains a LC3 interaction region (LIR) motif (FVMV) at amino acids 357-360.[64–66] Through this domain, ULK1 is able to interact with ATG8-family proteins (i.e. LC3, GABARAP), which act as scaffolds to recruit proteins to the phagophore surface. The interactions of ULK1 with GABARAP and GABARAPL1 are the strongest, however it also interacts with GABARAPL2, LC3A, and LC3C. ULK1 can also interact with LC3B, however this interaction is much weaker than that of other ATG8-family proteins. Mutation of the critical residue at position 357 to alanine (F357A) abolishes the interaction between ULK1 and ATG8-family proteins.[64]

The C-terminal domain (CTD) (amino acids 829-1051) of ULK1 shares homology with that of yeast Atg1 and is believed to play a role in its interaction with both proteins and membranes.[57,58] The C-terminus of Atg1 is better characterized than that of ULK1, and is known to contain an early autophagy targeting/tethering (EAT) domain. Work with synthetic liposomes has suggested that the Atg1 EAT domain acts as a dimeric membrane curvature sensor that is capable of tethering liposomes between 20-30 nm.[67] The EAT domain is comprised of two antiparallel three-helix bundles called MIT (microtubule-interacting and transport) domains.[68,69] Each of these MIT domains are

known to bind to MIT-interacting motifs (MIMs) in the Atg13 C-terminus, which is essential to the Atg1-Atg13 interaction.[68] Similarly, the interaction of ULK1 and ATG13 is known occur in residues 829-1001 of the ULK1 CTD. Residues 1038-1044 of ULK1 contain an IERRLSA motif that is required for a dominant-negative inhibitory function, likely through binding a yet unidentified autophagy-regulating protein.[58]

ULK1 regulates autophagy in response to changes in nutrient status, integrating AMPK and mTORC1 signaling. AMPK is a cellular sensor of low intracellular ATP levels, and is also activated upon mitochondrial stress.[70] AMPK binds to the S/P spacer domain of ULK1 and regulates the initiation of autophagy via the phosphorylation of at least 7 proposed sites (S317, S467, S555, T574, S637, S659, S777).[71] Phosphorylation of these sites by AMPK stimulates ULK1 activity in response to glucose starvation and regulates ATG9 localization.[3,63,72,73] Of these residues, phosphorylation of S555 (ULK1 p-S555) is the best characterized, and is commonly used as an indicator of activate ULK1. Conversely, phosphorylation of ULK1 at S757 (ULK1 p-S757) by mTORC1 is used as an indicator of inactivated ULK1. mTORC1 is a kinase complex that promotes cell growth and metabolism in response to metabolic and environmental signals.[74] mTORC1 binds to the ULK1 kinase domain via the complex protein Raptor, and phosphorylates ULK1 on S757. This phosphorylation event represses ULK1 kinase activity by inhibiting the interaction between ULK1 and AMPK.[3] Interestingly, S757 phosphorylation can be prevented through the phosphorylation of Raptor by AMPK, which blocks the interaction of Raptor and ULK1.[4]

ULK1 is also known to undergo autophosphorylation to regulate its activity.[58] In yeast, autophosphorylation of the Atg1 activation loop correlates with increased Atg1

kinase activity. The mutation of autophosphorylation sites disrupts starvation-induced autophagy, but does not affect Atg1 localization or complex formation.[75,76] This autophosphorylation event may correspond with that of T180 in the activation loop of ULK1, which has been shown to be required for ULK1 autophosphorylation activity.[77,78] Early studies noted that kinase dead (K46N or K46I) ULK1 migrates with a lower apparent molecular mass than wild-type ULK1 via western blot. Limited proteolysis of wild-type ULK1 with chymotrypsin *in vitro* generated distinct protected fragments ranging from approximately 350-380 residues. However, these distinct fragments were not as efficiently detected following the proteolysis of kinase dead ULK1 (K46I), consistent with internal regions of the protein being exposed to the protease.[58] Based on these results, it is hypothesized that the structure of ULK1 is regulated through autophosphorylation, possibly between residues 278-351. Kinase active ULK1 is proposed to undergo autophosphorylation to adopt a “closed” confirmation in which the Atg13-binding CTD is folded closely to the kinase domain, hiding the dominant-negative motif within the CTD. However, upon loss of autophosphorylation through ULK1 kinase inactivation, ULK1 adopts an “open” conformation which exposes the dominant-negative motif and inhibits autophagy.[58]

In addition to phosphorylation, ULK1 is regulated by the acetylation and ubiquitination of lysine residues. Upon growth factor withdrawal, the acetyltransferase TIP60 is activated via phosphorylation by the growth factor-sensitive kinase GSK3B. TIP60 then acetylates ULK1 on K162 and K606, stimulating ULK1 activity. This regulation further links ULK1 activity and autophagy initiation to growth factor levels.[79] It has also been observed that the activation of ULK1 upon amino acid starvation is

accompanied by a decrease in ULK1 protein levels, possibly acting as a feedback mechanism to limit autophagy as nutrients become available.[44] It is possible that this mechanism may be regulated, in part, by ubiquitination.[80,81] ULK1 is reported to be degraded in a proteasome-dependent manner following ubiquitination by the Cullin E3 ligase complex. During prolonged starvation, ULK1 is autophosphorylated at residues S1042 and T1046, which recruits the substrate adaptor protein KLHL20 and allows Cullin-3-mediated ubiquitination.[82] The E3-ligase NEDD4L may also regulate ULK1 degradation during prolonged starvation.[83] These regulatory mechanisms may prevent an excessive autophagic response in response to prolonged starvation.

ULK1 is known to phosphorylate a number of protein targets essential for starvation-induced autophagy. First, ULK1 is known to phosphorylate members of the ULK1 complex, including ULK1, ATG13, FIP200, and ATG101.[59,84–86] ATG13 phosphorylation is required for the clearance of depolarized mitochondria, while understanding the significance of FIP200 and ATG101 phosphorylation requires additional study.[81] Downstream, ULK1 is known to regulate the VPS34 complex through the phosphorylation of BECLIN-1 and ATG14L. These phosphorylation events enhance VPS34 activity, PI3P production, and autophagy induction.[10,11] ULK1 has also been shown to directly phosphorylate VPS34, but the significance of this event is unclear.[59] In addition to regulating VPS34 complex activity, ULK1 regulates its translocation to autophagy initiation sites through the phosphorylation of AMBRA1, a protein that mediates the tethering of the complex to the cytoskeleton.[87] ULK1 may further regulate autophagy initiation through the phosphorylation of ATG9, a protein thought to play a role in supplying membranes for autophagosome biogenesis.[20] ATG9 colocalizes to

nascent autophagosomes in an ULK1-dependent manner in response to starvation.[88] ULK1 also affects the regulation of LC3 processing by phosphorylating ATG4B. ULK1 phosphorylation inhibits ATG4B activity, affecting the conversion of pro-LC3 to LC3-I and the conversion of LC3-II back into LC3-I.[89] Finally, ULK1 activity may possibly act on autophagosome maturation. Recent work demonstrates that ULK1 inhibition not only blocks autophagy initiation, but also results in “stalled” autophagosomes that are positive for both early and late autophagosome markers.[90] The mechanism of this blocking requires further study, but these results suggest additional ULK1 substrates are involved in autophagosome maturation.

ULK1 may also regulate selective forms of autophagy, with evidence for a role in the autophagic turnover of mitochondria.[91,92] In response to mitochondrial depolarization, the PINK-Parkin pathway ubiquitinates outer mitochondrial membrane proteins which are recognized by the cargo receptors NDP52 and optineurin. These cargo receptors are also known to regulate ULK1 mitochondrial recruitment, suggesting that ULK1 may directly initiate autophagosome formation at depolarized mitochondria.[93] ULK1 has also been shown to translocate to the mitochondria under hypoxic conditions. This recruitment to the mitochondria is believed to be dependent on the binding of ULK1 to the mitochondrial cargo receptor FUNDC1. Upon recruitment, ULK1 phosphorylates FUNDC1 in a manner which enhances the interaction of FUNDC1 with LC3 at the phagophore surface.[92] This phosphorylation event presumably specifically enhances mitochondrial autophagy.

Dysfunctional autophagy, and ULK1, have been implicated in numerous human diseases. Only one disease-associated single nucleotide polymorphism (SNP) in ULK1

has been identified, implicating ULK1 with Crohn's disease.[94] However, altered ULK1 expression has been associated with a number of cancers. ULK1 expression correlates with poor prognosis in breast, colorectal, nasopharyngeal, and gastric cancers.[95–98] ULK1 down regulation results in inhibited cell growth, suggesting that autophagy acts as a survival mechanism in these cancers. But this effect of ULK1 expression may be context dependent, as an immunohistochemical analysis of breast cancer tissue identified low ULK1 expression as an adverse marker for disease progression and metastasis.[99] Additionally, knockdown of ULK1 in hypoxia-treated cells results in cell death, implying that tumor cells in hypoxic environments rely on ULK1-dependent autophagy for survival. The clinical significance of ULK1 activity has become increasingly important in light of the unexpected failures of mTOR inhibitors as anticancer therapy. mTOR inhibition results in the activation ULK1 and autophagy, which may provide tumor cells a survival mechanism during treatment. Several specific inhibitors of ULK1 have recently been identified, including ULK-101, SBI-0206965, and MRT68921.[59,90,100] Work has begun to test the efficacy of co-treatment with mTOR and ULK1 inhibitors, with preliminary work showing that dual inhibition promoted apoptotic cell death in cell lines.[59]

Mitophagy in cellular stress response and homeostasis

Mitophagy is a selective form of macro-autophagy through which mitochondria are preferentially targeted for degradation at the autolysosome.[101] Mitophagy serves an important housekeeping function by eliminating mitochondria that have become dysfunctional, thus limiting the production of damaging reactive oxygen species (ROS). In response to stresses such as hypoxia and nutrient deprivation, mitophagy can also

promote the efficient use of limiting metabolites and oxygen by eliminating healthy mitochondria to reduce overall mitochondrial mass. In order to specifically target mitochondria for degradation via mitophagy, cells rely on the activity of a growing list of mitochondrial cargo receptors (MCRs), which includes BNIP3, BNIP3L (NIX), FUNDC1, and the mitochondrial substrates for Parkin/PINK-mediated ubiquitination.[101] Upon localization to the mitochondria, these MCRs promote mitophagy through direct interaction with LC3/GABARAP via conserved LC3 interaction regions (LIR) (Figure 1.3). The expression and activity of MCRs are modulated by the upstream sensing of mitochondrial or environmental stressors that induce mitophagy.[101]

The primary mechanism through which depolarized mitochondria are eliminated by the cell involves Parkin/PINK-dependent mitophagy. PTEN-induced putative kinase-1 (PINK1) is a serine/threonine ubiquitin kinase that accumulates at the outer mitochondrial membrane (OMM) upon membrane depolarization ($\Delta\Psi_M$). At the OMM, PINK1 recruits and phosphorylates the E3 ubiquitin ligase Parkin within its ubiquitin-like domain, derepressing Parkin auto-inhibition.[93,102] PINK1 may also phosphorylate other E3 ubiquitin ligases (e.g. MARCH5, ARIH1, and MUL1), however these interactions are less well characterized.[103–106] The de-repression of Parkin leads to the ubiquitination and phosphorylation of proteins at the OMM, notably the voltage-dependent anion channel-1 (VDAC-1) and Mitofusin-2 (Mfn2), which then interact with LIR-containing cargo receptors optineurin (OPTN), NDP52, or p62/Sqstm1.[93,107–109] In addition to activation by mitochondrial depolarization, Parkin/PINK-dependent mitophagy is also known to be activated upon the accumulation of unfolded proteins in the mitochondrial matrix.[110,111]

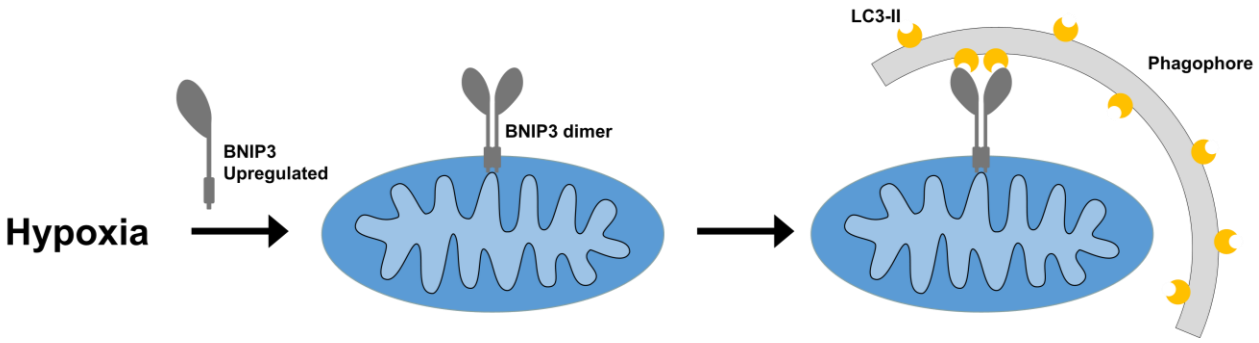

Figure 1.3: BNIP3 mediates mitophagy in response to hypoxia. Mitophagy is a selective form of macro-autophagy through which mitochondria are preferentially targeted for degradation at the autolysosome. In order to specifically target mitochondria for degradation via mitophagy, cells rely on mitochondrial cargo receptors. Parkin/PINK mediates the degradation of dysfunctional mitochondria to limit ROS. Stress-induced mitochondrial cargo receptors, including BNIP3 (above) and BNIP3L, are upregulated in response to cellular stresses such as hypoxia or nutrient depravation to promote the efficient use of limiting metabolites and oxygen by reducing mitochondrial mass. Mitochondrial cargo receptors, such as BNIP3, localize to the mitochondria and promote mitophagy through direct interaction with LC3/GABARAP at the phagophore surface via conserved LC3 interaction regions.

BNIP3 and its homolog BNIP3L are tail-anchored (TA) proteins that integrate into the OMM via their C-terminal transmembrane (TM) domains. The bulk of each protein remains cytosolic upon integration, allowing their N-terminal LIR motifs to interact with LC3/GABARAP at the phagophore surface.[112–114] At the OMM, BNIP3 and BNIP3L form SDS-resistant homodimers, which recent evidence suggests is required for efficient interaction with LC3/GABARAP.[115] BNIP3 and BNIP3L have also been reported to heterodimerize, however the physiological context and effect of heterodimerization on mitophagy remain undetermined.[116] Stressors, such as hypoxia and nutrient deprivation, lead to the rapid transcriptional upregulation of BNIP3 and BNIP3L. Both proteins are transcriptionally activated by HIF1α in response to hypoxia and elevated ROS.[117,118] BNIP3 and BNIP3L are also known to be multiply phosphorylated, however little is known about which kinases are responsible for regulating their levels and activity. Transcriptional and post-translational regulation of BNIP3 and BNIP3L will be described in greater detail in later sections of this chapter. Neither BNIP3 nor BNIP3L require Parkin/PINK1 to promote mitophagy. However, BNIP3 facilitates, but is not required for, PINK1 accumulation and Parkin recruitment to the OMM.[119] Additionally, BNIP3L is a ubiquitination target of Parkin and can promote Parkin/PINK1-dependent mitophagy.[120,121] Parkin/PINK1 loss results in HIF1α accumulation, which may allow compensation of mitophagy by BNIP3 and BNIP3L upon Parkin loss.[122,123]

Similar to BNIP3 and BNIP3L, FUNDC1 (FUN14 Domain Containing 1) promotes hypoxia-induced mitophagy. FUNDC1 is a multi-pass protein that integrates into the OMM with three TM domains. The cytosolic N-terminus of FUNDC1 contains a LIR motif that interacts with LC3 family proteins.[124] Unlike BNIP3 and BNIP3L, which are

predominantly transcriptionally regulated, FUNDC1 activity is primarily regulated at the post-translational level via phosphorylation.[124] In response to hypoxia, ULK1 phosphorylates S17, the residue adjacent to the FUNDC1 LIR motif, to enhance the interaction of FUNDC1 and LC3B.[92] FUNDC1-dependent mitophagy can be inhibited by the phosphorylation of Y18 by oncogenic SRC, or the phosphorylation of S13 by Casein Kinase 2 (CK2).[92] PGAM phosphatase, which also plays a role in PINK1 accumulation, dephosphorylates S13 to promote LC3 interaction and mitophagy.[125] FUNDC1 also appears to be required for the recruitment of DRP1 and Calnexin to mitochondrial-ER junctions, as FUNDC1 mutants that cannot bind DRP1 cannot elicit mitophagy.[126] To limit hypoxia-induced mitophagy, FUNDC1 may also be degraded at the proteasome upon the ubiquitination of K119 by the E3 Ub ligase MARCH5.[106] While both BNIP3/BNIP3L and FUNDC1-induced mitophagy are promoted by hypoxia, the extent to which these processes overlap is unknown.

BNIP3: A stress-induced mitophagy receptor

BNIP3 (BCL2/Adenovirus E1B 19kDa Interacting Protein 3) is a tail-anchored stress response protein that targets mitochondria for degradation at the autolysosome. BNIP3 was initially identified in a yeast two-hybrid screen as a pro-apoptotic protein that interacts with the anti-apoptotic proteins Bcl-2 and E1B 19kDa.[127] Based on weak homology to other Bcl-2 and Bcl-X_L interacting proteins, and BH3-only proteins in particular, it was suggested that BNIP3 was a pro-apoptotic molecule. However, BNIP3 protein is highly expressed in healthy liver, heart, and muscle tissues in the absence of cell death, casting doubt on the regulation of programmed cell death being a primary role of BNIP3.[128] Instead, more recent work has demonstrated that BNIP3 primarily acts

as a mitochondrial cargo receptor.[114,128–131] BNIP3 integrates into the OMM via its C-terminal transmembrane (TM) domain and interacts with LC3-II at the surface of the phagophore membrane via its cytosolic N-terminus to selectively target mitochondria for degradation.[128,131]

The BNIP3 protein sequence contains the following domains: the N-terminal domain, the LC3 interaction region (LIR), the PEST sequence, the Bcl-2 homology 3 (BH3) domain, the conserved domain (CD), and the C-terminal TM domain (Figure 1.4). The N-terminal domain (amino acids 1-49) remains cytosolic upon integration of BNIP3 into the OMM. The primary known function of this domain is to heterodimerize with Bcl-2 and Bcl-X_L.[127,132] The heterodimerization of BNIP3 with Bcl-X_L has been shown to enhance the interaction of the BNIP3 LIR motif to LC3.[133] LIR motifs allow the targeting of autophagy receptors, such as BNIP3, to the LC3-family proteins anchored in the phagophore membrane. The core LIR consensus sequence is four residues long, with an aromatic residue (W/F/Y) at the first position and a hydrophobic aliphatic residue (L, I, V) at the fourth position.[134] The BNIP3 LIR motif (amino acids 18-21), located within the N-terminal domain, is the site of the interaction between BNIP3 and LC3-II, which is critical for BNIP3-indcued mitophagy.[114] Within the motif is a critical tryptophan residue at position 18 of BNIP3, which when mutated to alanine (W18A) ablates the BNIP3-LC3-II interaction. Serine or threonine residues are found at the -1 position of 25% of LIR motifs, many of which are proposed to be regulated via phosphorylation.[92,133–136] Serine residues at positions 17 and 24 in BNIP3 have been reported as putative phosphorylation sites, the modification of which are proposed to increase the interaction

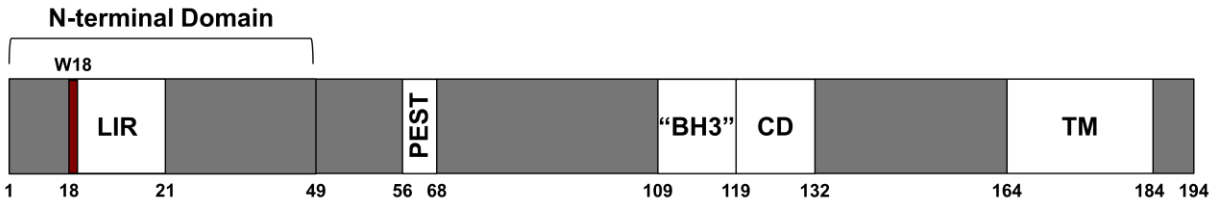

Figure 1.4: Schematic of BNIP3 protein domains. The BNIP3 protein sequence contains the following domains: the N-terminal domain, the LC3 interaction region (LIR), the PEST sequence, the “BH3” domain, the conserved domain (CD), and the C-terminal TM domain. BNIP3 integrates into the outer mitochondrial membrane as a tail-anchored protein, where it then homodimerizes via its TM domain. Following integration, the majority of the BNIP3 protein sequence (amino acids 1-163) remains cytosolic, while the C-terminal tail (amino acids 184-194) is localized in the mitochondrial intermembrane space.

of BNIP3 and LC3-II.[133] However, the kinase responsible for these phosphorylation events remains unknown.

BNIP3 is reported to contain a PEST sequence (amino acids 56-68), which is a sequence rich in proline (P), glutamic acid (E), serine (S), and threonine (T) residues, often flanked by charged amino acids.[137,138] PEST sequences are commonly associated with proteins that have short intracellular half-lives, and are therefore hypothesized to play a role in targeting proteins for degradation at the proteasome.[138,139] BNIP3 is known to be subject to both autophagic and proteasomal degradation, however the mechanism through which BNIP3 is targeted to the proteasome and whether its PEST sequence plays a role is not known.[140]

BNIP3 was originally identified as a BH3-only protein due to its interaction with E1B 19kDa and Bcl-2, as well as its putative BH3 domain (amino acids 109-118).[127] BH3 domains typically consist of 11 amino acids.[141] While there is no strict domain conservation between the BH3-only proteins, an 11-residue consensus motif has been proposed based on structural studies and sequence analyses.[142] However, when comparing the putative BH3 domain of BNIP3 to that of canonical BH3-only proteins (e.g. BIM, PUMA, and NOXA), the BNIP3 BH3 domain is poorly conserved.[141] Additionally, the BH3 domain of pro-apoptotic proteins typically mediates heterodimerization with pro-survival Bcl-2 family proteins.[132,143] However, in the case of BNIP3, the BH3 domain is redundant for function, and heterodimerization with Bcl-2 and Bcl-XL instead relies on the N-terminal domain.[132] Therefore, it remains to be determined whether the putative BH3 domain of BNIP3 serves any function. Adjacent to the putative BH3 domain lies the CD (amino acids 119-132)[144]. This region of the BNIP3

protein is homologous to that of the BNP3 homolog BNIP3L, however the significance of this homologous sequence is unclear.

BNIP3 is a tail-anchored protein, with its C-terminal TM domain (amino acids 164-184) required for its localization to the mitochondria.[145] Tail-anchored proteins are a class of membrane protein containing a single C-terminal TM domain, which is integrated post-translationally into the target membrane (e.g. mitochondria, endoplasmic reticulum, peroxisome).[146–149] Upon integration of its TM domain into the OMM, the N-terminal portion (amino acids 1-163) of BNIP3 remains cytosolic and a 10 amino acid C-terminal tail (amino acids 184-194) is located within the mitochondrial intermembrane space (IMS). It is reported that this 10 amino acid tail interacts with Opa1 in the IMS, possibly inhibiting Opa1-mediated mitochondrial fusion.[150,151] Upon targeting BNIP3 to the OMM, the TM domain forms SDS-resistant homodimers.[137,152] Homodimeric BNIP3 forms a right-handed parallel helix-helix structure with critical interfacial residues at S172, H173, A176, L179, G180, I183, and G184.[153–155] Within this structure lies a tandem glycine zipper motif (AxxxGxxxG), as well as intermonomeric hydrogen bonding between residues S172 and H173, lending stability to the helix-helix interaction.[153,156] The arginine residues that flank the TM domain, Arg185 and Arg186, are also important for dimerization, possibly due to the proximity of these positively charged resides to negatively charged lipid headgroups.[153] Mutation of the interfacial residues, including G180, blocks BNIP3 homodimerization, resulting in monomeric BNIP3. These BNIP3 dimerization mutants are known to have significantly reduced interaction with LC3 as compared to wild-type, suggesting that BNIP3 dimer binds more strongly to LC3.[114] Additional studies have suggested that the TM domain of BNIP3 may act as an acid-

sensitive proton channel in the OMM, however these results have been inconsistent.[157–159]

Unlike Parkin/PINK-mediated mitophagy, which specifically targets depolarized mitochondria for degradation, BNIP3 is activated in response to metabolic stress to promote mitophagic turnover and reduce mitochondrial mass.[131,160] Hypoxia is a key promoter of BNIP3 transcriptional upregulation.[130,161] Under hypoxic conditions, hypoxia-inducible factor-1 alpha (HIF1α) binds to the hypoxia response element (HRE) in the BNIP3 promoter, resulting in the rapid transcriptional upregulation of BNIP3.[117,130,161] In addition to hypoxia, BNIP3 is also transcriptionally regulated by several other stress-related proteins including Rb/E2F, NF-κB, PPARα, FoxO3, p53, oncogenic Ras, and GR.[130,162–168] Transcriptional mechanisms take time to elicit a response, therefore mechanisms often exist to post-translationally regulate the activity of preexisting stress response proteins upon exposure to stress.[169] Preliminary work suggests that BNIP3 is regulated post-translationally via phosphorylation and oxidation events. Hypoxia-reoxygenation is reported to induce BNIP3 phosphorylation, while dephosphorylation was coordinated with extreme acidosis.[170] BNIP3 is also reported to act as a redox sensor, with increased oxidative stress reported to result in the oxidation of the N-terminus and promotion of homodimerization.[159] Additional work has suggested that phosphorylated forms of BNIP3 may interact more strongly with binding partners, including Bcl-2, Bcl-$_X$L, Opa1, and LC3.[133,151,171]

BNIP3 protein is also known to play several specific roles in the liver. Unlike in many other tissues, BNIP3 protein is constitutively expressed and stabilized in the liver, however this expression is superinduced by PPARα in response to fasting.[128,164] BNIP3

is also required for glucagon-induced mitophagy.[172] Within the liver, BNip3 exhibits a zonal expression pattern that correlates with levels of oxygenation in the tissue. BNIP3 is highly expressed around the hypoxic central vein of the liver lobule, while its expression is lower around the oxygenated periportal vein.[172] This, in turn affects mitochondrial mass, with lower mitochondrial mass correlating with high expression of BNIP3. Metabolic activities, such as glutamine synthesis and the urea cycle, lipogenesis and fatty acid oxidation, and gluconeogenesis and glycolysis, are spatially organized across the liver lobule based on proximity to the periportal and central veins.[173] Interestingly, loss of BNIP3 disrupts the metabolic zonation of the liver, such that processes normally performed in proximity of the periportal vein, such as the urea cycle, were expanded at the expense of central vein processes, such as glycolysis. These results demonstrate that BNIP3-induced mitophagy plays an important role in the coordination of metabolic processes in the liver.

BNIP3L: Similarities and differences in regulation and function

BNIP3L (BCL2/adenovirus E1B 19 kDa protein-interacting protein 3-like), also known as NIX, was originally cloned from a human placenta cDNA library based on its 56% identical homology to BNIP3.[174] Similar to BNIP3, BNIP3L was originally characterized as a pro-apoptotic BH3-only protein which interacts with Bcl-2 and Bcl-x_L.[175] However, BNIP3L is highly expressed during erythroid development and the differentiation of both retinal ganglion and inflammatory macrophages in the absence of cell death, contrary to a primary role in regulating programmed cell death.[176,177] Instead, more recent work has demonstrated that, like BNIP3, BNIP3L is a tail-anchored stress response protein that acts as a mitochondrial cargo receptor in mitophagy.[113,178,179]

BNIP3L integrates into the OMM via its C-terminal TM domain and interacts with LC3-II at the surface of the phagophore membrane via its cytosolic N-terminus to selectively target mitochondria for degradation.[115] Like that of BNIP3, the BNIP3L protein sequence contains the following domains: the N-terminal domain, the LIR motif, the PEST sequence, the BH3 domain, the CD, and the C-terminal TM domain (Figure 1.5). While the history and chemistry of these domains was described in detail in the previous section, additional detail specific to BNIP3L will be described below.

The N-terminal domain of BNIP3L (amino acids 1-76) is the site of the interaction of BNIP3L with Bcl-2 and Bcl-X_L. Within this domain lies the LIR motif (amino acids 36-39) with a critical tryptophan residue at position 36 of BNIP3L, which when mutated to alanine (W36A) blocks the interaction of BNIP3L with LC3-II.[101] Serine residues at positions 34 and 35 in BNIP3L have been reported as putative phosphorylation sites, the modification of which are proposed to increase the interaction of BNIP3L and LC3-II.[135] However, the kinase responsible for these phosphorylation events remains unknown. BNIP3L is thought to contain a PEST sequence, however there is no consensus on its location. While BNIP3L is known to be subject to both autophagic and proteasomal degradation, whether its PEST sequence is involved in the targeting of BNIP3L to the proteasome remains unknown.[180] Like BNIP3, the putative BH3 domain of BNIP3L (amino acids 133-144) is poorly conserved when compared to canonical BH3-only proteins, and is redundant for function.[141] Adjacent to the putative BH3 domain lies the CD (amino acids 145-156) which is a region of homology between BNIP3L and BNIP3, however the significance of this homologous sequence is unclear.[181] While no in-depth study has been performed on the BNIP3L TM domain

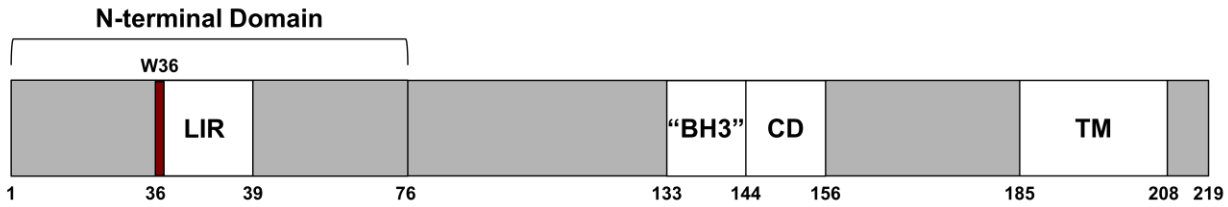

Figure 1.5: Schematic of BNIP3L protein domains. Similar to its homolog, BNIP3, the BNIP3L protein sequence contains the following domains: the N-terminal domain, the LC3 interaction region (LIR), the “BH3” domain, the conserved domain (CD), and the C-terminal TM domain. BNIP3L is also thought to contain a PEST sequence, however there is no consensus on its location. BNIP3L integrates into the outer mitochondrial membrane as a tail-anchored protein, where it then homodimerizes via its TM domain. Following integration, the majority of the BNIP3L protein sequence (amino acids 1-185) remains cytosolic, while the C-terminal tail (amino acids 208-219) is localized in the mitochondrial intermembrane space.

(amino acids 185-208), it is highly homologous to the BNIP3 TM domain. It contains all of the critical interfacial residues of the BNIP3 domain at S196, H197, A200, L203, G204, I207, and G208, as well as the flanking charged residues at K209 and R210. Upon integration of its TM domain into the OMM, the N-terminal portion (amino acids 1-184) of BNIP3L remains cytosolic and an 11 amino acid C-terminal tail (amino acids 209-219) is located within the mitochondrial IMS.[101] Upon targeting BNIP3L to the OMM, the TM domain forms SDS-resistant homodimers. BNIP3L homodimerization is essential for its binding to LC3/GABARAP-family proteins at the phagophore surface.[115,180] BNIP3 and BNIP3L are also known to form heterodimers, however understanding the significance and physiological context of this interaction requires further investigation.[116]

Much like BNIP3, BNIP3L is a stress response protein that is regulated both transcriptionally and post-translationally. In response to hypoxia or increased levels of ROS, both BNIP3 and BNIP3L are transcriptionally activated by HIF-1. Both proteins are also transcriptionally regulated by p53, however while BNIP3 is repressed by p53, BNIP3L is known to be transcriptionally upregulated.[182,183] These data suggest that BNIP3 and BNIP3L may play different roles in response to signals that activate p53, such as DNA damage. Preliminary work has demonstrated that BNIP3L is regulated post-translationally by both phosphorylation and ubiquitination.[120,121] Several putative phosphorylation sites (S34, S35, and S82) have been identified as modulating the interaction of BNIP3L with LC3/GABARAP family proteins, however, the kinases responsible for these events have yet to be identified.[135,184] BNIP3L has also been shown to be phosphorylated by PKA on S212 to prevent localization to the OMM and

reduce rates of mitophagy.[185] In addition to phosphorylation, BNIP3L is known to be ubiquitinated by Parkin, which promotes Parkin/PINK1-mediated mitophagy.[120,121] However, Parkin and PINK1 are not required for BNIP3L-induced mitophagy.

Additionally, BNIP3L has been demonstrated to have several important functions in tissue differentiation. BNIP3L-induced mitophagy has been implicated in erythroid maturation. Erythroid cells undergo organelle removal and enucleation during terminal differentiation.[186] Erythrocytes of BNIP3L-null mice exhibited mitochondrial retention and reduced lifespan, suggesting a critical role for BNIP3L in erythroid development.[176,187,188] A BNIP3L-dependent glycolytic switch also plays a role in the differentiation of retinal ganglion and polarization of M1 macrophages, and BNIP3L-dependent mitophagy is also required for the generation of robust natural killer cell memory.[177,179,189]

Both BNIP3 and BNIP3L are also known to interact with Ras homolog enriched in brain (Rheb), however the outcomes of these interactions differ. Rheb is a small GTP-binding protein that promotes the lysosomal localization and activity of the growth promoting kinase mTOR. The binding of BNIP3 to Rheb repressed its activity, resulting in decreased mTOR activity and decreased cell growth, which is consistent with a tumor-suppressive role for BNIP3.[190] The interaction of BNIP3L with Rheb occurred upon high rates of oxidative phosphorylation (OXPHOS) to enhance mitochondrial turnover and renewal. The interaction of Rheb with BNIP3L at the mitochondria affected growth in an mTOR-independent manner through a tri-molecular complex with LC3.[191] Additional work is required to elucidate the physiological significance of the interactions of BNIP3 and BNIP3L with Rheb.

Role of mitophagy and its regulators in cancer

Due to the critical role of mitophagy in maintaining cellular homeostasis, it is unsurprising that many of the proteins involved in the mitophagic process have been found to be dysregulated in human cancers. Dysregulation of mitophagy-related genes has been shown to contribute to the Warburg Effect, affect HIF-1α stabilization, and alter rates of OXPHOS, all of which play important roles in tumor cell progression and survival.[101,192]

The genetic loci encoding for Parkin and PINK1 (PARK2 and PARK6, respectively) are commonly disrupted in several human cancers. The PARK2 locus is frequently deleted in breast, lung, bladder, and ovarian cancer, while mutations have been linked to glioblastoma, lung, and colon cancer.[193,194] Rare mutations in the PARK6 locus have been found in neuroblastoma, and expression is down-regulated in ovarian cancer and glioblastoma.[195] The loss of either Parkin or PINK1 in KRas-driven pancreatic ductal adenocarcinoma (PDAC) increased both tumor burden and metastasis.[123,196] Additionally, Parkin-null mice are sensitized to irradiation-induced lymphomagenesis and susceptible to spontaneous hepatocellular carcinoma (HCC).[197,198] Due to their well-characterized role in mitophagy, Parkin and PINK1 have been hypothesized to function in mouse and human disease by clearing depolarized mitochondria to prevent excess ROS and Warburg metabolism.[198,199] However, additional work has also demonstrated a role of Parkin and PINK1 in the suppression of HIF1α stabilization.[122,123,195] The elevated levels of glycolysis and ROS observed in Parkin- or PINK1-null mouse models of PDAC was rescued by the deletion of HIF1α.[123] Parkin has been shown to ubiquitinate HIF1α on K477 to promote its degradation.[122] In

human breast cancer, low Parkin levels correlate with high HIF1α levels and reduced metastasis-free survival.[122] However, it is also important to note that Parkin is poorly expressed in most cancers and cell lines, and that other E3 ubiquitin ligases may substitute for Parkin in mitophagy.[200] ARIH1, another E3 ubiquitin ligase, promotes drug resistance when it is recruited by PINK1 to promote mitophagy in response to chemotherapeutic agents. ARIH1 functions similarly to Parkin, however its mitochondrial substrates remain uncharacterized.[103] Investigating the roles of additional mitochondrial E3 ubiquitin ligases in mitophagy remains an open area of interest in the field.

The genetic locus encoding for BNIP3 is commonly disrupted in several human cancers. In various solid cancers, such as pancreatic and breast cancers, BNIP3 protein levels are induced by hypoxia in early, pre-malignant stages of the disease but are subsequently down-regulated as the tumors progress.[201–203] Epigenetic silencing of BNIP3 is associated with poor prognosis in a number of human cancers, including hematological malignancies, lung, liver, gastric, and pancreatic cancer.[201,204–206] The BNIP3 locus is also known to be deleted in a number of cancers including prostate, and, most frequently, triple negative breast cancer (TNBC).[131,207] In TNBC patients, the loss of BNIP3 combined with high HIF1α expression is predictive of poor metastasis-free survival. In mice, BNIP3 knockdown promoted tumor growth and metastasis in a 4T1 orthotopic model of mammary tumorigenesis, and the loss of BNIP3 in a MMTV-PyMT mouse model of breast cancer increased tumor burden and accelerated the progression to invasive and metastatic disease.[131] This phenotype was associated with reduced mitophagy and increased ROS, which led to HIF-1α stabilization and increased glycolysis. Quenching of ROS attenuated HIF1α and reduced metastasis, indicating that

BNIP3 acts as a tumor suppressor by reducing mitochondrial mass and limiting ROS.[131] Similarly, work with the breast cancer cell line MCF7 demonstrated that resistance to IFG-1 receptor kinase inhibitor was associated with reduced BNIP3 levels, increased ROS, and increased glycolysis.[208] Conversely, BNIP3 has also been shown to promote cancer cell survival, with high BNIP3 levels correlated with worse patient outcomes in both kidney cancer and sarcoma.[209] These differences in the effect of BNIP3 on tumorigenesis may be explained by differential roles of BNIP3 depending on cell type or other factors. The BNIP3 homolog BNIP3L has also been implicated in tumor progression. In the KPC model of PDAC, loss of BNIP3L delayed tumor progression from the PanIN stage to malignant PDAC.[210] Consistently, elevated BNIP3L expression in PDAC patients was linked to worse prognosis. Why BNIP3 and BNIP3L are reported to play opposing roles in PDAC development requires further investigation, however it may be due to their expression in different cell types or at different stages of tumor progression.

Changes in FUNDC1 expression have also been implicated in cancer. In both prostate and glioblastoma cells, silencing FUNDC1 resulted in increased cellular motility and invasion due to increased rates of focal adhesion assembly and disassembly.[211] Similarly, decreased FUNDC1 expression was associated with increased liver metastasis in xenograft models, however this was also accompanied by decreases in tumor cell proliferation.[212] A study of The Cancer Genome Atlas (TCGA) database found an association between low levels of FUNDC1 and increased ROS and metastasis in lung cancer, while increased FUNDC1 expression was associated with increased levels of genes involved in mitochondrial bioenergetics.[212] Consequently, some have

postulated that the effects of FUNDC1 on cell proliferation, migration, and invasion may be the result of mitophagy-independent functions of FUNDC1 in mitochondrial bioenergetics. FUNDC1 knockdown in prostate cancer cells was associated with increased degradation of electron transport chain (ETC) complexes and resulted in lowered respiration rates, decreased levels of TCA cycle intermediates, and increased ROS production.[211] FUNDC1 knockdown resulted in the misfolding of the LonP protease, which maintains the integrity of ETC complexes. Exogenous overexpression of LonP rescued the metabolic effects of FUNDC1 knockdown, as well as the effects on cell proliferation and invasion.[213] These results suggest that the effect of FUNDC1 on tumorigenesis may be independent of its mitophagy function.

Summary

Response to external stressors is essential to cell survival, resulting in the development of a number of mechanisms to cope with a variety of cellular stressors. Autophagy is an adaptive process that involves the sequestration, lysosomal degradation, and recycling of intracellular components and other cytoplasmic contents.[1] This process is critical to maintaining cellular homeostasis, and is upregulated in response to a number of cellular stressors including oxidative stress, nutrient depravation, and hypoxia.[2] The kinase ULK1, a major regulator of autophagy initiation, regulates general autophagy in response to changes in nutrient status by integrating AMPK and mTORC1 signaling.[44,62] In addition to its role in general autophagy, recent work has suggested that ULK1 plays a role in forms of selective autophagy, including the autophagic turnover of mitochondria, termed mitophagy.[91,92] Mitophagy serves an important housekeeping function by eliminating mitochondria that have become

dysfunctional, thus limiting the production of damaging ROS. In response to stresses such as hypoxia and nutrient depravation, mitophagy can promote the efficient use of limiting metabolites and oxygen by eliminating healthy mitochondria to reduce overall mitochondrial mass.[101,192] In order to achieve this, cells rely on the activity of mitochondrial cargo receptors, which specifically target mitochondria to the autophagosome. These proteins include BNIP3, BNIP3L, FUNDC1, and Parkin/PINK1, among others.[101] The mitochondrial cargo receptor BNIP3 is a stress response protein that is transcriptionally upregulated in response to a number of stressors, including hypoxia.[130,162–168] While the transcriptional upregulation of BNIP3 in response to stressors is well characterized, the role of post-translational modification in BNIP3 protein stability and BNIP3-induced mitophagy remains poorly understood.

ULK1 has recently been demonstrated to regulate the mitochondrial cargo receptor FUNDC1 by phosphorylating a residue adjacent to its LIR motif, thereby enhancing the interaction of FUNDC1 with ATG8 family proteins and increasing rates of mitophagy.[92] Interestingly, studies have suggested that the residues adjacent to the LIR motifs of BNIP3 and BNIP3L (S17 and S35, respectively) are also phosphorylated, but the kinase responsible remains unknown.[133,135] The work in this dissertation explores the hypothesis that BNIP3-induced mitophagy is regulated by the phosphorylation of BNIP3 at S17 by ULK1, resulting in an increased affinity for LC3 and therefore an increase in rates of mitophagy. In addition to the regulation of BNIP3-induced mitophagy, we investigate a novel role for ULK1 in stabilizing BNIP3 protein by protecting it from regulation by the proteasomal machinery. Taken together, the results of this work explore an additional layer of post-translational regulation, key to the

function of BNIP3 as a stress response protein. In concordance with the published work on FUNDC1, these findings demonstrate and strengthen an additional role for ULK1 in specifically upregulating mitophagy, as opposed to general autophagy, which may occur upon specific cellular stressors, such as hypoxia or nutrient depravation. While this study helps lay the foundation on which this role of ULK1 can be assessed, additional work is required to fully understand the cellular context and scope of this role.

CHAPTER 2

MATERIALS AND METHODS

Reagents

ULK-101 (MedChemExpress HY-114490) was used at 5 μM. MG132 (Enzo Life Sciences BML-PI102) was used at 10 μM. Bafilomycin A_1 (Enzo Life Sciences BML-CM110) was used at 0.1 μM. Cycloheximide (Sigma 01810) was used at 10 μM. Deferoxamine (Sigma BP987) was used at 260 μM.

Genotyping

Mice were weaned and had their tail tips snipped for genotyping at 3 weeks of age by technicians at the University of Chicago Animal Resource Center. Tail tips were digested overnight at 55°C in tail lysis buffer (100 mM Tris pH 8.0, 5 mM EDTA pH 8.0, 0.2% SDS, 200 nM NaCl, 100 nM proteinase K). Genomic DNA was isolated by isopropanol precipitation, resuspended in nuclease-free deionized water, and used in subsequent genotyping analysis. The following primers were used to detect the WT, Floxed-in, and Floxed-out alleles: WT (intron 1), 5'-GCATCACTAAGATCGAGCCT-3'; Floxed-IN (exon 2), 5'-CATGCTGGGCATCCAACAGT-3'; Floxed-OUT (intron 5), 5'-ACCTTCCACTACACGGGATT-3'. These primers generate a 545 bp product for the WT allele, a 645 bp product for the Floxed-in allele, and a 350 bp product for the Floxed-out allele.

Whole cell protein extraction

For harvesting protein from cells, plates were washed in ice-cold DPBS followed by scraping in 1 mL of DPBS containing protease and phosphatase inhibitors (0.5 mM PMSF, 1 μg/mL aprotinin, 1 μg/mL leupeptin, 1 mM Na_3VO_4). Cells were pelleted at

3000xg for 3 minutes at 4°C and resuspended in RIPA lysis buffer (10 mM Tris-HCl pH 8.0, 150 mM NaCl, 1% sodium deoxycholate, 0.1% SDS, 1% Triton X-100) containing a Roche PhosSTOP inhibitor cocktail in addition to the aforementioned protease and phosphatase inhibitors. Samples were incubated on ice for 15 minutes with vortexing every 5 minutes, and centrifuged at full speed for 15 minutes at 4°C. The supernatant was transferred to fresh, pre-chilled Eppendorf tubes and protein concentration was measured on a NanoDrop spectrophotometer and stored frozen at -80°C.

Immunoprecipitation

For harvesting protein from cells, plates were washed in ice-cold DPBS followed by scraping in 1 mL of DPBS containing protease and phosphatase inhibitors (0.5 mM PMSF, 1 µg/mL aprotinin, 1 µg/mL leupeptin, 1 mM Na_3VO_4). Cells were pelleted at 3000xg for 3 minutes at 4°C and resuspended in 250 µL NP-40 IP lysis buffer (50 mM Tris-HCl pH 7.5, 150 mM NaCl, 1 mM EDTA, 1% IGEPAL, 0.01% β-mercaptoethanol), and sonicated at 10% power for 5 seconds using a Fisher Sonic Dismembrator Model 500 while keeping samples cold in an ethanol-ice bath. Samples were incubated on ice for 5 minutes and centrifuged at full speed for 15 minutes at 4°C. The supernatant was transferred to fresh, pre-chilled Eppendorf tubes and protein concentration on a NanoDrop spectrophotometer. For immunoprecipitation of exogenously-expressed GFP-tagged proteins, 25 µL GFP-Trap or agarose control-Trap magnetic beads (Chromotek) were washed twice in 500 µL IP lysis buffer using a magnetic bead rack, followed by resuspension in 1 mL IP lysis buffer and addition of 2 mg protein lysate. For FLAG-tagged proteins, 25 µL of anti-FLAG M2 magnetic beads (Sigma M8823) were used. Lysates were incubated on beads for 1 hour at 4°C on a rotator followed by three

1 mL washes with IP lysis buffer using a magnetic bead rack. Beads were transferred to a fresh Eppendorf tube for the final wash and resuspended in 50 µL 2x sample loading buffer (1:2:2 10x SDS:5x BPB: ddH_2O) and boiled for 10 minutes. Supernatant containing denatured was transferred to a fresh Eppendorf tube and frozen at -80°C.

Western blot

Protein samples were denatured by boiling for 5 minutes with SDS reducing sample buffer (400 mM Tris pH 6.8, 10% SDS, 500 mM β-mercaptoethanol) and sample loading dye (60% glycerol and bromophenol blue). The amount of protein loaded per sample varied depending on the proteins being probed, but typically 75 ug was loaded onto SDS-PAGE gels, followed by transfer to nitrocellulose (0.2 µm or 0.45 µm pore, GE Healthcare) or PVDF (0.45 µm pore, GE Healthcare) membranes. Membranes were blocked in 5% nonfat milk in TBS/0.05% Tween (TBS-T) for 30 minutes at room temperature for non-phosphorylated protein detection, and 5% BSA in TBS-T for 30 minutes at room temperature for phosphorylated protein detection. Primary antibodies were incubated overnight at 4°C on a rocker, in 5% BSA/TBS-T for antibodies from Cell Signaling Technology and in 5% nonfat milk/TBS-T for non-Cell Signaling Technology antibodies. The next day membranes were washed three times with TBS-T for 10 minutes and incubated with HRP-conjugated secondary antibody (Dako) in 5% nonfat milk/TBS-T for 2 hours at room temperature on a shaker. Membranes were washed three times in TBS-T for 10 minutes and proteins were visualized by chemiluminescence and exposure on X-ray film.

Immunofluorescence & confocal microscopy

U2OS$^{\Delta BNIP3}$ cells were grown on sterile glass coverslips in 6-well tissue culture plates overnight before transfection with HA-tagged BNIP3 mutants. At 20hr post transfection, cells were treated with Bafilomycin A_1 (100nM) for 4hr. Cells were fixed for 15 min in 4% paraformaldehyde at RT, and 10min in ice cold methanol at -20°C. Coverslips were incubated in 0.1% Saponin in PBS for 10min, then blocked in 10% goat serum in 0.05% TBS-T for 1hr. Coverslips were then incubated with primary antibodies in 10% goat serum in TBS-T for 1hr at RT. Anti-TOMM20 (Abcam, ab56783, 1:200), anti-LC3B (Cell Signaling, 3868S, 1:200), anti-HA-Tag (Bethyl, A190-106A, 1:200). Coverslips were washed in TBS-T for 3x5 min, followed by incubation with Alexa Fluor conjugated secondary antibodies (Thermo Fischer Scientific, 1:1000) for 1hr at RT. Coverslips were washed in TBS-T for 3x5 min and mounted with 10µL ProlongGold containing DAPI (Thermo Fisher, P36931). Slides were allowed to cure for 24hr in the dark at RT, with subsequent storage at 4°C. Imaging was performed using the Leica TCS SP8 laser scanning confocal microscope in the Integrated Microscopy Core Facility at the University of Chicago. All images were collected using a 100X oil-immersion objective. Ten representative images per sample were obtained.

Cell culture

Human cell lines were maintained in a humidified CO_2 incubator at 5% CO_2 and 37°C. U2OS, SaOS2, PANC-1, and HEK-293T cell lines were cultured in Dulbecco's Modified Essential Medium (DMEM) supplemented with 10% fetal bovine serum (FBS) and 1% penicillin/streptomycin. HCC38 cells were cultured in Roswell Park Memorial Institute (RPMI) media supplemented with 10% fetal bovine serum (FBS) and 1%

penicillin/streptomycin. MiaPaca2 cells were cultured in DMEM supplemented with 10% FBS, 2.5% horse serum, and 1% penicillin/streptomycin. Cells treated with hypoxia were cultured in a humidified 37°C Tissue Culture Glove Box (Coy Laboratory Products) at 5% CO_2 and 1% O_2.

Transient transfections

For the transient transfection of human cell lines, including HEK-293T cells, cells were seeded onto 10 cm plates at a density of $1.0x10^6$ cells. The next day, 0.5 µg of pLVX-IRES-hygro-HA-BNIP3 plasmid and/or 1.0 ug of pcdna3 FLAG-ULK1 plasmid were added to Lipofectamine 3000 reagents at a 1:1 ratio (ug plasmid DNA:uL Lipofectamine 3000) in 0.5 mL of Opti-MEM media and allowed to incubate for 15 minutes at room temperature. After incubation, the solution was added to the 10 cm plates containing 8 mL of cell culture media. The plates were incubated in transfection media overnight, washed once with DPBS and returned to cell culture media. Cell lysates were harvested 36-48 hours post-transfection.

Stable transfections

For the stable transfection of human cell lines, cells were seeded onto 6 well plates at a density of $2.0x10^5$ cells. The next day 1.0 µg of plasmid and Lipofectamine 2000 reagent were added in a 1:1 ratio in 250 µL of Opti-MEM media and allowed to incubate for 15 minutes at room temperature. After incubation, the solution was added to the well containing 1 mL of cell culture media. The wells were incubated in transfection media overnight, washed once with DPBS and returned to cell culture media. Cells were selected 36-48 hours post transfection and either seeded sparsely

onto 15 cm plates for clonal growth or expanded onto 10 cm plates for pooled growth. Stable expression

Lentivirus production and transduction

Lentivirus were produced using Lenti-X^{TM} Packaging Single Shots (Clontech) using the manufacturer's protocol. Briefly, 7 µg of diluted lentiviral vector plasmid was added to the Lenti-X^{TM} Packaging Single Shot, vortexed and incubated for 10 minutes. The resulting nanoparticle complexes were added to 293T cells plated at 80-90% confluence. The complexes were allowed to incubate overnight at 37°C, after which additional fresh growth media was added. Viruses were collected at 48 hours by centrifuging the growth media to pellet any contaminating cells and passing the supernatant through a 0.45 µm pore filter. Lentiviral-containing media was frozen at -80°C.

For infection, 500 µL of lentivirus was added to target cells in media containing 8 µg/mL polybrene. Cells were transduced for 24 hours, followed by removal of viral media, washing with PBS twice, and replacement with normal growth media. After 24 hours of growth post-transduction, cells were selected using the appropriate selective marker to generate stable cell lines.

Generation of CRISPR/Cas9 *Bnip3*-KO cell lines

The *Bnip3* locus was genetically deleted in 293T and U2OS cell lines. *Bnip3* CRISPR/Cas9 and HDR plasmids were purchased from Santa Cruz Biotechnologies (sc-400985 and sc-400985-HDR). Cell lines were transfected with 2 µg of each plasmid using Lipofectamine 3000 at a ratio of 2:1 Lipofectamine to DNA. After 24 hours of transfection, media was changed and dual fluorescence of GFP and RFP was

confirmed using the Incucyte S3 imaging system. Cells were selected 48-72 hours post-transfection with 0.5-1 µg/mL puromycin and seeded sparsely onto 15 cm plates for clonal growth. Single clones were isolated using cloning cylinders, expanded in 6-well plates, and further expanded onto 10 cm plates. At confluence, plates were placed in a hypoxia chamber (1% O_2) for 16-24 hours and protein was extracted as described previously. Lysates were run on western blots and probed for BNIP3 to confirm deletion of the *Bnip3* gene and the absence of BNIP3 protein compared to control parental cells. The U2OS cells with confirmed deletion of BNIP3 were transiently transfected with Cre recombinase to remove the puromycin resistance genes and RFP, both of which were flanked by loxP sites introduced by the CRISPR plasmids. RFP-negative cells were sorted and collected at the Cytometry and Antibody Technology core at the University of Chicago with the assistance of core staff. RFP deletion was then confirmed by western blot.

Cloning

Site-directed mutagenesis was used for the generation of pLVX-IRES-hygro-HA-BNIP3 plasmids expressing mutant forms of BNIP3, and pcdna3 FLAG-ULK1 plasmids expressing mutant forms of ULK1. Primers were designed and recommended annealing temperatures were calculated using the NEBaseChanger website. Site-directed mutagenesis was then performed using the Q5 Site-directed Mutagenesis Kit (New England BioLabs).

Growth curves

For manual cell counts, human cell lines were seeded at a density of $2x10^4$ cells per well in 6 well plates. Each condition was seeded in duplicate for each day of

counting. The next day (D1), culture medium was changed. On D2 through D7, each well was rinsed in PBS, trypsinized, and resuspended in media for counting by hemocytometer.

For automated cell counts, U2OS$^{\Delta BNIP3}$ cells were stably infected using Incucyte® NucLight Green Lentivirus Reagent (Sartorius). Cells expressing NucLight Green were selected as previously described. For cellular proliferation experiments, NucLight Green expressing cells were seeded at a density of $2x10^4$ cells per well in 6 well plates. Each condition was seeded in duplicate. The next day (D1), culture medium was changed, and the plates were placed in the Incucyte S3 Imaging system. The Incuyte S3 Imaging system counted fluorescent nuclei at 25 defined locations in each well once per day for D1 through D7. All counts were normalized to D1 values to account for seeding error.

Statistics

Data were plotted and analyzed using Graphpad Prism software and presented as the mean ± SEM. Statistical significance was determined using unpaired, two-tailed Student's t-test for comparisons of two groups. *p<0.05, **p<0.01, ***p<0.001, ***p<0.0001.

Analysis of oxygen consumption rates (Seahorse)

U2OS$^{\Delta BNIP3}$ cells stably expressing pLVX-IRES-hygro-HA-BNIP3 mutants were seeded in Seahorse XF96 microplates at a density of $2x10^4$ cells/well. Following drug treatments, cells were rinsed with DPBS prior to the addition of 175 µL of 1X DMEM supplemented with 4.5 g/L glucose, 2 mM glutamine, and 1 mM sodium pyruvate, and adjusted to a pH of 7.35. Following a 1-hour incubation in the absence of CO_2, the Seahorse Cell Mito Stress Test was performed according to the manufacturer's protocol

using the Seahorse XF96 analyzer in the Biophysics Core at the University of Chicago. Data were normalized by cell density using Hoechst 33342 nuclear counterstain and fluorescence quantification using a microplate reader. Normalized OCR data was then analyzed using Agilent Seahorse Wave software.

Southern blot

During collaboration with the Transgenics/ES Cell Technology Mouse Core Facility at the University of Chicago, a targeting vector was electroporated into murine ES cells, which were grown and selected in 96-well plates. DNA was collected from the ES cells using the Gentra Puregene Blood Kit (Qiagen) as described by the manufacturer. To test for homologous recombination, PCR screening was used to find likely-positive clones, followed by confirmation with Southern blot. 5 µg of DNA was loaded into a 0.5% agarose gel. After the gel was finished running, it was submerged in denaturation solution (0.5 M NaOH, 1.5 M NaCl) for 15 minutes, twice. The gel was then submerged in neutralization solution (0.5 M Tris HCl pH 7.5, 1.5 M NaCl) for 15 minutes, twice, followed by equilibration for 10 minutes in 20X SSC (3 M NaCl, 0.3 M Na citrate). DNA was transferred to a membrane overnight in transfer buffer (20X SSC), followed by UV crosslinking to fix DNA to the blot. The blot was then incubated with DIG Easy Hybridization buffer (Sigma) at 42°C for 30 minutes, followed by incubation with a DIG-labeled probe overnight. The membrane was then washed for 5 minutes in washing buffer and incubated in blocking solution (Sigma DIG Wash and Block Buffer Set) for 30 minutes. After blocking, the membrane was incubated in anti-AP antibody (1:2000) in blocking buffer, followed by two 15-minute washes in washing buffer and equilibration for 3 minutes in detection buffer (Sigma). The membrane was then placed face up in a

development cassette and 1 mL of CDP-Star was added to the membrane. The membrane was incubated for 15 minutes and exposed to X-ray film.

Lambda phosphatase assays

Cells were plated on two 10 cm dishes at $1x10^6$ cells per plate. The following day, one plate was placed in the hypoxia chamber (1% O_2 concentration) overnight while the other was left at atmospheric oxygen. Protein was then harvested as described above, but in the absence of phosphatase inhibitors. Protein concentration was measured by nanodrop. A total of 75 µg of the hypoxia-treated lysate was added to 10X Lambda Protein Phosphatase (λPPase) buffer and $MnCl_2$ (New England Biolabs), and either left untreated, treated with 1 µL of λPPase, or treated with 1 µL of λPPase and Na_3VO_4 (phosphatase inhibitor). All samples were then incubated for 30 minutes at 30°C, diluted 1:1 in 2x sample loading buffer (1:2:2 10x SDS:5x BPB: ddH_2O), and boiled for 5 minutes. The atmospheric oxygen and hypoxic lysates were then run on a western gel alongside the experimentally treated lysates as described above.

Recombinant protein expression in BL21 cells

pGEX2T-BNIP3 was transformed into BL21 cells and grown overnight on agar plates at 37°C. A single colony was then grown overnight in 25 mL of LB-Amp. The following day, the 25 mL culture was added to a 250 mL flask of LB-Amp and grown in a 37°C shaker for 1 hour. 275 µL of IPTG (stock 0.24 g/10 mL) was then added and the cells were placed back in the shaker for 4 hours. The bacteria were centrifuged, and the pellet was frozen overnight. The pellet was then thawed, resuspended in 50 mL NETN buffer with inhibitors, and sonicated at 15% amplitude 3x10 sec with 10 sec rest. The sonicated bacteria were then centrifuged and supernatant was added to 250 µL of a

Glutathione Sepharose 4B (GE Healthcare) bead slurry. Following pulldown and 3 washes with the Glutathione Sepharose 4B beads, rBNIP3 was eluted from the beads via thrombin cleavage (30 minutes at room temp). Recombinant protein was aliquoted and stored at -80°C. Relative protein concentrations were determined using western blots in which 1 µL, 3 µL, and 6 µL of each sample were run on a western, probed with BNIP3 antibody (Sigma B7931), and band intensity was compared.

Radioactive *in vitro* kinase assays

Recombinant GST-BNIP3 and GST-BNIP3L was produced and purified as described above. *In vitro* kinase assays were performed using recombinant ULK1 (ThermoFisher PV6430), 5X Kinase Buffer A (ThermoFisher PV3189), recombinant BNIP3/BNIP3L, ATP (0.2 mM), ULK-101 (0.5 µM), and ATP [γ-32P] (PerkinElmer BLU002Z250UC). Assays were incubated at 37°C for 30 minutes, diluted 1:1 in 2x sample loading buffer (1:2:2 10x SDS:5x BPB: ddH_2O), and boiled for 5 minutes. Samples were loaded onto an SDS-PAGE gel overnight, followed by gel drying and visualization by exposure on X-ray film.

CHAPTER 3

ULK1 PROMOTES MITOPHAGY VIA PHOSPORYLATION OF BNIP3

Introduction

Autophagy is a highly conserved process through which cells maintain homeostasis by sequestering, degrading, and recycling intracellular components including dysfunctional organelles and other cytoplasmic contents.[1] Autophagy initiation is regulated by the kinase ULK1, which phosphorylates and activates a number of protein targets essential for starvation-induced autophagy. ULK1 integrates AMPK and mTORC1 signaling, allowing the cell to initiate autophagy in response to changes in nutrient status and other stressors.[62,71] ULK1 may also regulate selective forms of autophagy, with evidence for a role in mitophagy, the autophagic turnover of mitochondria.[91,92] ULK1 has been implicated to localize mitochondria in response to hypoxic stress where it is reported to phosphorylate the mitochondrial cargo receptor FUNDC1 adjacent to its LIR motif, enhancing its interaction with LC3 at the phagophore surface to increase rates of mitophagy.[92] While FUNDC1 is known to induce mitophagy in response to hypoxia, it is not transcriptionally upregulated under these conditions. However, the mitochondrial cargo receptors BNIP3 and BNIP3L are transcriptionally upregulated in response to hypoxia and play an important role in upregulating mitophagy in response to hypoxic stress.[101] Similarly to FUNDC1, both BNIP3 and BNIP3L have previously been reported to be phosphorylated adjacent to their respective LIR motifs, however the kinases responsible for these phosphorylation events remain unknown.[133,135]

In this chapter, we sought to determine the kinase responsible for phosphorylating BNIP3 and BNIP3L adjacent to their respective LIR motifs, and how these phosphorylation events affect rates of mitophagy. Our findings led us to investigate a novel role for ULK1 in phosphorylating both BNIP3 and BNIP3L, suggesting a broader role for ULK1 in specifically regulating rates of mitophagy in response to cellular stressors including hypoxia.

ULK1 phosphorylates BNIP3 and BNIP3L adjacent to the LIR motif

While the transcriptional regulation of BNIP3 is relatively well characterized, its post-translational regulation remains poorly understood.[101] To confirm that BNIP3 is post-translationally regulated via phosphorylation, we began by performing an *in vitro* phosphatase assay (Figure 3.1). Indeed, BNIP3 is a highly phosphorylated protein, and the treatment of U2OS cellular lysates with lambda protein phosphatase resulted in a change of the BNIP3 protein banding pattern via western blot, with an increase in the intensity of lower molecular weight bands. Both BNIP3 and its homolog BNIP3L have previously been reported to be phosphorylated (serine 17 and 24 for BNIP3 and serine 34 and 35 for BNIP3L), but the kinase responsible for these phosphorylation events has not been identified.[133,135] Interestingly, both S17 and S35 are adjacent to the critical tryptophan residues in their respective LIR motifs, which are critical for the binding of BNIP3 and BNIP3L to processed LC3 family member proteins (Figure 3.2).[101] Recent work has shown that the mitochondrial cargo receptor FUNDC1 is phosphorylated adjacent to its LIR motif by the autophagy-regulating kinase ULK1, which led us to consider whether ULK1 may also phosphorylate BNIP3 and BNIP3L.[92] The optimal ULK1 phosphorylation consensus sequence includes an affinity for serine (S) over

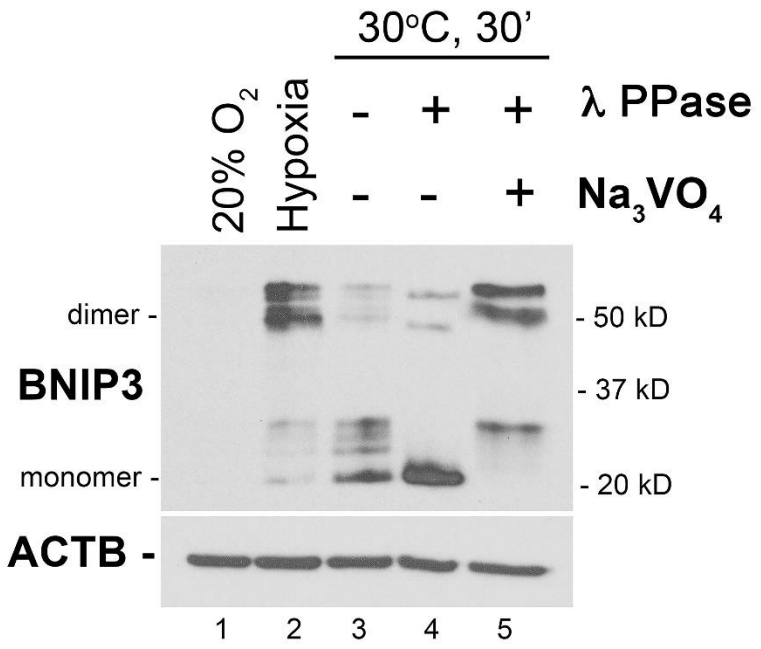

Figure 3.1: BNIP3 is a highly phosphorylated protein. U2OS cells were treated with hypoxia to induce BNIP3 expression. A lysate was harvested in the absence of phosphatase inhibitors and 75 µg of protein was either left untreated, treated with λ phosphatase (λ PPase), or a combination of λ PPase and phosphatase inhibitor (Na_3VO_4) at 30° for 30 minutes. The BNIP3 banding pattern shifted in the presence of λ PPase, but this shift was prevented by Na_3VO_4, suggesting that BNIP3 is a phosphorylated protein.

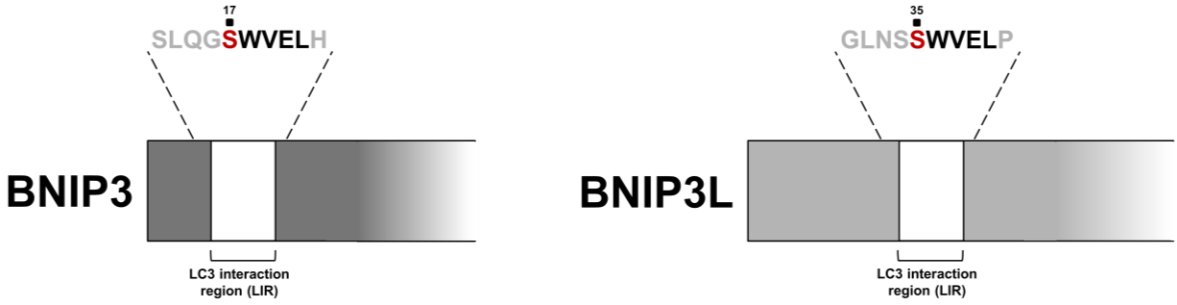

Figure 3.2: BNIP3 and BNIP3L contain serine residues adjacent to their LIR motifs. Schematic demonstrating the sequence surrounding (gray) the BNIP3 (left) and BNIP3L (right) LIR motifs (black). Each LIR motif has a serine residue at the -1 position (red), adjacent to the tryptophan residue critical for LC3 binding. These serine residues have previously been reported to be phosphorylation sites, but the kinase(s) responsible have not been identified.

threonine (T) at the phosphorylation site, leucine (L) or methionine (M) at the -3 position, and aliphatic or aromatic amino acids at positions +1 and +2.[59] When we compared the primary amino acid sequences surrounding S17 of BNIP3 and S35 of BNIP3L to the published ULK1 phosphorylation consensus sequence, we found that both BNIP3 and BNIP3L have leucine (L) at the -3 position, serine (S) at position 0, and tryptophan (W) and valine (V) at positions +1 and +2. We then aligned the putative ULK1 phosphorylation sites of BINP3 and BNIP3L with validated ULK1 substrates and observed strong sequence similarity (Table 3.1).[59,62]

To examine whether BNIP3 and/or BNIP3L are phosphorylated by ULK1, we performed *in vitro* kinase assays by incubating recombinant BNIP3 or BNIP3L protein with recombinant ULK1 and ^{32}P-γ-ATP in the presence or absence of the ULK1 inhibitor ULK-101.[100] ULK1 is known to autophosphorylate, which acts as a useful internal control for ULK1 activity in this assay. As expected, ULK1 autophosphorylation was inhibited by the addition of ULK-101. Additionally, ULK1 strongly phosphorylated BNIP3 and BNIP3L *in vitro*, and this phosphorylation was inhibited by ULK-101 (Figure 3.3A, lanes 4-5; Figure 3.3B, lanes 4-5). The mutation of S35 in BNIP3L to alanine (S35A) ablated BNIP3L phosphorylation by ULK1. The mutation of S17 in BNIP3 to alanine (S17A) decreased the phosphorylation of BNIP3 by ULK1, but did not eliminate ULK1 phosphorylation as effectively as the S35A mutation in BNIP3L, suggesting the existence of additional ULK1 phosphorylation sites in BNIP3 (Figure 3.3A, lanes 4 and 7; Figure 3.3B, lanes 4 and 7).

ULK1 substrate	Phosphorylation site	Protein sequence
BNIP3	S17	ES**L**QG**S**W**V**ELH
BNIP3L	S35	AG**L**NS**S**W**V**ELP
ATG101	S11 S203	EV**L**EV**S**V**V**EGRQ DA**L**TG**S**V**T**TTM
ATG9	S14	QR**L**EA**S**Y**S**DSP
ATG14	S29	RD**L**VD**S**V**D**DAE
BECLIN-1	S15	ST**M**QV**S**F**V**CQR
ATG4B	S316	AE**L**DP**S**I**V**GF
FUNDC1	S17	ESDDD**S**Y**V**LD
VPS34	S249	SPILT**S**F**V**LVK

Table 3.1: BNIP3 and BNIP3L sequences surrounding S17 and S35, respectively, share sequence similarity with known ULK1 substrates. The primary amino acid sequences of putative ULK1 phosphorylation sites in BNIP3 and BNIP3L were aligned to ULK1 phosphorylation sites in validated ULK1 substrates (ATG101, ATG9, ATG14, BECLIN-1, ATG4B, FUNDC1, VPS34).[59,62] The optimal ULK1 phosphorylation consensus sequence includes an affinity for serine (S) over threonine (T) at the phosphorylation site, leucine (L) or methionine (M) at the -3 position, and aliphatic or aromatic amino acids at positions +1 and +2.[59] The putative ULK1 phosphorylation sites in BNIP3 and BNIP3L share sequence similarity to known ULK1 targets as well as the ULK1 target consensus sequence.

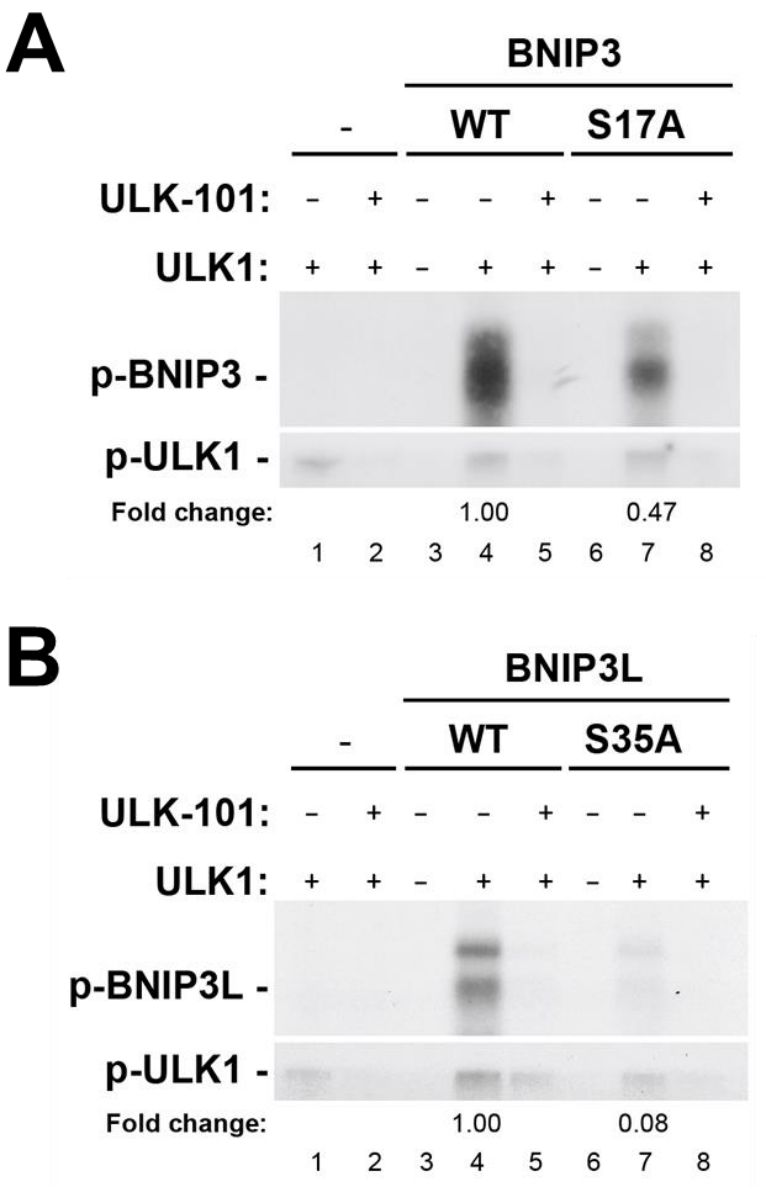

Figure 3.3: BNIP3 and BNIP3L are phosphorylated by ULK1 on S17 and S35 respectively. (A) *In vitro* kinase assay testing the ability of recombinant ULK1 kinase to phosphorylate recombinant BNIP3 (lanes 3 – 5) or BNIP3 mutated to S17A (lanes 6 -8) in the presence or absence of ULK-101 to inhibit ULK1 kinase activity (lanes 2, 5, 8) and using ULK1 autophosphorylation as a control for ULK1 activity (lower panel). (B) *In vitro* kinase assay testing the ability of recombinant ULK1 kinase to phosphorylate recombinant BNIP3L (lanes 3 – 5) or BNIP3L mutated to S35A (lanes 6 -8) in the presence or absence of ULK-101 to inhibit ULK1 kinase activity (lanes 2, 5, 8) and using ULK1 autophosphorylation as a control for ULK1 activity (lower panel). In each quantification, levels are standardized relative to 1.00 representing the phosphorylation of wild-type rBNIP3 (A) and rBNIP3L (B), respectively.

Using the published ULK1 phosphorylation consensus sequence, we scrutinized the BNIP3 primary amino acid sequence for additional phosphorylation sites and identified three possible sites at serine 24, 172, and 190 (Table 3.2). These additional sites have leucine (L) at the -3 position and serine (S) at position 0, however the consensus for aliphatic or aromatic amino acids at positions +1 and +2 is poorly maintained. Of the possible BNIP3 phosphorylation sites, only S17 is conserved in BNIP3L. Additionally, two of the sites, S172 and S190, are located in domains inaccessible from the cytosol following BNIP3 mitochondrial integration (in the TM domain and intermembrane space, respectively) which may pose a challenge to phosphorylation *in vivo*. To examine whether these sites are phosphorylated by ULK1, we performed additional *in vitro* kinase assays on recombinant BNIP3 with either individual or multiple serine residues mutated to alanine (Figure 3.4). Mutation of the additional serine residues in combination with S17A had no effect on the ULK1 phosphorylation of BNIP3 when compared to S17A alone, suggesting that these sites are not ULK1 phosphorylation targets. Due to the *in vitro* nature of this assay, it is possible that ULK1 may be phosphorylating sites on BNIP3 with less specificity than in a physiological setting, resulting in a nonspecific phosphorylation signal following the S17A mutation. Therefore, we opted to proceed with studying S17 alone.

Phosphorylation site	Protein sequence
S17	ES**L**QG**SWV**ELH
S24	VE**L**HF**S**NNGNG
S172	PS**L**LL**SH**LLAI
S190	RR**L**TT**ST**STF

Table 3.2: The ULK1 target consensus motif is poorly maintained in additional possible BNIP3 phosphorylation sites. The primary amino acid sequences of additional possible ULK1 phosphorylation sites in BNIP3 were aligned to the putative ULK1 phosphorylation site at S17 of BNIP3. The leucine is present at the -3 position of all sites, but the aliphatic or aromatic amino acids at positions +1 and +2 are poorly maintained

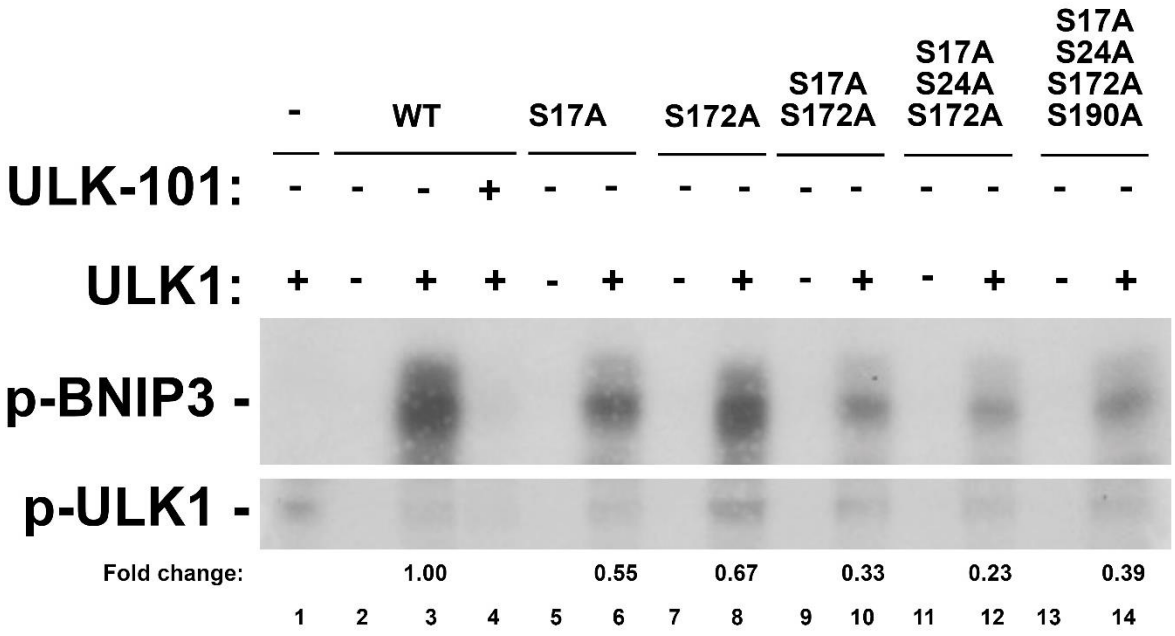

Figure 3.4: ULK1 does not phosphorylate additional sites in BNIP3 in vitro. *In vitro* kinase assay testing the ability of recombinant ULK1 kinase to phosphorylate different mutant forms of BNIP3. Quantification levels are standardized relative to 1.00 representing the phosphorylation of wild-type rBNIP3.

ULK1 mediated phosphorylation of BNIP3 on S17 promotes its interaction with LC3B and mitophagy

Having identified S17 of BNIP3 as an ULK1 phosphorylation site, we next examined how phosphorylation of S17 affected BNIP3-dependent mitophagy. Serine 17 was mutated to alanine (S17A) to produce a phospho-null mutant, or glutamic acid (S17E) to mimic phosphorylation. We first examined the interaction of each mutant with LC3B by transiently overexpressing HA-BNIP3 constructs in HEK-293T cells genetically deleted for BNIP3 ($293T^{\Delta BNIP3}$) that were engineered to stably overexpress GFP-LC3 (293T-ΔB + GFP-LC3). The S17A mutation diminished the interaction of BNIP3 with GFP-LC3 to a similar extent as mutation of the critical W18 residue in the BNIP3 LIR motif to alanine (W18A), indicating that inhibiting phosphorylation of BNIP3 on S17 was sufficient to block its interaction with LC3B (Figure 3.5). Mutation to S17E resulted in apparently lower binding of HA-BNIP3 to GFP-LC3 than wild-type. However, blocking autophagic turnover with 100 nM bafilomycin A_1 in S17E-expressing cells resulted in a greater increase in the binding of HA-$BNIP3^{S17E}$ to GFP-LC3 (6.68-fold increase in dimer) when compared to the effect of bafilomycin A_1 on HA-$BNIP3^{WT}$ (1.97-fold increase in dimer). This result suggests that the S17E mutation promotes mitophagic flux to a greater extent than wild-type.

We next sought to assess the effects of FLAG-ULK1 on the interaction of HA-BNIP3 and GFP-LC3. Interestingly, we found that overexpressing FLAG-ULK1 resulted in an increase in overall protein levels of all forms of BNIP3 examined, suggesting that ULK1 modulated BNIP3 protein levels (Figure 3.6, lanes 2-5 compared to lanes 6-9). FLAG-ULK1 overexpression increased the interaction of HA-$BNIP3^{WT}$ and

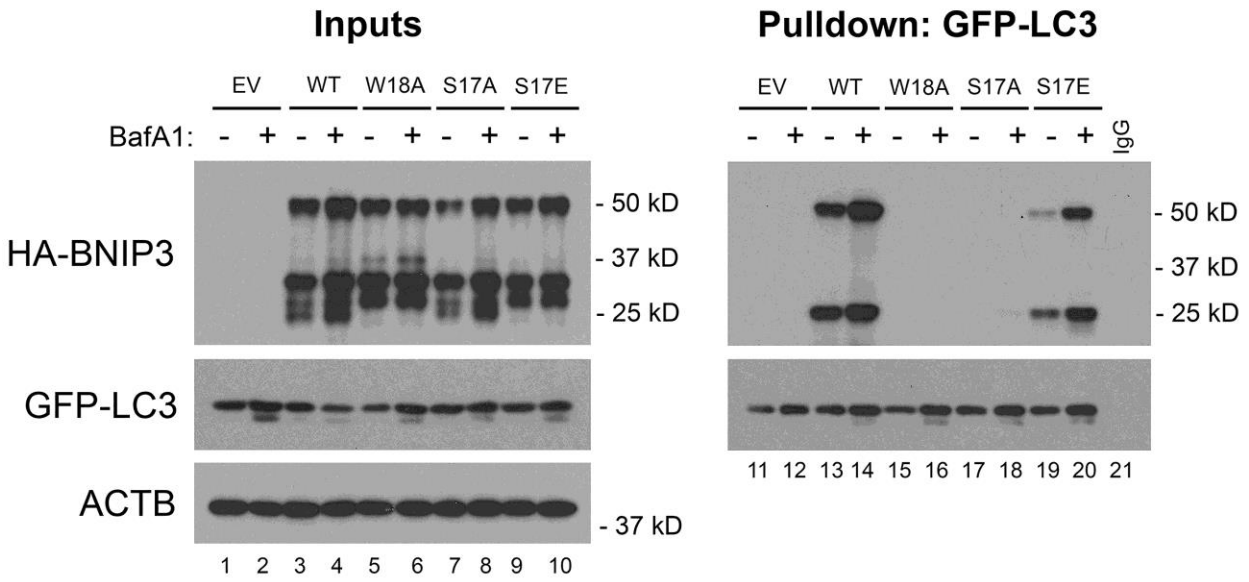

Figure 3.5: Mutation of S17 in BNIP3 modulates its LC3 interaction. Pulldown of GFP-LC3 stably expressed in 293T cells with transiently expressed HA-BNIP3 (WT) and different HA-BNIP3 mutants (W18A, S17A, S17E) or empty vector (EV) control, in the presence or absence of 100 nM bafilomycin A1. Inputs to the pulldown are shown on the left and the result of the pulldown on the right. HA-BNIP3^{S17E} dimer pulldown with GFP-LC3 increased by 6.68-fold with bafilomycin A1 while HA-BNIP3^{WT} dimer pulldown increased by 1.97-fold, suggestive of increased mitophagic flux with S17 phosphorylation.

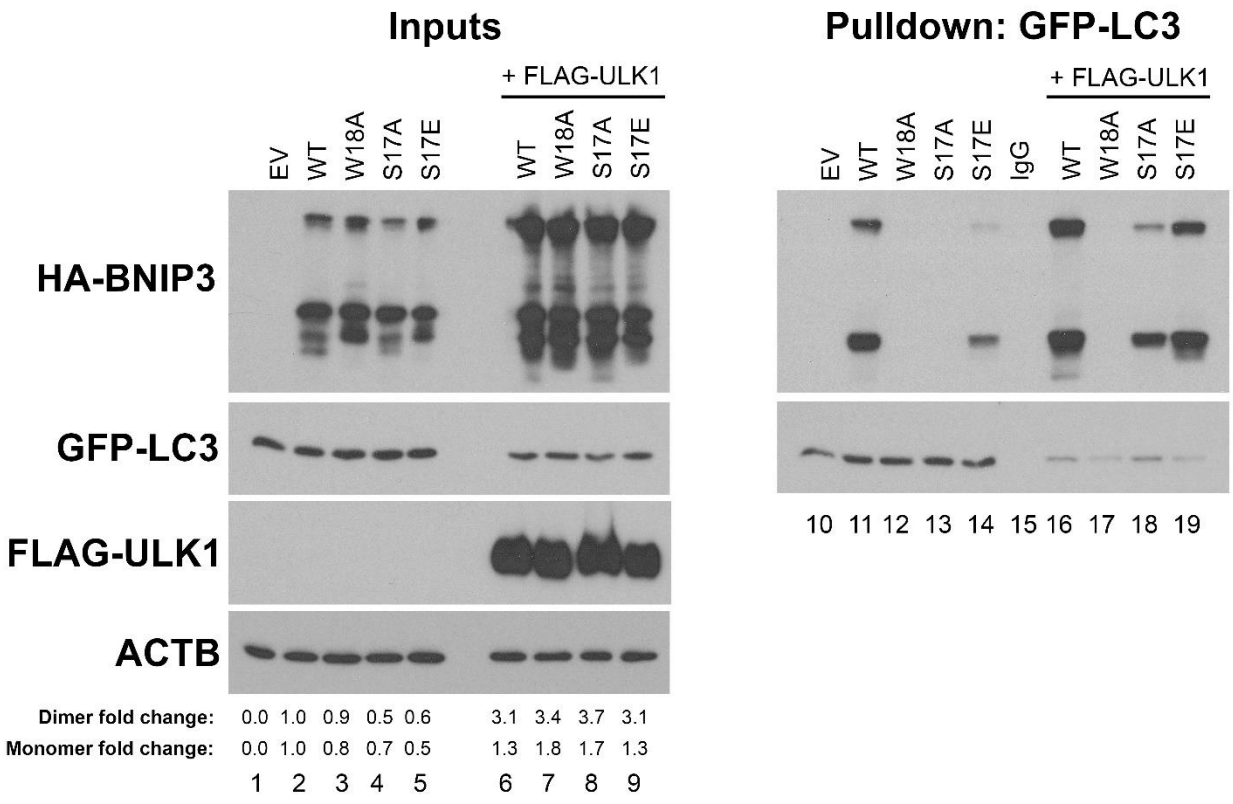

Figure 3.6: FLAG-ULK1 overexpression increases HA-BNIP3 protein levels. Pulldown of GFP-LC3 stably expressed in 293T cells with transiently expressed HA-BNIP3 (WT) and different HA-BNIP3 mutants (W18A, S17A, S17E) or empty vector (EV) control, in the presence (lanes 6-9, 16-19) or absence (lanes 1-5, 10-15) of exogenous FLAG-ULK1. Inputs to the pulldown are shown on the left and the result of the pulldown on the right. Quantification levels are standardized relative to 1.0 representing the HA-BNIP3^{WT}-expressing condition in the absence of FLAG-ULK1.

HA-BNIP3^{S17E} with GFP-LC3, however these increased interactions were proportionate to the relative increases in the input BNIP3 protein levels. The interaction of HA-BNIP3^{S17A} with GFP-LC3 was also modestly enhanced by FLAG-ULK1 overexpression, again possibly due to the increase in protein levels, while HA-BNIP3W18A still failed to interact with GFP-LC3. These results suggest that the S17A mutation weakens but does not abolish the interaction of HA-BNIP3 with GFP-LC3. The effect of ULK1 on BNIP3 protein stability will be assessed in depth later in the following chapter.

In order to further assess the effects of S17 phosphorylation status on BNIP3-induced mitophagy, we transiently expressed HA-BNIP3 mutant constructs in U2OS cells genetically deleted for BNIP3 (U2OS$^{\Delta BNIP3}$). The interactions of HA-BNIP3 with endogenously expressed proteins were then visually assessed using immunofluorescence imaging. Because the expression of HA-BNIP3 was transient and not all cells expressed the vector, the non-expressing/BNIP3-null cells acted as a useful BNIP3-null control within each image. Imaging of LC3B and TOMM20 in these cells showed that HA-BNIP3^{WT}, HA-BNIP3^{S17A}, and HA-BNIP3^{S17E} expression increased the overlap between TOMM20 and LC3B, while the HA-BNIP3^{W18A} mutant, which is deficient for LC3B binding, did not (Figure 3.7). Interestingly, the HA-BNIP3^{S17A} mutant, which dramatically reduced binding to GFP-LC3 in 293T-ΔBNIP3 cells, was able to promote overlap of LC3-TOMM20 staining. However, HA-BNIP3^{S17A} did not decrease mitochondrial staining as effectively as wild-type, suggesting decreased mitophagic efficacy (Figure 3.7, bottom left). In contrast, the HA-BNIP3^{S17E} mutant strikingly reduced mitochondrial staining in cells, consistent with a more effective clearance of mitochondria by mitophagy (Figure 3.7, bottom right).

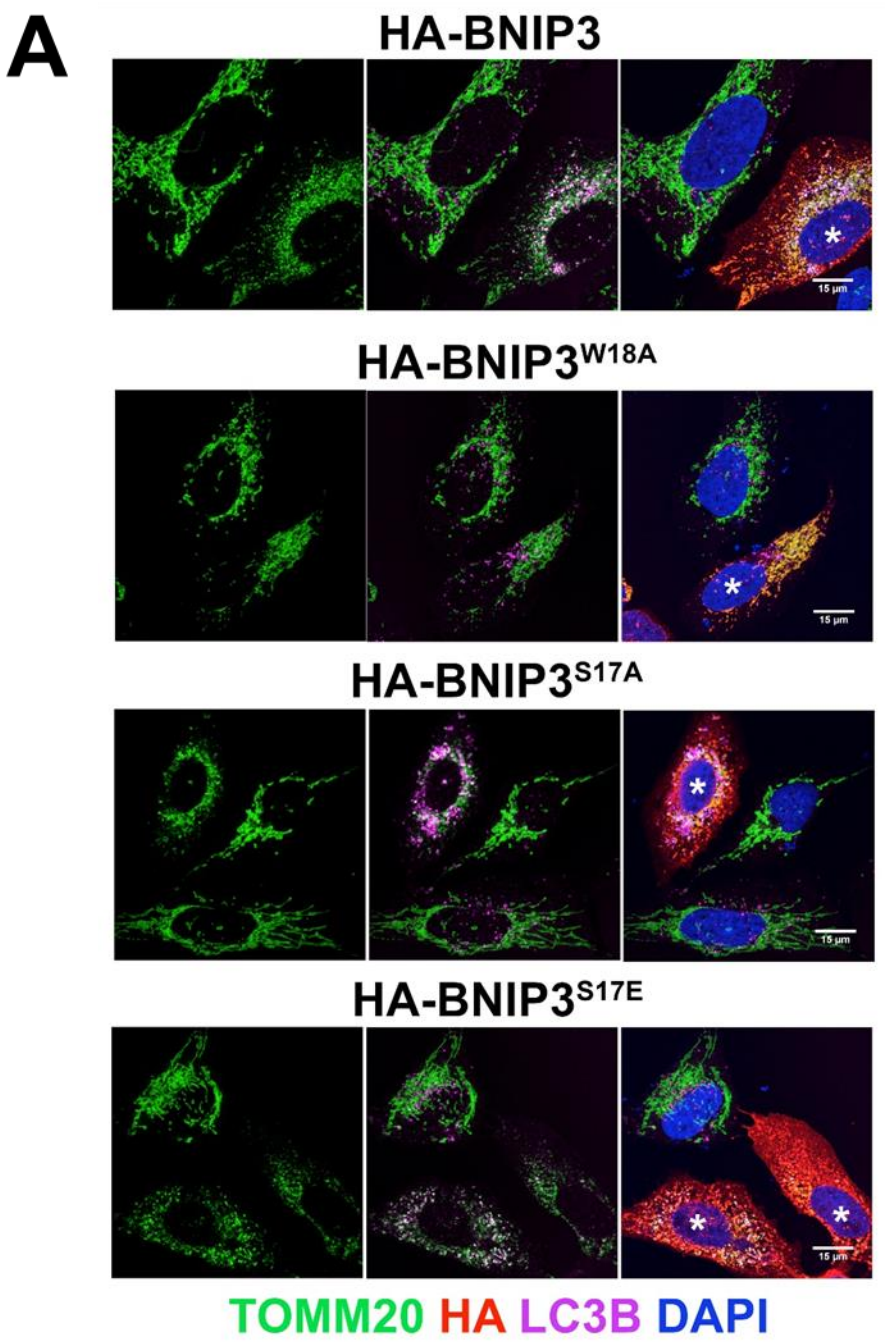

Figure 3.7: Mutation of S17 in BNIP3 modulates colocalization of LC3 and TOMM20. (A) Immunofluorescent staining for TOMM20 (green, mitochondria), LC3B (magenta, autophagosomes), HA-BNIP3 (red) and DAPI (blue) in U2OS$^{\Delta BNIP3}$ cells transiently expressing HA-BNIP3, HA-BNIP3^{W18A}, HA-BNIP3^{S17A}, or HA-BNIP3^{S17E}. Cells expressing exogenous HA-BNIP3 are asterisked (*) and LC3B/TOMM20 overlap is detected as white puncta (green and magenta overlap). (Done in collaboration with Althea Bock-Hughes)

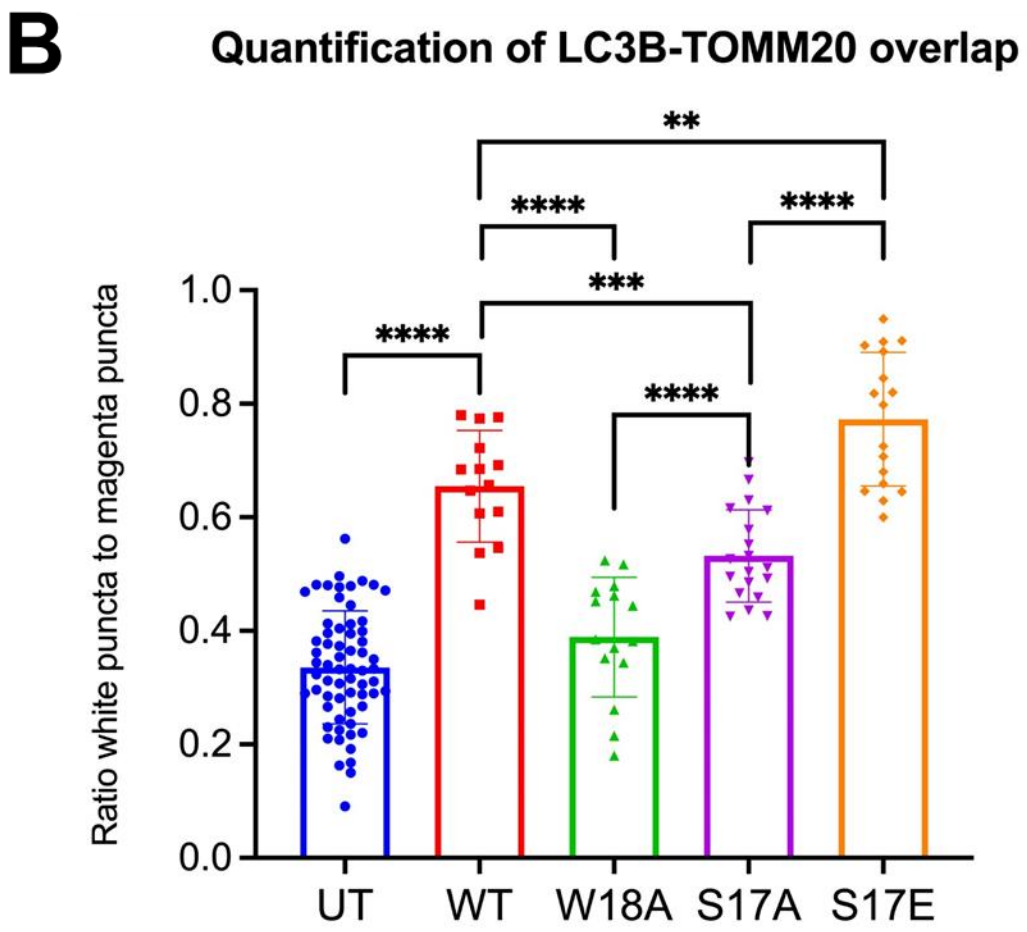

Figure 3.7: Mutation of S17 in BNIP3 modulates colocalization of LC3 and TOMM20 (continued). (B) Quantification of LC3B/TOMM20 overlap for each of the different forms of BNIP3 compared to cells not expressing BNIP3. *p<0.05, **p<0.01, ***p<0.001, ***p<0.0001.

To corroborate these findings, we then co-stained for TOMM20 and LAMP1, a lysosomal marker, in order to examine mitochondrial turnover at the lysosome. Consistent with the previous result, HA-BNIP3^{S17A} displayed a diminished ability to promote LAMP1 and TOMM20 overlap as compared to wild-type, suggesting a defect in the targeting of mitochondria to the lysosome (Figure 3.8, bottom left). However, HA-BNIP3^{S17A} remained more effective than the mitophagy-null mutant HA-BNIP3^{W18A} (Figure 3.8, top right). Once again, HA-BNIP3^{S17E} expression resulted in a dramatic decrease in TOMM20 staining, having essentially removed most of the cellular mitochondrial mass via mitophagy (Figure 3.8, bottom right).

To assess the inconsistencies between the protein-protein interaction studies in 293T$^{\Delta BNIP3}$ cells and the immunofluorescence colocalization studies in U2OS$^{\Delta BNIP3}$ cells, we then performed pulldowns in U2OS$^{\Delta BNIP3}$ cells co-expressing GFP-LC3 and HA-BNIP3 mutants. We hypothesized that the interaction of GFP-LC3 and HA-BNIP3 in U2OS$^{\Delta BNIP3}$ cells would be consistent with the observed outcomes of the immunofluorescence data as opposed to the previous pulldown data, possibly due differences in the physiology of 293T cells. 293T cells are commonly used for exogenous overexpression of proteins due easy transfectability and high rates of expression, however these cells are typically not used for functional studies.[214] Indeed, the results of the GFP-LC3 pulldown in U2OS$^{\Delta BNIP3}$ cells were consistent with the immunofluorescence data (Figure 3.9). HA-BNIP3^{S17A} exhibited similar rates of GFP-LC3 binding to wild-type in both the presence and absence of bafilomycin A_1, consistent with the immunofluorescence data in which we observed similar degrees of LC3B and TOMM20 overlap. Interestingly, both HA-BNIP3^{WT} and HA-BNIP3^{S17E} displayed similar

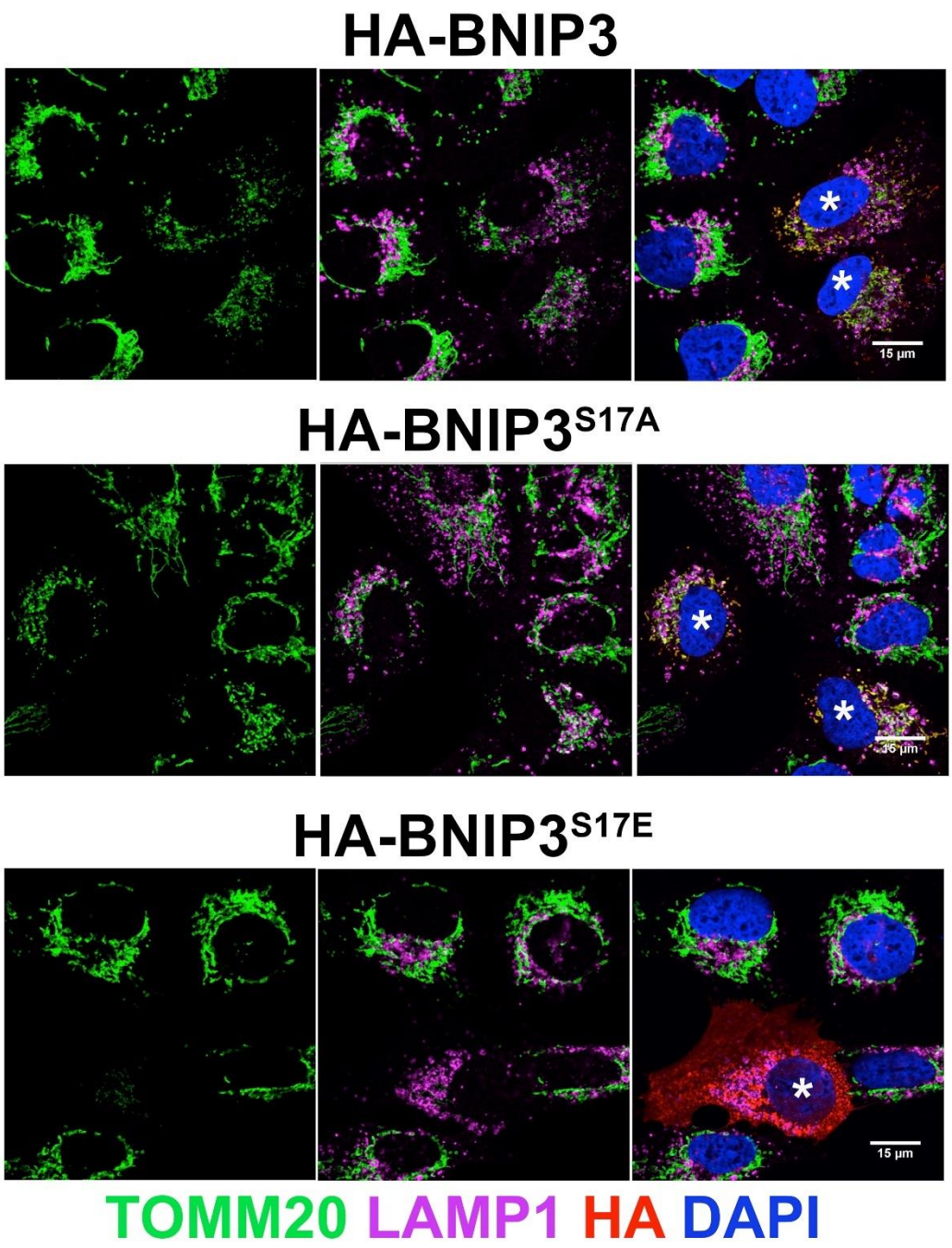

Figure 3.8: Mutation of S17 in BNIP3 modulates colocalization of LAMP1 and TOMM20. Immunofluorescent staining for TOMM20 (green, mitochondria), LAMP1 (magenta, lysosomes), HA-BNIP3 (red) and DAPI (blue) in U2OS$^{\Delta BNIP3}$ cells transiently expressing HA-BNIP3, HA-BNIP3^{S17A}, or HA-BNIP3^{S17E}. Cells expressing exogenous HA-BNIP3 are asterisked (*) and LAMP1/TOMM20 overlap is detected as white puncta (green and magenta overlap). (Done in collaboration with Althea Bock-Hughes)

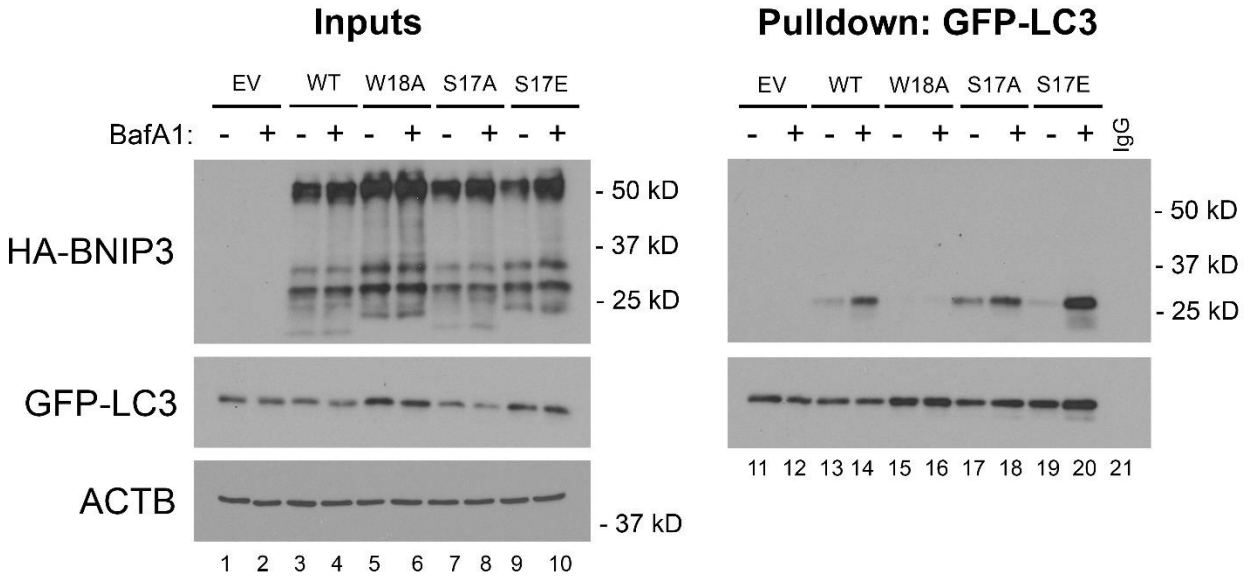

Figure 3.9: Mutation of S17 in BNIP3 modulates its LC3 interaction in U2OS cells consistent with immunofluorescence data. Pulldown of GFP-LC3 transiently expressed in U2OS$^{\Delta BNIP3}$ cells with stably expressed HA-BNIP3 (WT) and different HA-BNIP3 mutants (W18A, S17A, S17E) or empty vector (EV) control, in the presence or absence of 100 nM bafilomycin A1. Inputs to the pulldown are shown on the left and the result of the pulldown on the right.

levels of interaction with GFP-LC3 in the absence of bafilomycin A_1, however blocking autophagic flux resulted in a dramatic increase in the interaction of GFP-LC3 and HA-BNIP3^{S17E} as compared to wild-type (Figure 3.9, lanes 4 and 10). This effect on the interaction is consistent with the striking removal of mitochondrial mass by HA-BNIP3^{S17E} in the immunofluorescence data, and is suggestive of enhanced mitochondrial flux. Together, these findings indicate that the S17E mutation that mimics ULK1 phosphorylation markedly increases mitophagy while the S17A mutation that blocks ULK1 phosphorylation decreases mitophagy relative to wild-type BNIP3.

Mitochondrial turnover as a result of S17 phosphorylation suppresses oxygen consumption and cellular proliferation

Given the effect of S17 mutation on apparent rates of mitophagy and changes in mitochondrial mass, we next examined its effect on mitochondrial respiration. Oxygen consumption rates were measured in U2OS$^{\Delta BNIP3}$ cells stably expressing HA-BNIP3 constructs. HA-BNIP3^{WT}-expressing U2OS$^{\Delta BNIP3}$ cells displayed repressed oxygen consumption compared to cells expressing empty vector (EV), consistent with a reduction in mitochondrial mass due to BNIP3-dependent mitophagy (Figure 3.10, red versus black). The S17A mutant was modestly less effective than wild-type at decreasing oxygen consumption, although the differences in basal oxygen consumption rates were withing the margin of error (Figure 3.10, red versus blue). Strikingly, expression of HA-BNIP3^{S17E} resulted in a marked reduction in both basal and maximal oxygen consumption rates, consistent with the dramatic reduction in mitochondrial mass we observed in our immunofluorescence studies (Figure 3.10, green; Figure 3.7).

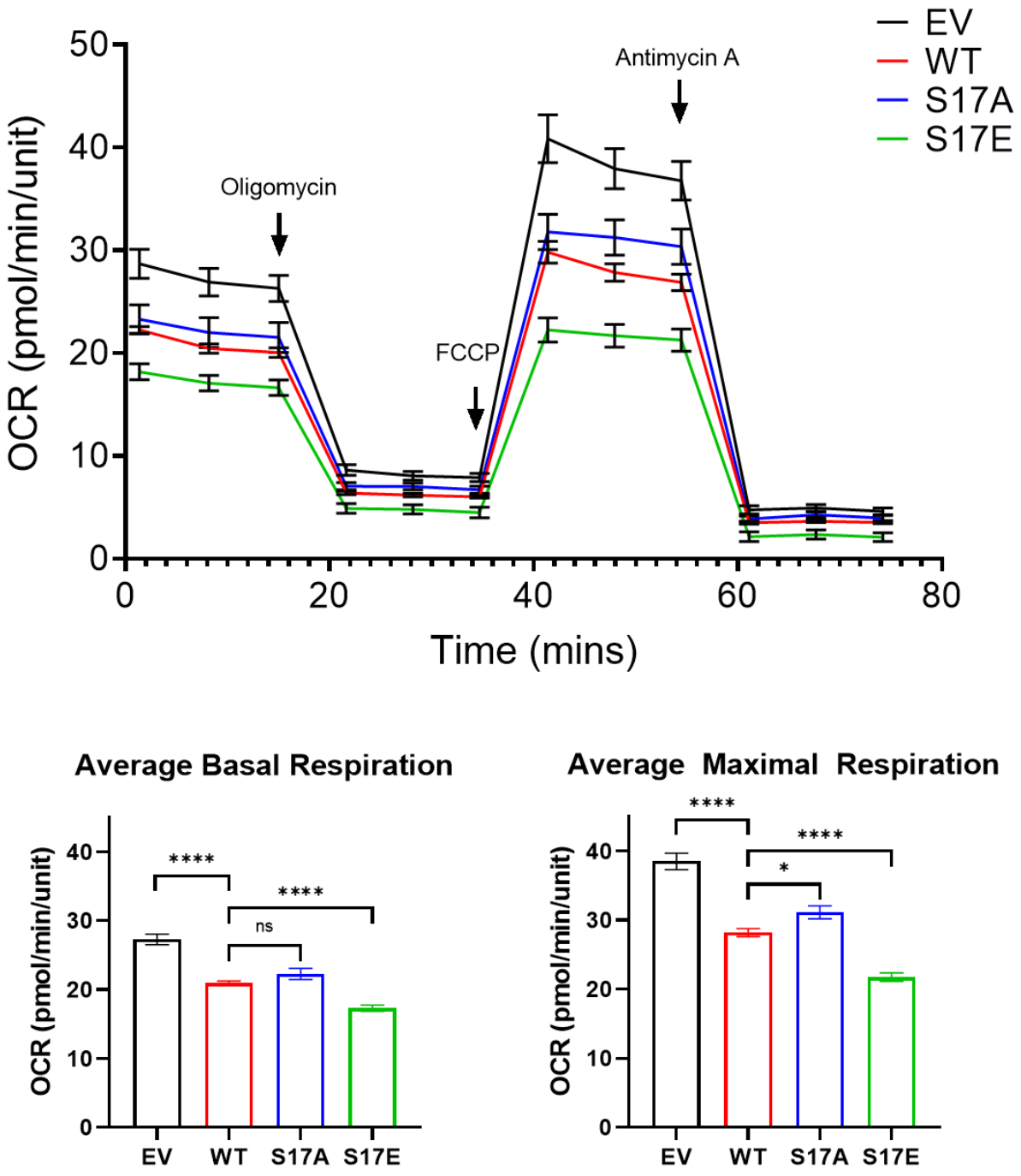

Figure 3.10: Phosphorylation of S17 decreases oxygen consumption. Oxygen consumption rate (OCR) of U2OS$^{\Delta BNIP3}$ cells stably expressing HA-BNIP3, HA-BNIP3^{S17A} or HA-BNIP3^{S17E} compared to empty vector control (EV). *p<0.05, **p<0.01, ***p<0.001, ***p<0.0001.

Finally, given the effect of S17 mutation on oxygen consumption rates, we next investigated how S17 mutation affects cellular proliferation. Previous work from our laboratory has established a growth suppressive function for BNIP3, due in part to decreased mitochondrial mass resulting from BNIP3-dependent mitophagy.[131] Therefore, due to the effect of S17 mutation, particularly S17E, on mitochondrial mass, we expected to observe an effect on cellular proliferation. To assess this effect, we generated U2OS$^{\Delta BNIP3}$ cells stably co-expressing a nuclear GFP marker (NucLight-GFP) and HA-BNIP3 constructs. Consistent with previous observations, overexpression of HA-BNIP3^{WT} decreased cellular proliferation as compared to empty vector (Figure 3.11, red line). Similarly, expression of HA-BNIP3^{S17A} resulted in a decrease in cellular proliferation indistinguishable from that of wild-type (Figure 3.11, blue line). Finally, in line with the immunofluorescence and oxygen consumption rate data, expression of HA-BNIP3^{S17E} led to a dramatic slowdown in the growth of U2OS$^{\Delta BNIP3}$ cells (Figure 3.11, green line). Taken together, these results indicate that the phosphorylation of S17 on BNIP3 by ULK1 promotes the interaction of BNIP3 with LC3, increases mitophagy, lowers rates of cellular respiration, and decreases cellular proliferation.

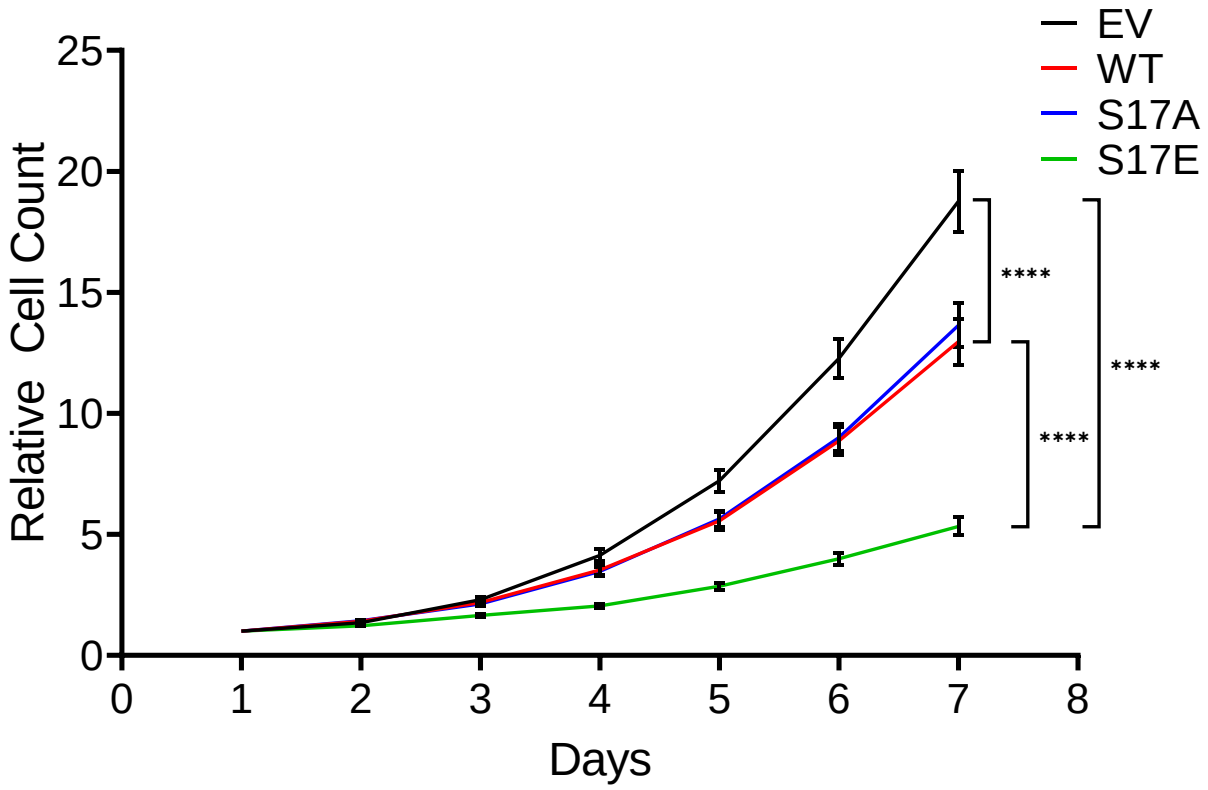

Figure 3.11: Phosphorylation of S17 decreases cellular proliferation. Cellular proliferation rate of U2OS$^{\Delta BNIP3}$ cells stably expressing HA-BNIP3, HA-BNIP3^{S17A} or HA-BNIP3^{S17E} compared to empty vector control (EV). Comparison of HA-BNIP3 to HA-BNIP3^{S17A} was not significant. *p<0.05, **p<0.01, ***p<0.001, ***p<0.0001.

Conclusions

In this chapter, we identified a novel role for ULK1 in regulating BNIP3-induced mitophagy through phosphorylation of S17, adjacent to its LIR motif. In addition to BNIP3, we also identified BNIP3L as an ULK1 target that is phosphorylated adjacent to its LIR motif at S35. Both S17 of BNIP3 and S35 of BNIP3L closely matched the established ULK1 consensus motif, and mutation of these sites decreased phosphorylation by ULK1 in *in vitro* kinase assays.[59] Mutation of S17 did not fully ablate the *in vitro* phosphorylation of BNIP3 by ULK1, suggesting the possibility of additional sites. However, further analysis of the BNIP3 sequence yielded only poor patches to the ULK1 consensus motif, and mutation of these sites did not affect *in vitro* phosphorylation. Therefore, it is likely that the remaining phosphorylation signal is due to nonspecific phosphorylation as a result of the highly concentrated conditions of the assay.

We next sought to determine the effects of S17 phosphorylation on the interaction of BNIP3 and LC3. Phospho-null mutation of S17 to alanine (S17A) greatly decreased the interaction of HA-BNIP3 to GFP-LC3 in a 293T exogenous protein expression system. Phosphomimetic mutation of S17 to glutamic acid (S17E) slightly decreased the interaction of HA-BNIP3 with GFP-LC3 as compared to wild-type. However, treatment with the inhibitor bafilomycin A_1, which inhibits turnover of autophagosomes at the lysosome, yielded a greater change in S17E pulldown than that of wild-type, suggesting that S17E results in enhanced autophagic flux.

In order to gain a greater understanding of the effects of S17 status on mitophagy, we next assessed the colocalization of mitochondria with GFP-LC3 in the

presence of HA-BNIP3 mutants in an osteosarcoma cell line. Interestingly, in this system S17A mutation resulted in mitochondrial and GFP-LC3 localization that was less than that of wild-type but greater than the LC3-binding-null W18A mutant, in contrast with the previous pulldown results. Additionally, S17E mutation strikingly reduced mitochondrial staining in cells relative to wild-type, consistent with a more effective clearance of mitochondria by mitophagy. To address the discrepancy between the pulldown and immunofluorescence data, we next assessed the interaction of HA-BNIP3 and GFP-LC3 in the osteosarcoma cell line. Interestingly, these results were consistent with the immunofluorescent data, suggesting that 293T cells, which are infrequently used for assessment of cell physiology, may yield slightly different results, possibly due to physiological defects in mitophagy.

Given the effect on rates of mitophagy, we next sought to assess the effect of S17 phosphorylation on oxygen consumption rates and cellular proliferation. Consistent with the pulldown and immunofluorescence data, S17A oxygen consumption rates and cellular proliferation were similar to that of wild-type. Expression of S17E, however, resulted in dramatically reduced oxygen consumption rates and cellular proliferation. These results are consistent with S17E decreasing mitochondrial mass due to increased rates of mitophagy.

Taken together, the above results indicate that mimicking ULK1 phosphorylation at S17 markedly increases mitophagy while blocking S17 phosphorylation decreases mitophagy relative to wild-type (Figure 3.12). Interestingly, these results are consistent with those reported for the ULK1 phosphorylation of FUNDC1, suggesting a broader role for ULK1 in the specific upregulation of mitophagy as opposed to general

autophagy. This regulation of several mitophagy cargo receptors by ULK1 may emphasize the critical nature of mitophagy, specifically, in response to cellular stressors such as hypoxia. How intracellular conditions, such as hypoxia, trigger the specific upregulation of mitophagy by ULK1 should be the focus of future studies.

Finally, we aimed to determine how FLAG-ULK1 overexpression affected the interaction of HA-BNIP3 with GFP-LC3, expecting to find enhanced interaction of wild-type HA-BNIP3 with GFP-LC3 in the presence of FLAG-ULK1. This result was unexpectedly obfuscated by an observation that FLAG-ULK1 overexpression dramatically increased HA-BNIP3 protein levels, irrespective of S17 status, suggesting a distinct, mitophagy-independent mechanism of BNIP3 stabilization by ULK1. In the next chapter, we focus on uncovering the mechanism of this mitophagy-independent regulation of BNIP3 stability by ULK1.

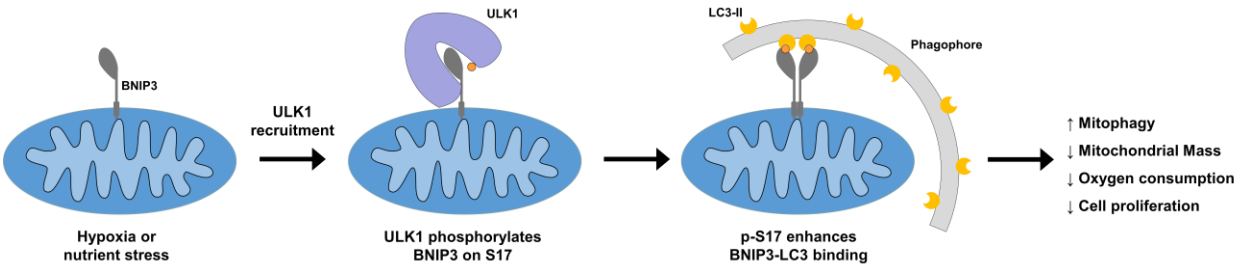

Figure 3.12: Model of the phosphorylation of S17 in BNIP3 by ULK1. BNIP3 integrates into the OMM in response to hypoxia and nutrient stress. Following ULK1 recruitment to the mitochondria, phosphorylation of S17 by ULK1 promotes mitophagy, thereby decreasing mitochondrial mass, oxygen consumption, and cellular proliferation.

CHAPTER 4

ULK1 PROMOTES THE STABILIZATION OF BNIP3 BY INHIBITING ITS PROTEASOMAL TURNOVER

Introduction

In the previous chapter, we described our novel finding that ULK1 regulates the interaction of BNIP3 with LC3 via phosphorylation of S17 of BNIP3. This phosphorylation event was shown to result in increased mitochondrial turnover by BNIP3-induced mitophagy, as well as decreased rates of oxygen consumption and cellular proliferation, likely due to decreased mitochondrial mass. Interestingly, we also noted that overexpression of FLAG-ULK1 resulted in increased levels of HA-BNIP3 protein, possibly due to an effect of FLAG-ULK1 on HA-BNIP3 protein stabilization. Our work with phospho-null and phosphomimetic mutants of S17 showed no indication of an effect on protein stability outside of changes in rates of mitophagy, and protein levels of S17-mutant constructs of HA-BNIP3 were equally affected by FLAG-ULK1 overexpression, suggesting a mitophagy- and S17-independent mechanism.

Previous studies have demonstrated that BNIP3 acts as a stress response protein through increased rates of transcription in response to cellular stressors including hypoxia.[101] However, many stress response proteins are regulated both transcriptionally and post-translationally in response to cellular stressors.[169] Little is known about the post-translational modification or stabilization of existing BNIP3 protein in response to hypoxia and other stressors.

In this chapter, we examined the mechanism through which the presence of active ULK1 affects BNIP3 protein levels. We investigated the effects of ULK1 protein

inhibition by ULK-101 on endogenous BNIP3 protein levels, and how this inhibition effects levels of BNIP3 protein in response to hypoxic stress. We also further explored the effect of FLAG-ULK1 overexpression on HA-BNIP3 protein levels. We assessed a series of HA-BNIP3 point and domain deletion mutants for resistance to FLAG-ULK1-induced BNIP3 protein stabilization and found that deletion of the “BH3” domain resulted in increased protein stability in the absence of FLAG-ULK1 and resistance to FLAG-ULK1-induced protein stabilization. We also identified the ULK1 domain responsible for interaction with BNIP3 and determined that deletion of this domain ablates the stabilization effect on HA-BNIP3 protein. Finally, we sought to identify the domain or domains of BNIP3 responsible for interaction with ULK1.

ULK1 promotes BNIP3 and BNIP3L protein stability by preventing their proteasomal degradation

Our studies thus far have indicated a role for ULK1 in phosphorylating BNIP3 and BNIP3L. In the case of BNIP3, exogenous expression of a phosphomimetic mutant resulted in an increased interaction with LC3 as compared to wild-type, leading to enhanced mitochondrial clearance via mitophagy. Given these results, we next sought to determine the effect of ULK1 inhibition on endogenous BNIP3 and BNIP3L. It is well established that BNIP3 and BNIP3L are induced by hypoxia and localize to mitochondria to promote hypoxia-induced mitophagy.[101] ULK1 was also reported to be induced and recruited to mitochondria by hypoxia, therefore we speculated that ULK1 may be modulating the mitophagy functions of BNIP3 and BNIP3L during hypoxia.[92] Following 8 hours at 1% oxygen, BNIP3 and BNIP3L protein levels were maximally induced in both parental U2OS and Saos2 cells, and these levels were sustained

through 16 hours (Figure 4.1, Figure 4.2). Surprisingly, ULK1 protein levels were not significantly affected by hypoxia as observed by western or immunofluorescence, nor was ULK1 activity as indicated by no change in phospho-S555 ULK1 or ULK1-medaited phospho-S29 ATG14 levels (Figure 4.1, Figure 4.2, Figure 4.3). These results suggest that ULK1 is constitutively active in these osteosarcoma cell lines. When we inhibited ULK1 using ULK-101 following 16 hours of growth in hypoxia, we observed decreased phosphorylation of S555 of ULK1 and S29 of ATG14 despite no change in ULK1 or ATG14 levels, consistent with ULK-101 effectively inhibiting ULK1 kinase activity. Interestingly, after 16 hours of growth in hypoxia, ULK-101 treatment markedly decreased levels of both BNIP3 and BNIP3L protein, suggesting increased rates of BNIP3 and BNIP3L turnover in the absence of ULK1 activity (Figure 4.1, Figure 4.2). This decrease in hypoxia-induced BNIP3 levels following ULK-101 treatment was further confirmed via immunofluorescence in U2OS cells (Figure 4.4). In order to determine the cellular mechanism through which this turnover occurs, we added MG132 or bafilomycin A_1, to inhibit the proteasome or block autophagic turnover, respectively. Surprisingly, treatment with MG132 appeared to inhibit the effect of ULK-101 on BNIP3 and BNIP3L protein levels, while bafilomycin A_1 had no effect. This result suggested that ULK-101 promotes BNIP3 and BNIP3L turnover at the proteasome, which further implies that ULK1 limits the proteasomal degradation of BNIP3 and BNIP3L.

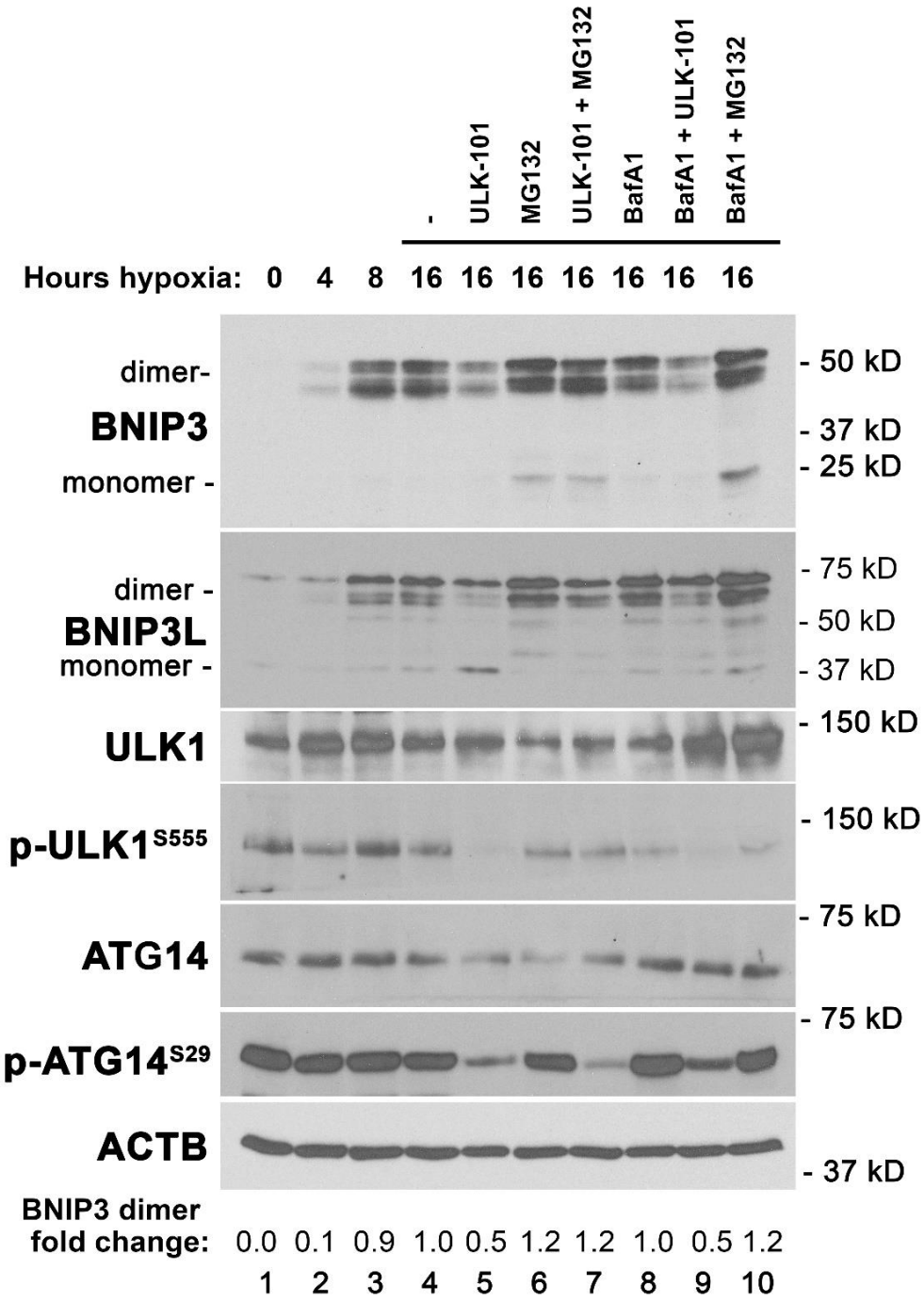

Figure 4.1: ULK1 inhibition limits BNIP3 accumulation under hypoxia in U2OS cells. Western blot for BNIP3, BNIP3L, ULK1, pS555-ULK1, ATG14, pS29-ATG14 and β-actin on. Whole cell lysates from U2OS cells exposed to hypoxia for 0, 4, 8 or 16 hours (lanes 1- 4) or for 16 hours in the presence of vehicle control and/or ULK-101, MG132 or bafilomycin A1 (lanes 6 – 10). Quantification levels are standardized relative to 1.0 representing the 16-hour hypoxia timepoint.

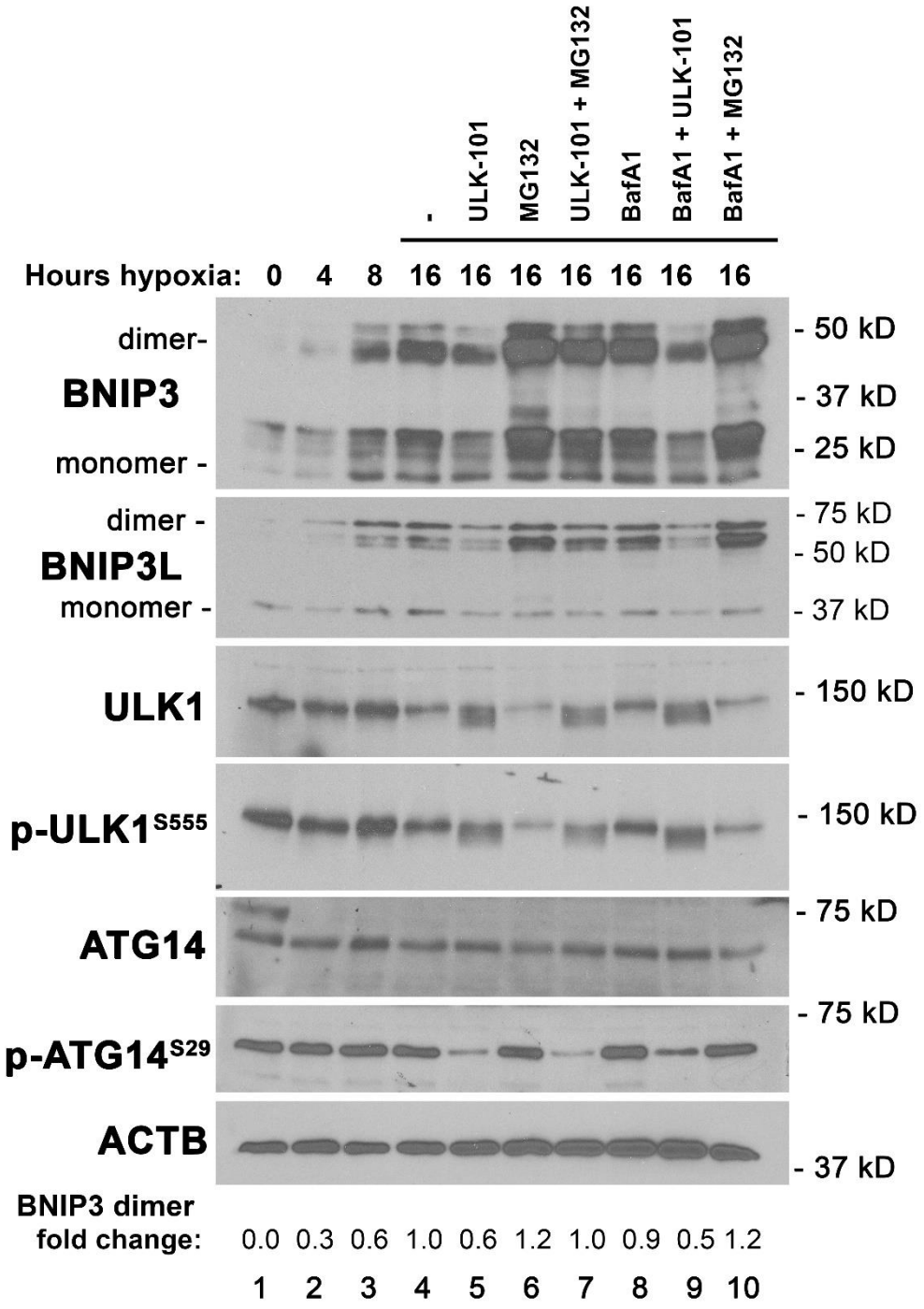

Figure 4.2: ULK1 inhibition limits BNIP3 accumulation under hypoxia in Saos2 cells. Western blot for BNIP3, BNIP3L, ULK1, pS555-ULK1, ATG14, pS29-ATG14 and β-actin on. Whole cell lysates from Saos2 cells exposed to hypoxia for 0, 4, 8 or 16 hours (lanes 1- 4) or for 16 hours in the presence of vehicle control and/or ULK-101, MG132 or bafilomycin A1 (lanes 6 – 10). Quantification levels are standardized relative to 1.0 representing the 16-hour hypoxia timepoint.

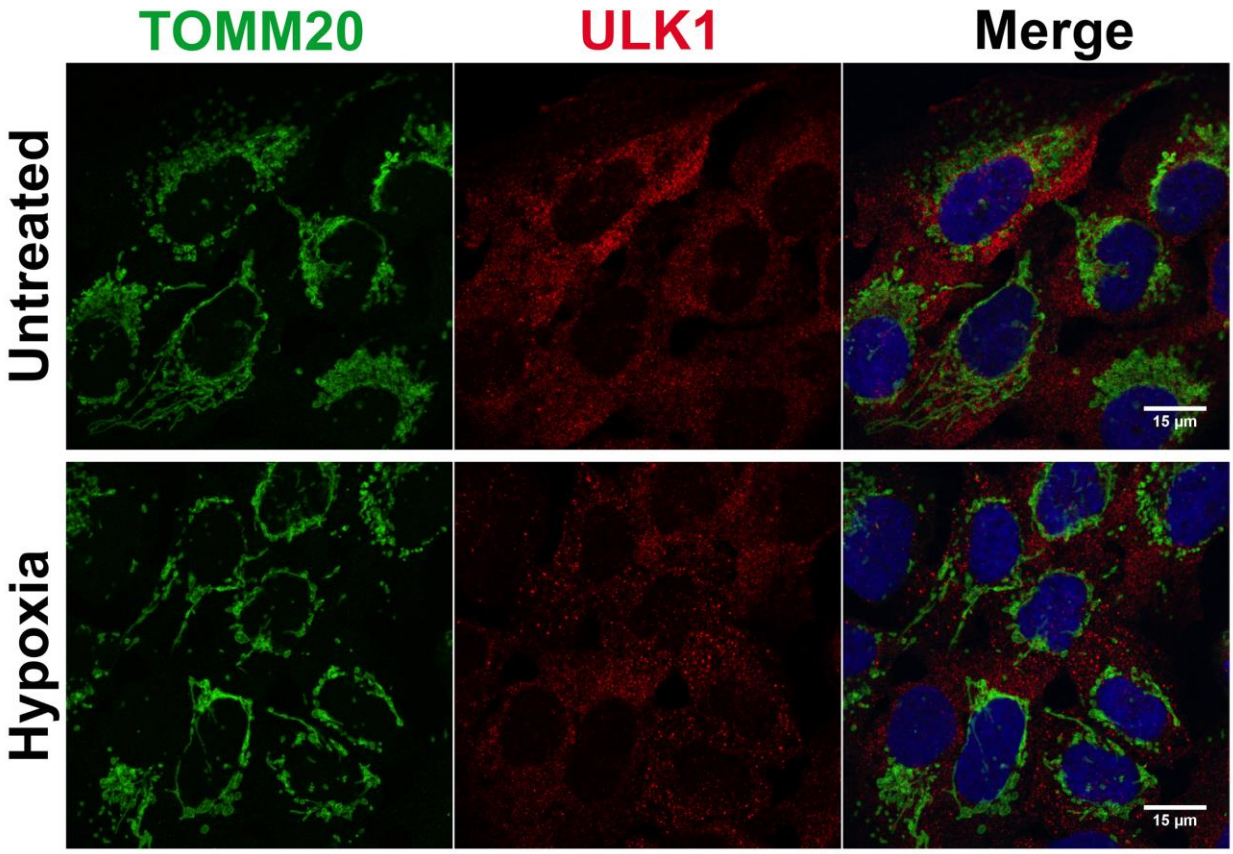

Figure 4.3: ULK1 protein levels are not significantly affected by hypoxia in U2OS cells. Immunofluorescent staining for TOMM20 (green, mitochondria), ULK1 (red, autophagosomes) and DAPI (blue) in U2OS cells at atmospheric oxygen (top panels) or 1% oxygen/hypoxia (bottom panels). (Done in collaboration with Althea Bock-Hughes)

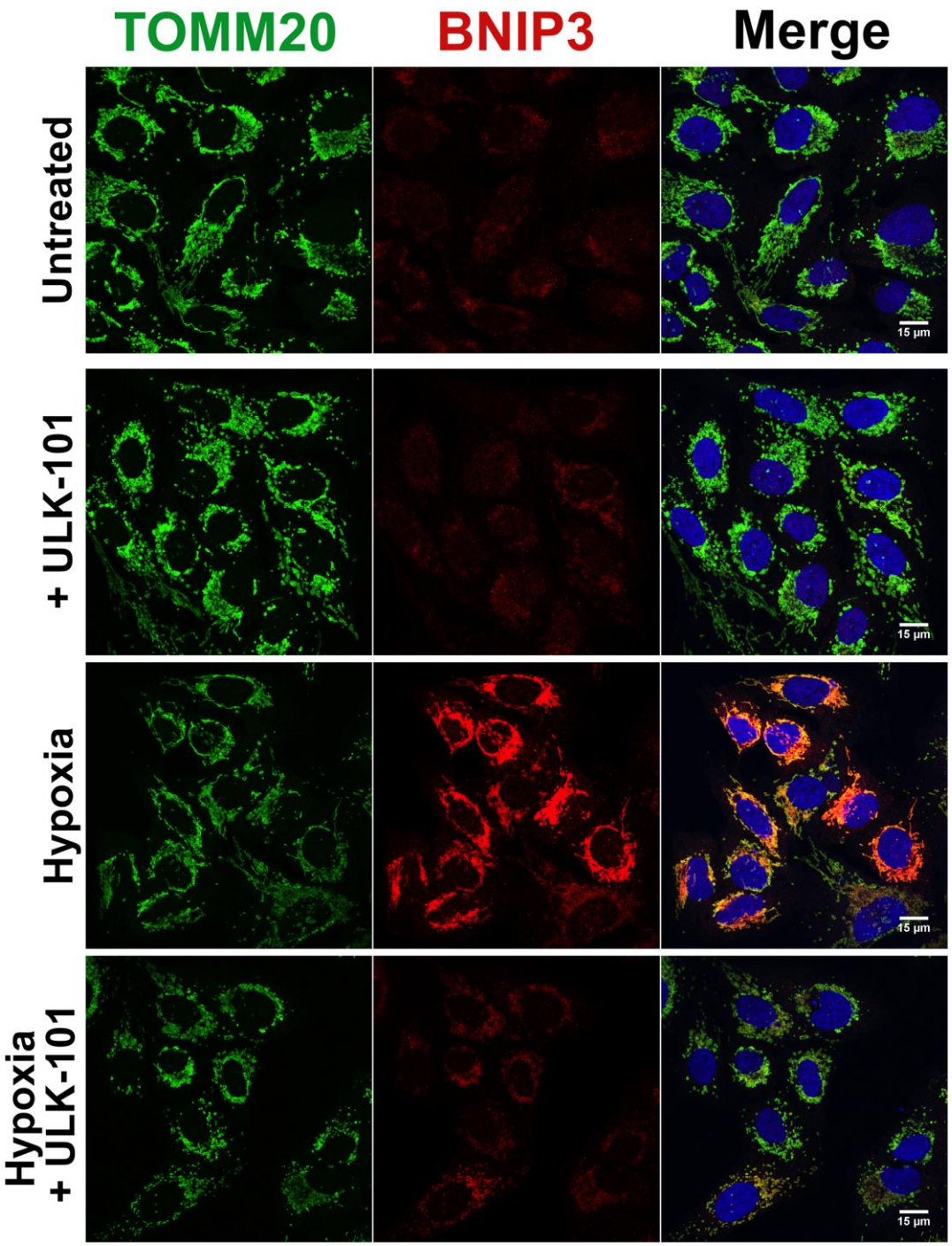

Figure 4.4: Immunofluorescence demonstrating ULK1 inhibition limits BNIP3 accumulation under hypoxia in U2OS cells. Immunofluorescent staining for TOMM20 (green, mitochondria), BNIP3 (red, autophagosomes) and DAPI (blue) in U2OS cells at atmospheric oxygen (Untreated), plus ULK1 inhibitor (+ ULK-101), 1% oxygen (hypoxia) or the combination of 1% oxygen plus the ULK1 inhibitor (hypoxia + ULK-101). (Done in collaboration with Althea Bock-Hughes)

Much of the analysis of BNIP3 and BNIP3L expression levels has largely focused on their transcriptional regulation by a number of transcription factors, including HIF1.[101] However, we have found that BNIP3 protein levels are also strongly regulated post-translationally through proteasomal degradation. BNIP3 levels are induced upon 4 hours of treatment with MG132 alone in all cell lines tested, including U2OS, Saos2, HCC38, and Panc1 (Figure 4.5). Interestingly, stably expressed exogenous HA-BNIP3 in MiaPaca2 cells, which are epigenetically silenced for endogenous BNIP3, also demonstrate a rapid stabilization of HA-BNIP3, indicating that the effects of MG132 on BNIP3 protein levels are not mediated through increased BNIP3 transcription (Figure 4.6). These results suggest that, like many stress response proteins, BNIP3 is consistently being expressed at a basal level and turned over at the proteasome in the absence of an expression-inducing stress, such as hypoxia. Treating cells grown in hypoxia with MG132 did not result in a further increase of BNIP3 protein levels, suggesting that hypoxia inhibits proteasomal turnover of BNIP3 protein (Figure 4.1, Figure 4.2). Combined with the observation that ULK-101 decreased BNIP3 protein levels in hypoxia-treated cells, these results further suggest that hypoxia limits the proteasomal degradation of BNIP3 in a manner that is dependent on ULK1.

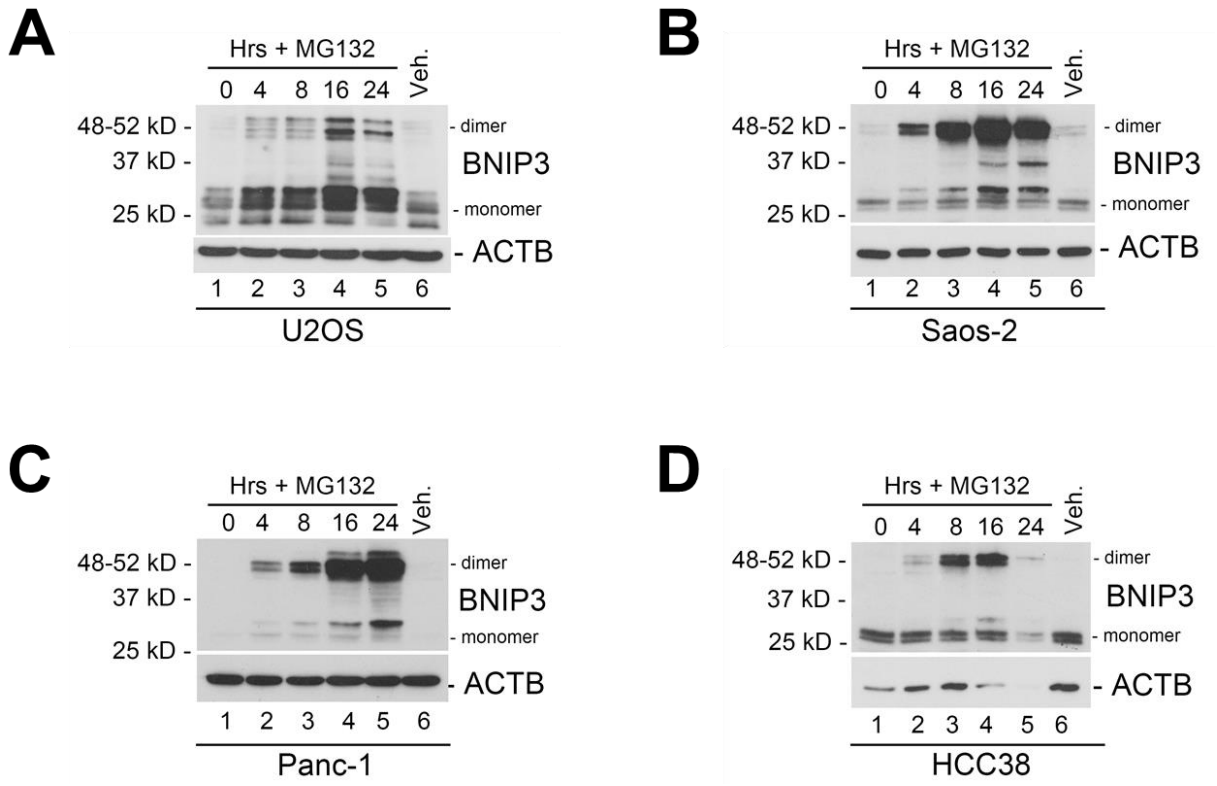

Figure 4.5: BNIP3 is turned over at the proteasome in the absence of stress. (A-D) Western blot for endogenous BNIP3 in U2OS (A), Saos2 (B), Panc-1 (C), HCC38 (D) cells in response to MG132 treatment for 0, 4, 8, 16, 24 hours.

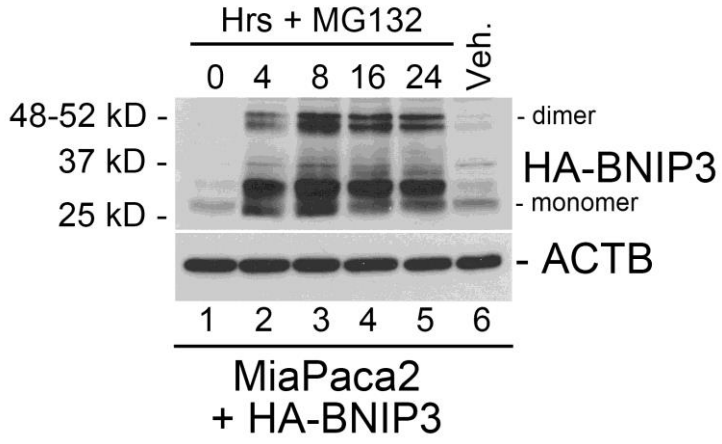

Figure 4.6: Exogenous HA-BNIP3 is turned over at the proteasome. Western blot for exogenous, stably expressed HA-BNIP3 in MiaPaca2 cells that are epigenetically silenced for endogenous BNIP3.

Given this observed role for ULK1 in limiting the proteasomal degradation of BNIP3, we next sought to determine how rapidly ULK1 inhibition increased the rate of BNIP3 protein turnover. Following 16 hours of treatment with DFO, which stabilizes HIF1α to increase BNIP3 expression without inducing ROS, we washed out the DFO and treated cells with cycloheximide to inhibit protein synthesis in the presence or absence of MG132 and ULK-101. Monitoring BNIP3 levels under these conditions allowed us to assess how inhibition of the proteasome or ULK1 affected the rate of decay of BNIP3. Following removal of DFO in the presence of cycloheximide, BNIP3 protein decayed rapidly and was barely detectable after 4 hours (Figure 4.7). However, treatment with MG132 blocked the decay of BNIP3, such that 4 hours of co-treatment with cycloheximide with MG132 resulted in similar protein levels as those seen at 0 hours following removal of DFO. Conversely, upon treatment with ULK-101 we observed a more rapid decay in BNIP3 protein levels, such that BNIP3 was barely detectable upon 2 hours of co-treatment with cycloheximide and ULK-101 following removal of DFO. Combining MG132 and ULK-101 treatment in the presence of cycloheximide following removal of DFO protected BNIP3 against decay, suggesting that ULK1 inhibition was causing the proteasomal degradation of BNIP3. These results indicate that ULK1 activity acts to stabilize BNIP3 protein levels by blocking its turnover at the proteasome.

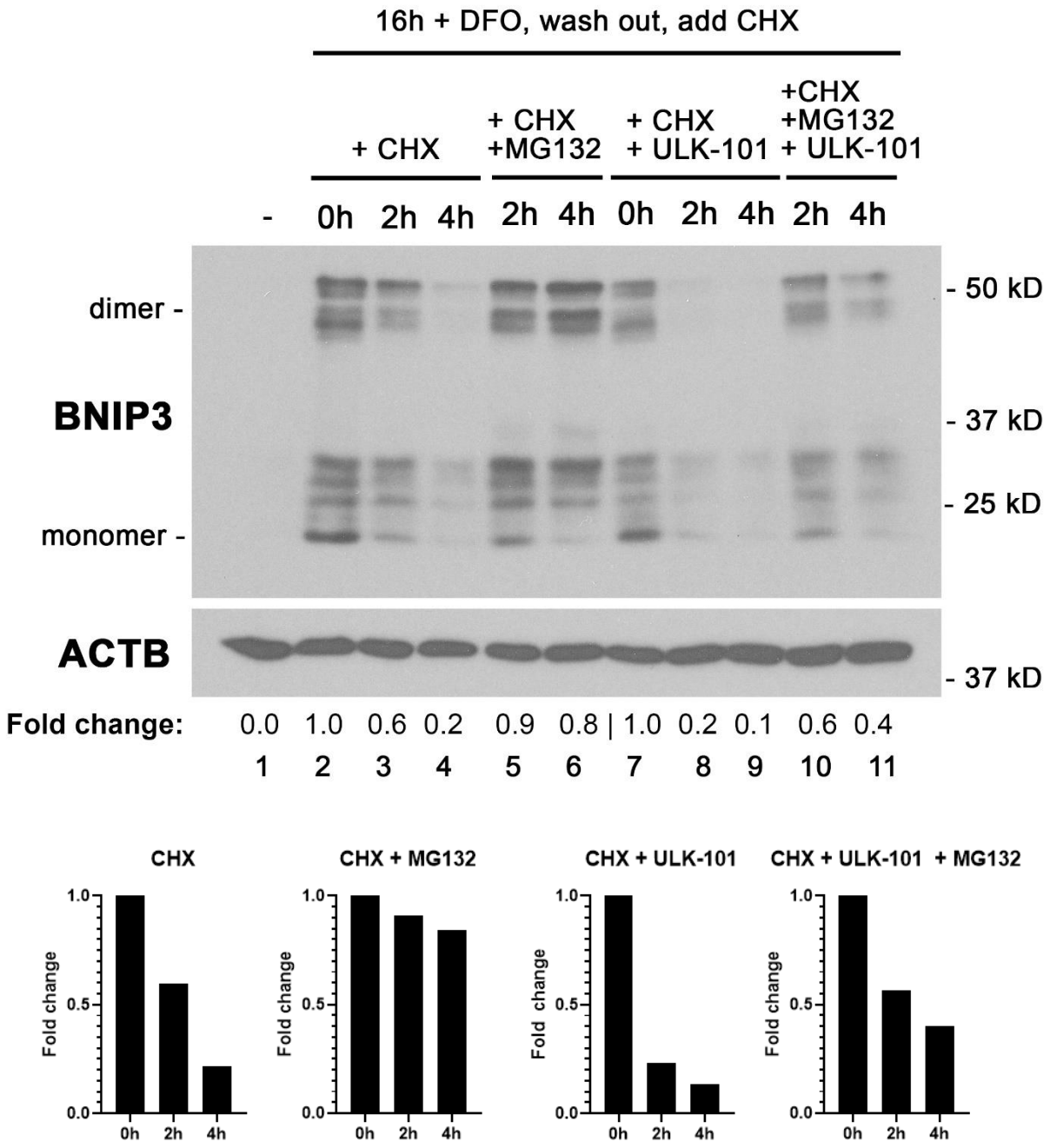

Figure 4.7: Inhibition of ULK1 increases the rate of BNIP3 protein decay. Western blot for endogenous BNIP3 in U2OS cells treated overnight with DFO to induce BNIP3, then washed out for DFO and immediately treated with cycloheximide (CHX) to block new protein synthesis and either MG132 to inhibit the proteasome and/or ULK-101 to inhibit ULK1 kinase activity. Visualized BNIP3 levels from western bands were quantified via densitometry and graphed. Quantification levels are standardized relative to 1.0 representing the 0-hour CHX (left, lane 2) and 0-hour CHX + ULK-101 (right, lane 7) timepoints, respectively.

ULK1 protects BNIP3 from proteasomal degradation in a manner dependent on its "BH3" domain

After having established that ULK1 inhibition leads to the proteasomal turnover of endogenous BNIP3, we aimed to uncover how ULK1 acts to block BNIP3 turnover at the proteasome. Overexpressing FLAG-ULK1 stabilized HA-BNIP3 protein independently of S17 mutation (Figure 3.6), therefore we explored the ability of FLAG-ULK1 to protect a variety of HA-BNIP3 mutants from degradation. In addition to the S17A and S17E mutants we have described thus far, we also assessed the effects of FLAG-ULK1 overexpression on HA-BNIP3 constructs with domain deletions a the "BH3", PEST, and TM domains, as well as a point mutation at G180A (Figure 4.8). As compared to BH3-only proteins, the BNIP3 "BH3" domain (amino acids 109-119) is very poorly conserved with only 2 of the 11 residues of the consensus sequence maintained.[141] No function of the BNIP3 "BH3" domain has been determined, as BNIP3 is known to bind Bcl2 and Bcl-X_L independently of its "BH3" domain and remains capable of promoting mitophagy in its absence (ΔBH3).[127] The BNIP3 PEST domain (amino acids 56-68) was originally identified based on an enrichment of proline (P), glutamic acid (E), serine (S), and threonine (T) which is found in other proteins targeted for proteasomal degradation.[137–139] Mutation of G180 to alanine (G180A) within the transmembrane domain of BNIP3 prevents dimerization of BNIP3 but allows the integration of BNIP3 into the outer mitochondrial membrane as a monomer.[155] Deletion of the transmembrane domain (amino acids 164-184; ΔTM) prevents both dimerization and integration of BNIP3 into the outer mitochondrial membrane.[137]

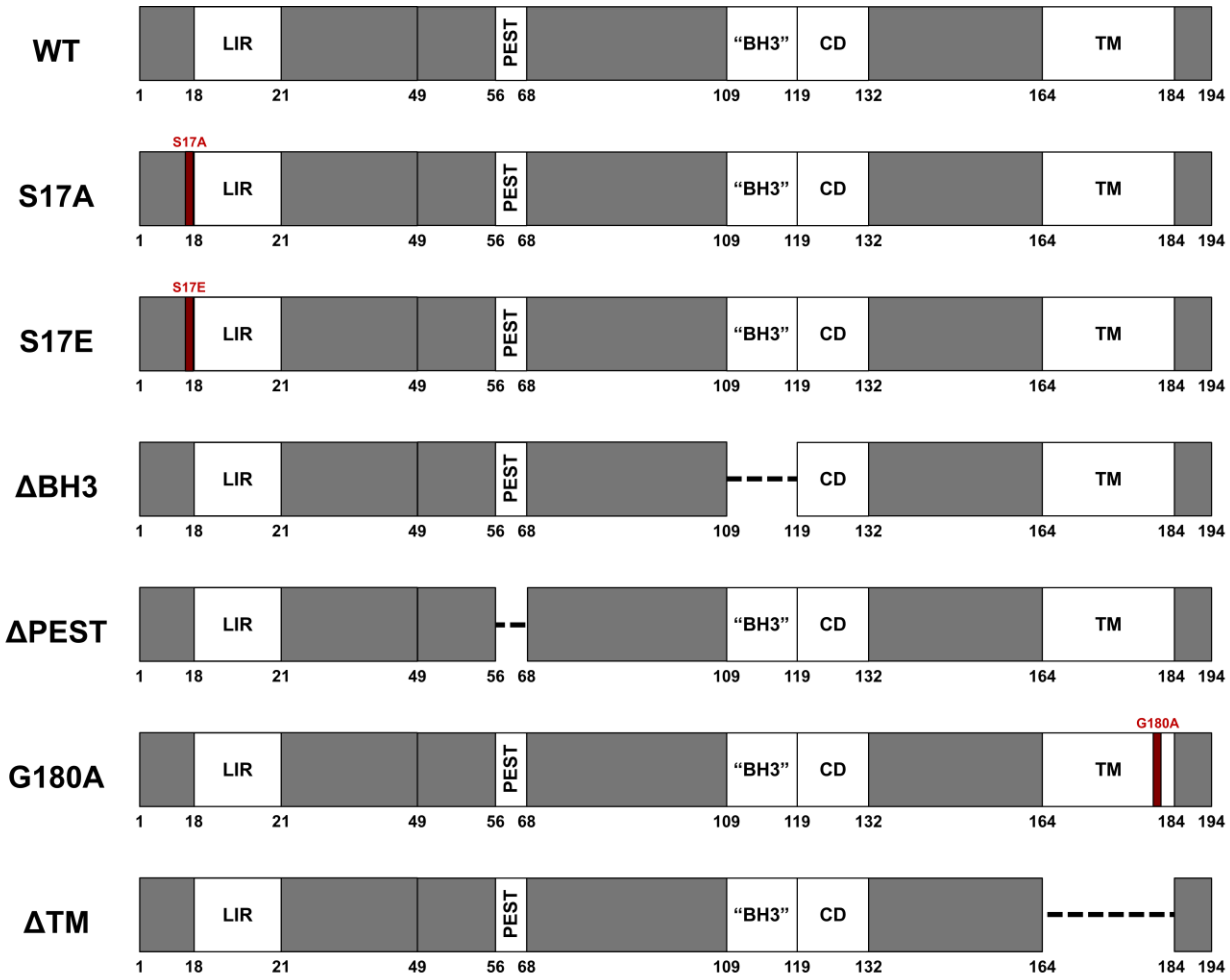

Figure 4.8: Schematic of BNIP3 point mutants and domain deletions. Wild-type, point mutants (S17A, S17E, G180A), and domain deletion mutants (ΔBH3, ΔPEST, ΔTM) of HA-BNIP3 were produced for pulldown assays. The ΔBH3 and ΔPEST deletions have no previously characterized function. The G180A mutation blocks BNIP3 dimerization. The ΔTM mutation blocks BNIP3 integration into the OMM, as well as BNIP3 dimerization.

To assess the effect of ULK1 on BNIP3 stability, we compared levels of HA-BNIP3 wild-type and mutant protein in the presence or absence of exogenously expressed FLAG-ULK1 (Figure 4.9). As we previously observed (Figure 3.6), FLAG-ULK1 overexpression increased the protein levels of HA-BNIP3^{WT}, HA-BNIP3^{S17A}, and HA-BNIP3^{S17E}, indicating that FLAG-ULK1 could promote BNIP3 protein stabilization independently of serine 17 phosphorylation (Figure 4.9, lanes 1-3 compared to lanes 8-10). Similarly, protein levels of the ΔPEST mutant were also increased by FLAG-ULK1 overexpression, suggesting that ULK1 stabilization of BNIP3 does not require the PEST domain (Figure 4.9, lane 5 compared to lane 12). Additionally, FLAG-ULK1 overexpression stabilized the G180 mutant, indicating that BNIP3 dimerization was not required for ULK1-induced stabilization (Figure 4.9, lane 6 compared to lane 13). Of note, protein levels of the ΔTM mutant were minimally affected by FLAG-ULK1 overexpression, suggesting that the stabilizing effect of ULK1 on BNIP3 protein may rely on the integration of BNIP3 into the outer mitochondrial membrane (Figure 4.9, lane 7 compared to lane 14). Interestingly, deletion of the “BH3” domain increased BNIP3 protein levels independently of FLAG-ULK1 expression, exhibiting the highest protein expression levels of all HA-BNIP3 constructs (Figure 4.9, lane 4 compared to lanes 1-3 and 5-7). The ΔBH3 mutant exhibited no change in protein levels upon FLAG-ULK1 overexpression (Figure 4.9, lane 4 compared to lane 11). Taken together, these results suggest that residues within the BNIP3 “BH3” domain promote the proteasomal degradation of BNIP3 and that this degradation may be suppressed by ULK1 in a manner dependent on BNIP3 integration into the outer mitochondrial membrane.

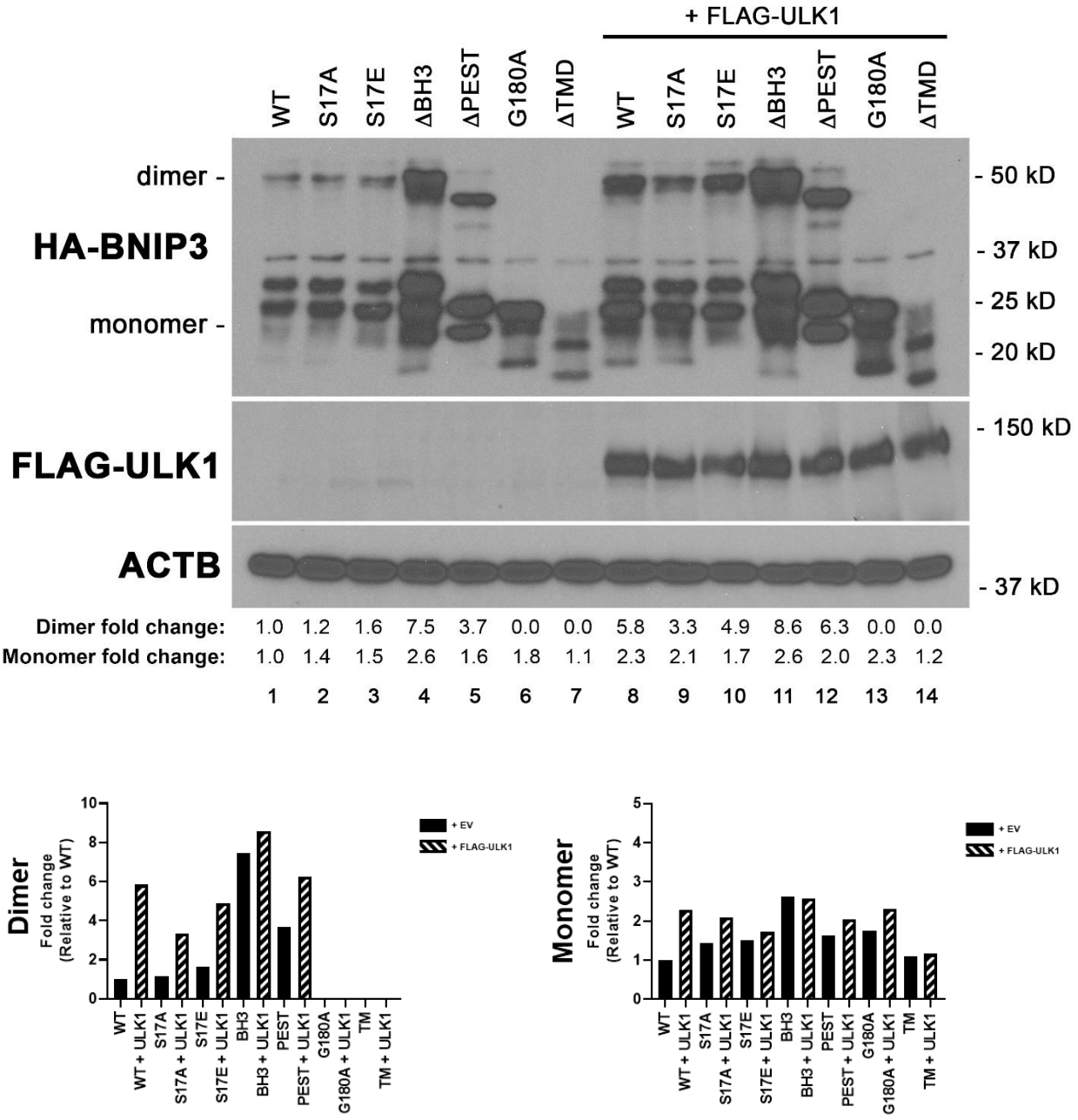

Figure 4.9: Deletion of the "BH3" domain of BNIP3 blocks the stabilization effect of ULK1. Western blot for HA-BNIP3 and different mutant forms of HA-BNIP3 expressed in 293T cells in the presence (lanes 8-14) or absence (lanes 1-7) of exogenous FLAG-ULK1. Quantification levels are standardized relative to 1.0 representing the HA-BNIP3^{WT}-expressing condition in the absence of FLAG-ULK1.

Having established the increased protein level of the ΔBH3 mutant and its resistance to ULK1 stabilization, we next investigated how the turnover of HA-BNIP3^{WT} and HA-BNIP3$^{\Delta BH3}$ differ, and how this turnover is affected by FLAG-ULK1. Cells expressing HA-BNIP3^{WT} and HA-BNIP3$^{\Delta BH3}$ were treated with cycloheximide to inhibit protein synthesis and HA-BNIP3 protein levels were monitored over time. We again noted that levels of the ΔBH3 mutant were higher than that of wild-type and observed that the ΔBH3 mutant did not decay as rapidly over time (Figure 4.10, lanes 1-6 compared to lanes 7-12). Overexpression of FLAG-ULK1 resulted in levels of HA-BNIP3^{WT} that were similar to that of HA-BNIP3$^{\Delta BH3}$, while levels of HA-BNIP3$^{\Delta BH3}$ remained unchanged. In the absence of FLAG-ULK1, wild-type HA-BNIP3 protein levels were visibly different following 4 hours of cycloheximide treatment. However, in the presence of FLAG-ULK1, the decay was slowed, with visible differences in protein levels following 8 hours of cycloheximide treatment (Figure 4.10, lanes 1-6 compared to lanes 13-18). Conversely, the turnover of HA-BNIP3$^{\Delta BH3}$ protein appeared to be relatively unaffected by the presence of FLAG-ULK1 as compared to HA-BNIP3^{WT}.

Based on our understanding of ULK1 phosphorylating BNIP3 on S17, we next sought to investigate the effect of combining the “BH3” domain deletion with either S17A or S17E on BNIP3 stability. Combining S17A or S17E with ΔBH3 increased levels of each combination mutant compared to the single mutation of S17A or S17E, but did not increase protein levels to that of ΔBH3 alone (Figure 4.11). Overexpression of FLAG-ULK1 increased levels of the combination mutants to levels comparable to that of the ΔBH3 mutant alone. The observation that deletion of the “BH3” domain in combination with the S17A and S17E mutants stabilizes BNIP3 in the absence of FLAG-ULK1, but

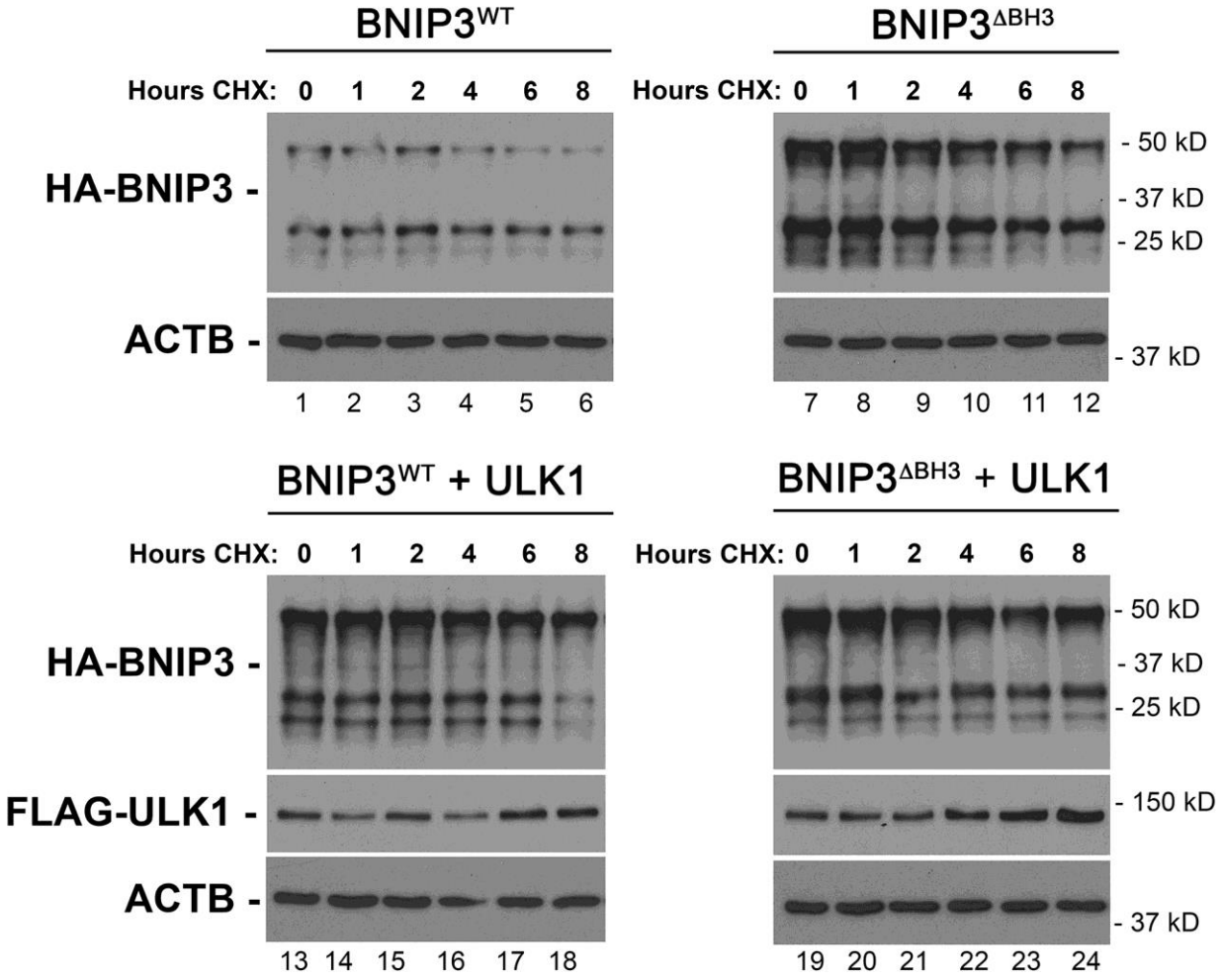

Figure 4.10: The ΔBH3 form of BNIP3 is stabilized in the absence of UKL1.
Western blot for HA-BNIP3 in cells expressing HA-BNIP3^{WT} or HA-BNIP3$^{\Delta BH3}$ mutant, in the presence or absence of FLAG-ULK1. Cells were treated with cycloheximide (CHX) to block new protein synthesis and harvested over time.

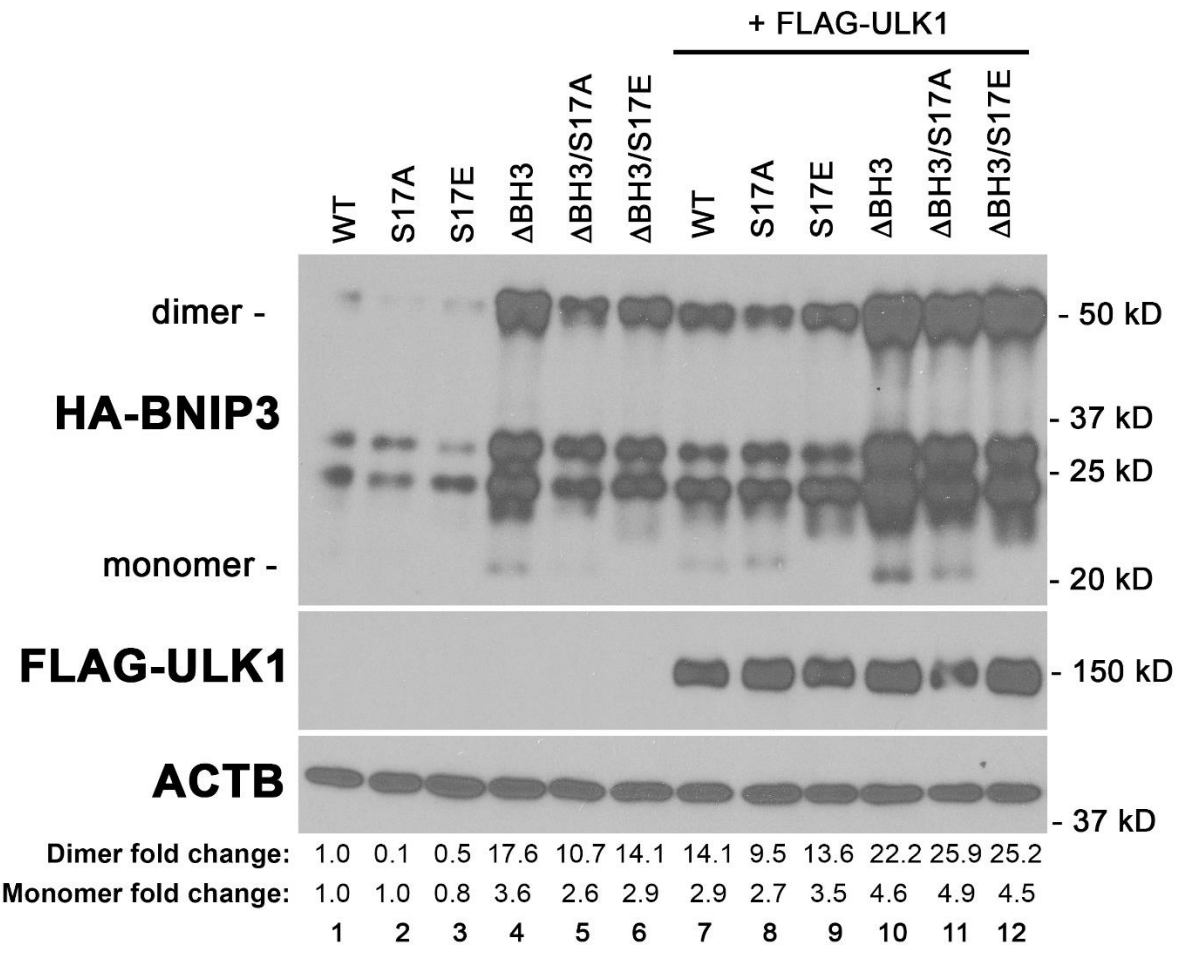

Figure 4.11: BNIP3 S17/ΔBH3 combination mutants are more stable that WT but further stabilized by ULK1. Western blot for HA-BNIP3 and different mutant forms of HA-BNIP3 expressed in 293T cells in the presence (lanes 7 - 12) or absence (lanes 1-6) of exogenous FLAG-ULK1. Quantification levels are standardized relative to 1.0 representing the HA-BNIP3^{WT}-expressing condition in the absence of FLAG-ULK1.

not to the extent to which it is stabilized in the presence of ULK1 suggests that the S17A/ΔBH3 and S17E/ΔBH3 mutants are still being turned over in the absence of ULK1 and that mutation of S17 affects BNIP3 protein turnover. These results further support the importance of the “BH3” region of BNIP3 in the stabilization of BNIP3 protein by ULK1, acting alongside ULK1-regulated post-translational events at S17.

Given the role of the BNIP3 “BH3” domain in the ULK1 stabilization of BNIP3, as well as the effect of S17 phosphorylation by ULK1 on BNIP3-induced mitophagy, we next assessed whether deletion of the “BH3” domain affected HA-BNIP3 and GFP-LC3 interaction. Once again, deletion of the “BH3” domain resulted in increased protein levels relative to HA-BNIP3^{WT}. An increase in HA-BNIP3$^{\Delta BH3}$ pulldown with GFP-LC3 relative to wild-type was observed, however this is likely explained by the increased HA-BNIP3 protein levels in the input, and not due to an enhancement in binding (Figure 4.12). Interestingly, while the combination of S17A and S17E mutation with “BH3” domain deletion did result in an increase in HA-BNIP3 protein levels relative to WT, there was no observed change in HA-BNIP3 and GFP-LC3 interaction compared to the observed results with S17A and S17E mutation alone (Figure 4.12, Figure 3.5). Similar to our previous results with single mutants, interaction of HA-BNIP3$^{S17A/\Delta BH3}$ with GFP-LC3 was undetectable, and the interaction of GFP-LC3 with HA-BNIP3$^{S17E/\Delta BH3}$ was less than that of wild-type. These results indicate that while the “BH3” domain deletion may enhance HA-BNIP3 and GFP-LC3 interaction via increased HA-BNIP3 protein levels, the phosphorylation status of S17 has a dominant effect in determining the interaction with GFP-LC3.

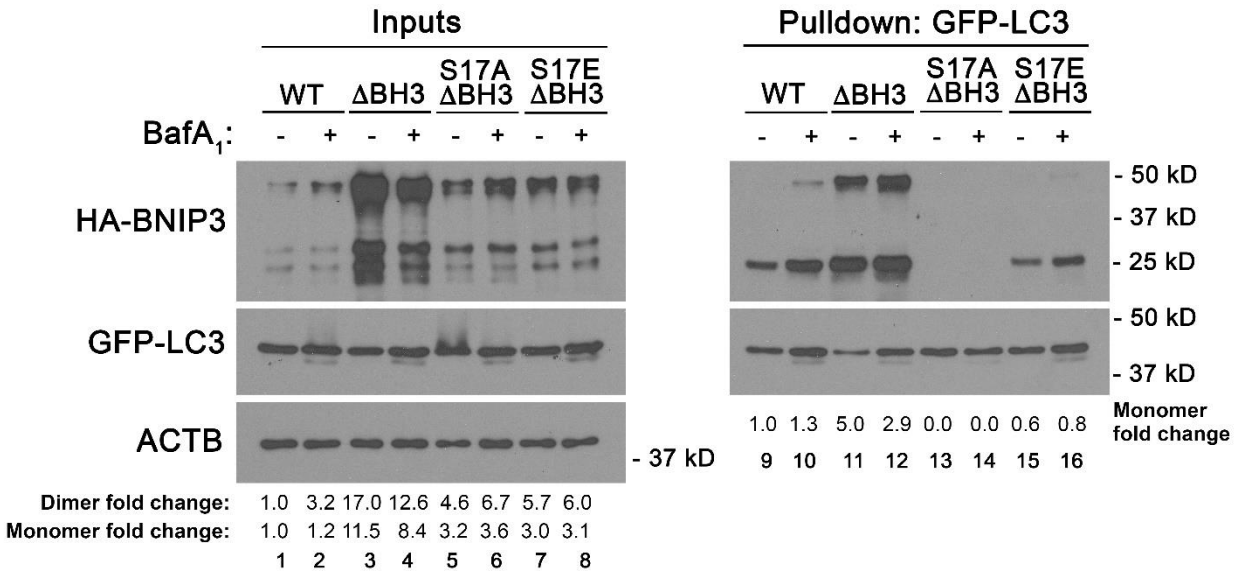

Figure 4.12: Deletion of the "BH3" domain increases HA-BNIP3 protein levels but does not affect LC3 interaction. Pulldown of GFP-LC3 stably expressed in HEK-293T cells with transiently expressed HA-BNIP3 (WT) and different HA-BNIP3 mutants (DBH3, S17A/DBH3, S17E/DBH3) in the presence or absence of 100 nM bafilomycin A1. Inputs to the pulldown are shown on the left and the result of the pulldown on the right. Quantification levels are standardized relative to 1.0 representing the HA-BNIP3^{WT}-expressing condition in the absence of BafA$_1$.

BNIP3 interacts with ULK1 via its C-terminal domain

Having uncovered two ways through which ULK1 affects BNIP3 stability and function, we next assessed how these two proteins interact. In order to determine the domain through which ULK1 interacts with BNIP3, we created FLAG-ULK1 vectors with domain deletions in regions previously identified as interaction sites with autophagy proteins. Deletion sites included amino acids 278-351 in the S/P spacer domain, amino acids 829-1051 constituting the entire c-terminal domain (CTD) which mediates interactions with ATG13 and other proteins, as well as the very C-terminal 14 amino acids from 1038-1051 which is believed to be required for the inhibitory dominant negative autophagy function of ULK1 (Figure 4.13).[58] Additionally, we mutated the active site at lysine 46 to asparagine (K46N) to create a kinase-dead mutant. Unfortunately, deletion of amino acids 278-351 as well as the K46N mutation resulted in unstable forms of FLAG-ULK1 that we were unable to express to adequate levels for comparison to wild-type and the remaining mutants (data not shown). Therefore, we proceeded with wild-type, Δ829-1051, and Δ1038-1051.

FLAG-ULK1 wild-type and mutants were co-overexpressed with wild-type HA-BNIP3, followed by FLAG-ULK1 pulldown. Wild-type HA-BNIP3 efficiently pulled down with FLAG-ULK1, indicating that BNIP3 is another autophagy protein that interacts with ULK1 (Figure 4.14). Interestingly, expression of the ΔCTD FLAG-ULK1 mutant resulted in reduced levels of HA-BNIP3 WT as compared to the effect of FLAG-ULK1^{WT}, suggesting that FLAG-ULK1$^{\Delta CTD}$ was incapable of stabilizing HA-BNIP3 protein (Figure 4.14, lane 3 compared to lane 4). Further supporting this observation, deletion of the CTD markedly decreased the binding of HA-BNIP3 to FLAG-ULK1 (Figure 4.14, lane 7

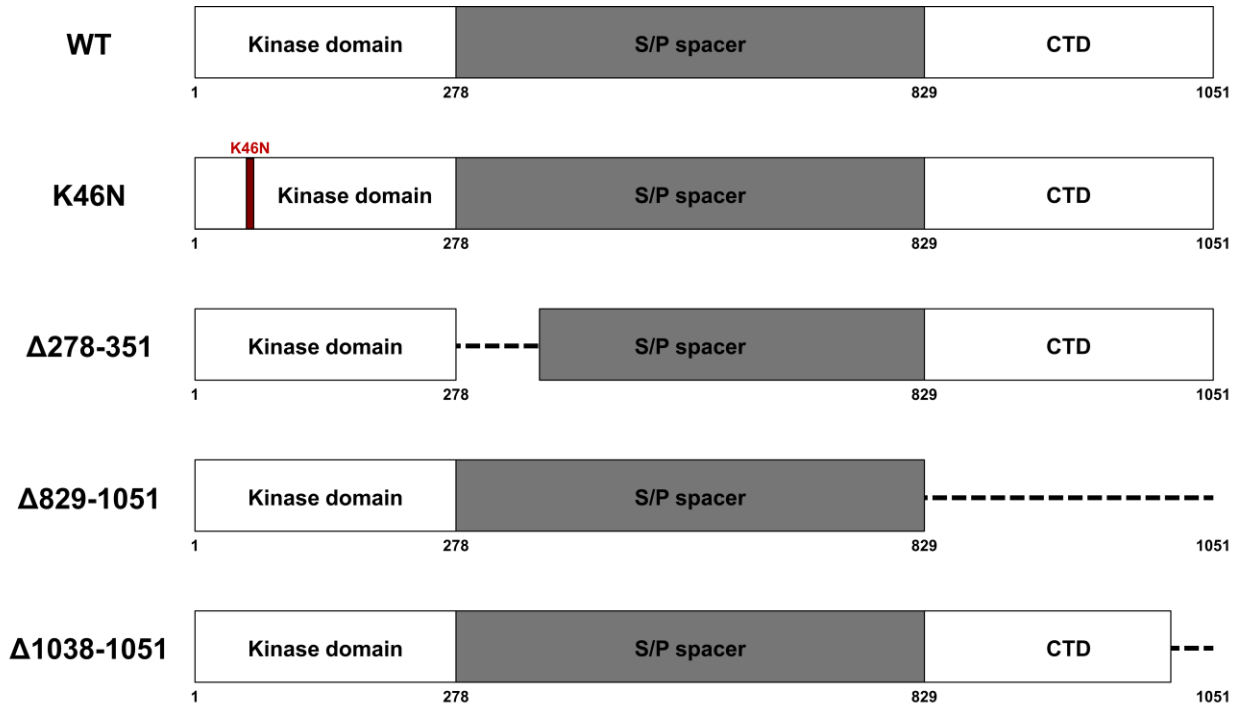

Figure 4.13: Schematic of ULK1 point mutant and domain deletions. Wild-type, K46N point mutant, and domain deletion mutants (Δ278-351, Δ829-1051, Δ1038-1051) of FLAG-ULK1 were produced for pulldown assays. The K46N and Δ278-351 mutants were unstable and unable to express at adequate levels for study alongside wild-type and the remaining mutants. The Δ829-1051 deletion accounts for the entire ULK1 c-terminal domain (CTD). The Δ1038-1051 deletion accounts for the last 14 amino acids of ULK1, which are thought to bind an unknown autophagy regulator protein critical for a dominant-negative autophagy inhibitory function of ULK1.

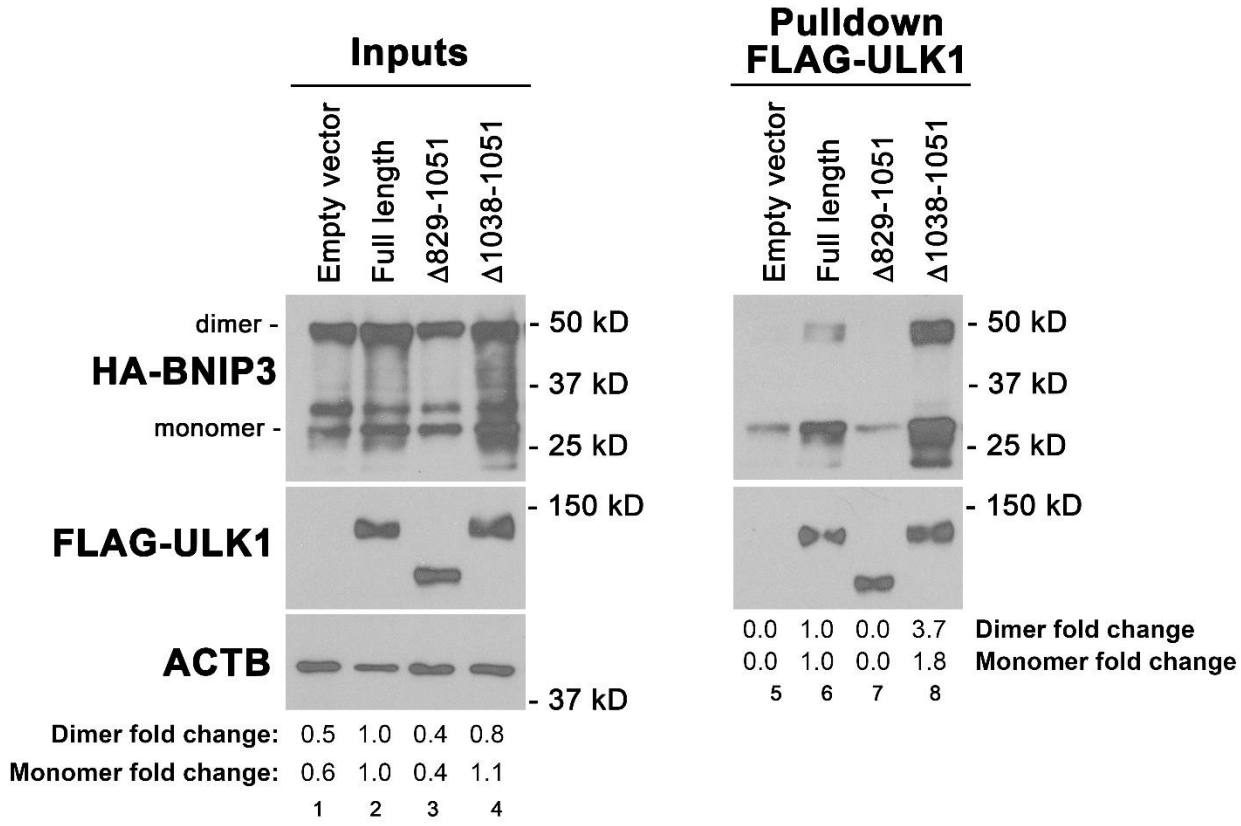

Figure 4.14: BNIP3 interacts with the ULK1 CTD (amino acids 829-1051). Pulldown of FLAG-ULK1 stably expressed in 293T cells with transiently expressed HA-BNIP3 (WT) and different mutant forms of FLAG-ULK1 (full-length, Δ 829-1051, Δ1038-1051). Inputs to the pulldown are shown on the left and the result of the pulldown on the right. Quantification of HA-BNIP3 pulldown was adjusted for background signal in the empty vector lane. Quantification levels are standardized relative to 1.0 representing the FLAG-ULK1^{WT}-expressing condition.

compared to lane 6). Unexpectedly, FLAG-ULK1$^{\Delta 1038\text{-}1051}$ expression resulted in increased HA-BNIP3 protein levels relative to FLAG-ULK1^{WT} (Figure 4.14, lane 4 compared to lane 2), as well as enhanced binding to HA-BNIP3 (Figure 4.14, lane 8 compared to lane 6). These results suggest that deletion of amino acids 1038-1051 may have removed sequences that allow the interaction of FLAG-ULK1 with another protein that normally competes with BNIP3 for ULK1-binding. Together, these findings indicate that BNIP3 is another autophagy protein that interacts with ULK, and support a model in which ULK1 binds BNIP3 via its CTD to protect BNIP3 from degradation and phosphorylate BNIP3 on S17 to boost rates of mitophagy.

ULK1 interacts with BNIP3 at multiple sites, possibly including its "BH3" domain

Given our results demonstrating that ULK1 phosphorylates BNIP3 on S17, we next worked to determine how mutation of BNIP3 at S17 affected ULK1 binding to BNIP3. Wild-type FLAG-ULK1 was co-overexpressed alongside wild-type HA-BNIP3 or constructs mutated at S17 followed by FLAG-ULK1 pulldown in the presence or absence of the ULK1 active site inhibitor ULK-101. Treatment with ULK-101 resulted in an increased interaction of FLAG-ULK1 with all forms of HA-BNIP3 tested (Figure 4.15, lanes 9-16). This result is consistent with a hypothesis that an active kinase dissociates from its substrate following phosphorylation, and that inhibition of the kinase active site may delay or stop said detachment. In support of this hypothesis, HA-BNIP3^{S17A}, which is unable to be phosphorylated, exhibited increased binding to FLAG-ULK1 as compared to wild-type HA-BNIP3 (Figure 4.15, lanes 11-12 and 13-14). HA-BNIP3^{S17E}, which mimics phosphorylation, interacted with FLAG-ULK1 at levels similar to that of

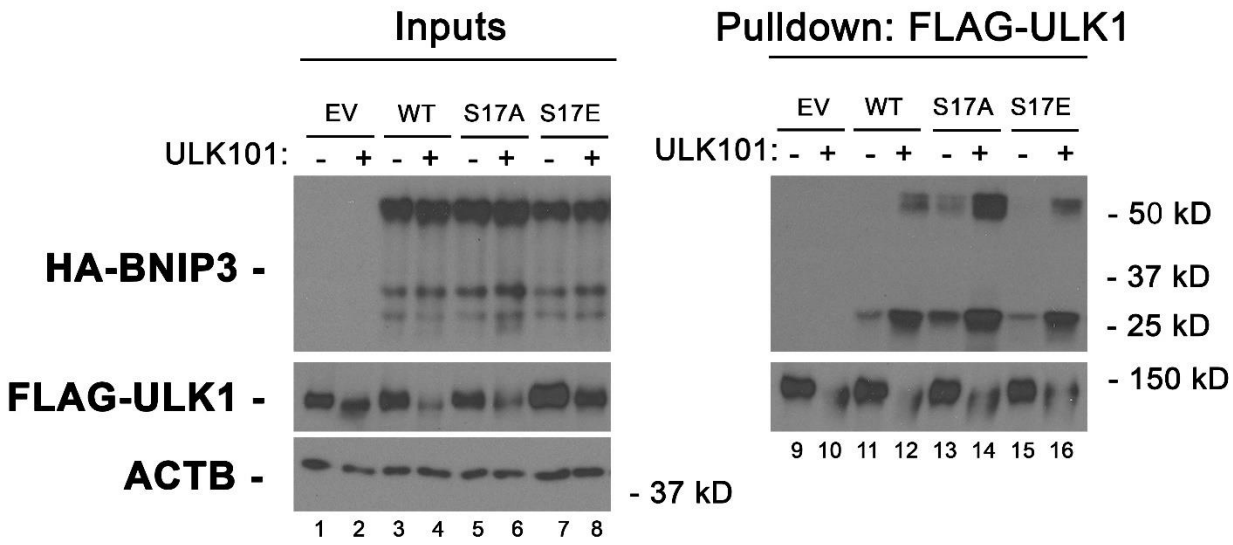

Figure 4.15: S17 mutation affects the interaction of BNIP3 with ULK1. Pulldown of FLAG-ULK1 transiently expressed in 293T cells with transiently expressing HA-BNIP3 (WT) and different HA-BNIP3 mutants (S17A, S17E) or empty vector (EV) control in the presence or absence of ULK-101. Inputs to the pulldown are shown on the left and the result of the pulldown on the right.

wild-type (Figure 4.15, lanes 11-12 and 15-16). In the absence of ULK-101, this may be due to the phosphorylation of HA-BNIP3^{WT} by FLAG-ULK1, resulting in a similar protein conformation at the S17 site between wild-type and S17E mutant. However, this does not explain why HA-BNIP3^{WT} and HA-BNIP3^{S17E} exhibit similar binding affinity to FLAG-ULK1 in the absence of ULK-101. We hypothesized that this may be due to FLAG-ULK1 interacting with HA-BNIP3 via multiple domains. Docking domains, or substrate binding regions that are not part of the active site, are frequently observed in kinase-substrate interactions and aid in substrate recognition and specificity.[215] Similarly, while the ULK1 kinase domain likely interacts with the region surrounding S17, the CTD of ULK1 may interact with a separate BNIP3 domain.

Given the apparent role of the “BH3” domain in the ULK1 stabilization of BNIP3, we next tested the interaction of HA-BNIP3$^{\Delta BH3}$ and S17/ΔBH3 combination mutants with FLAG-ULK1. Once again, HA-BNIP3$^{\Delta BH3}$ and the S17/ΔBH3 combination mutants displayed higher protein levels than that of wild-type or the S17 mutants alone (Figure 4.16, lanes 5-7). As observed in the previous experiment, HA-BHIP3^{S17A} interacted more strongly with FLAG-ULK1 than wild-type, and HA-BNIP3^{S17E} interacted to a similar degree as wild-type (Figure 4.16, lanes 9-11). The amount of HA-BNIP3$^{\Delta BH3}$ protein pulled down by FLAG-ULK1 was similar to that of wild-type, however when accounting for the increased input levels of HA-BNIP3$^{\Delta BH3}$ relative to wild-type, the “BH3” deletion may have decreased binding to FLAG-ULK1 (Figure 4.16, lanes 9 and 12). The interaction of HA-BNIP3$^{S17A/\Delta BH3}$ and FLAG-ULK1 was decreased as compared to S17A alone, and interestingly, was similar to that of the “BH3” deletion mutant, suggesting that

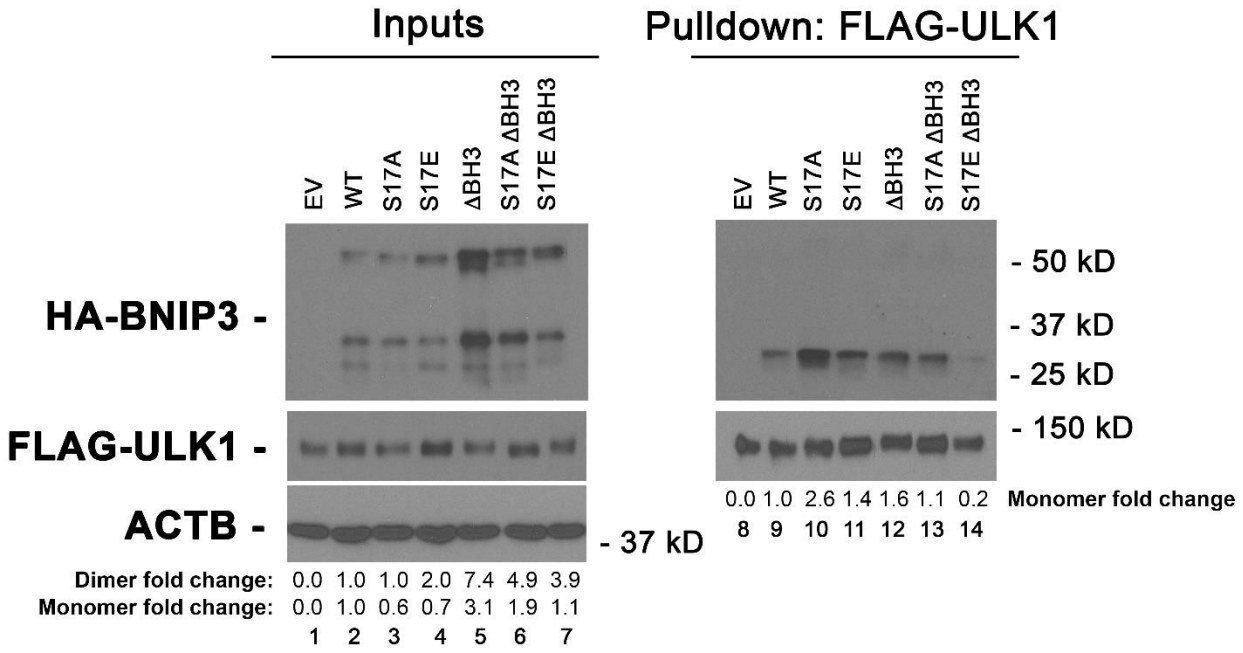

Figure 4.16: Deletion of the "BH3" domain may decrease the interaction of BNIP3 with ULK1. Pulldown of FLAG-ULK1 transiently expressed in 293T cells with transiently expressing HA-BNIP3 (WT) and different HA-BNIP3 mutants (S17A, S17E, ΔBH3, S17A/ΔBH3, S17E/ΔBH3) or empty vector (EV) control. Inputs to the pulldown are shown on the left and the result of the pulldown on the right. Quantification levels are standardized relative to 1.0 representing the HA-BNIP3^{WT}-expressing condition.

the “BH3” domain may play a dominant role over the S17 phosphorylation site in the interaction of BNIP3 and ULK1 (Figure 4.16, lanes 10 and 12-13). Finally, the S17E and “BH3” deletion combination mutant had dramatically reduced binding as compared to all forms of HA-BNIP3 tested, suggesting an additive effect (Figure 4.16, lane 14). This is consistent with a model in which the ULK1 CTD binds to BNIP3, possibly at the “BH3” domain, followed by phosphorylation of BNIP3 at S17 by the ULK1 kinase domain (Figure 4.17). It is important to note, however, that the S17E/ΔBH3 combination mutant does not fully inhibit the interaction of FLAG-UKL1 and HA-BNIP3, which implies that additional BNIP3 domains may be involved in the interaction. Based on the size disparity between ULK1 and BNIP3, it is not unreasonable to posit that the ULK1 CTD may interact with multiple BNIP3 domains, likely including the “BH3” domain (Figure 4.17).

Conclusions

In this chapter, we identified a novel role for ULK1 in promoting BNIP3 stability by limiting its turnover at the proteasome. We found that BNIP3 protein levels are rapidly increased upon inhibition of the proteasome, indicative of proteasomal regulation of BNIP3. However, treating cells grown in hypoxia with proteasome inhibitors did not further increase protein levels, suggesting that hypoxia inhibits proteasomal turnover of BNIP3. Interestingly, treating cells grown in hypoxia with the ULK1 inhibitor ULK-101 resulted in decreased BNIP3 protein levels which was reversed by proteasomal inhibition, suggesting that hypoxia limits the proteasomal degradation of BNIP3 in a manner that is dependent on ULK1. These results were further supported by observing

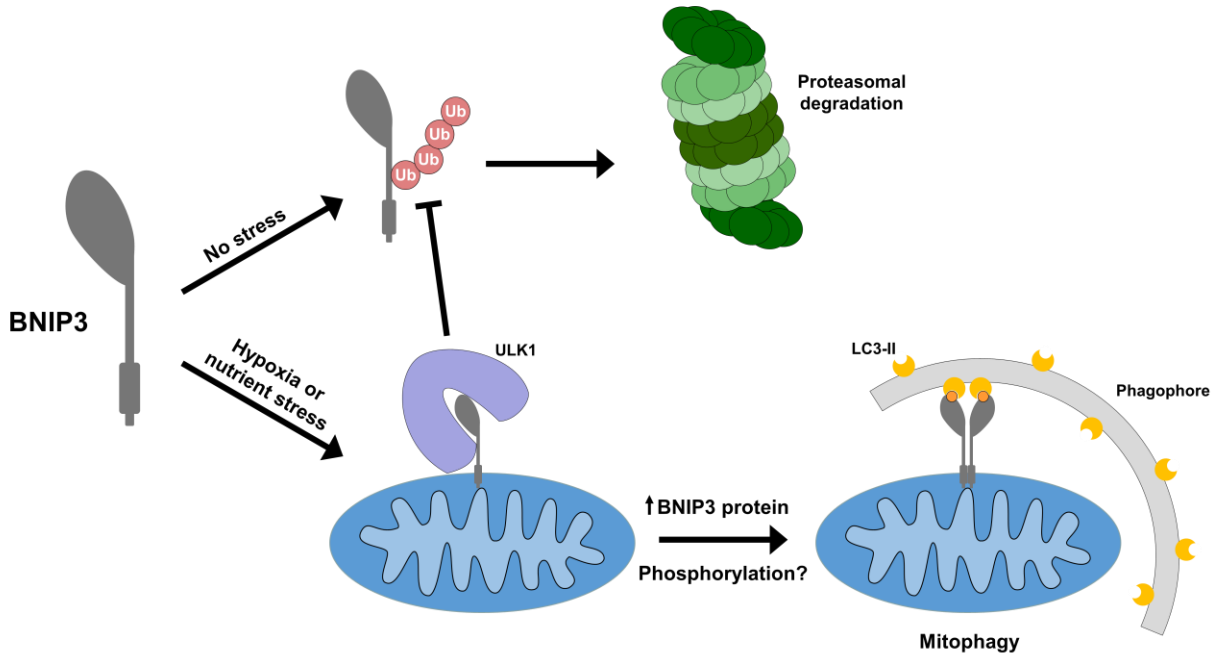

Figure 4.17: Model of the stabilization of BNIP3 protein by ULK1. Like many stress response proteins, *Bnip3* is consistently expressed but BNIP3 protein is rapidly turned over at the proteasome in the absence of stress (likely due yet unknown ubiquitination events). We find that ULK1 stabilizes BNIP3 protein under stressors such as hypoxia or nutrient stress, which increases BNIP3 protein levels to allow mitophagy to proceed. It remains unknown whether ULK1 always phosphorylates BNIP3 on S17 following the stabilization of BNIP3.

differences in the decay of endogenous BNIP3 protein in the presence of ULK-101, proteasomal inhibition, or a combination thereof.

Conversely, we observed that FLAG-ULK1 overexpression protected HA-BNIP3 from degradation. As observed in the previous chapter, this stabilizing effect was independent of S17 phosphorylation status, suggesting that an additional domain or domains may be involved. Indeed, upon testing a number of HA-BNIP3 point mutants and domain deletions, we found that HA-BNIP3 with a deleted “BH3” domain was relatively unaffected by the overexpression of FLAG-ULK1. Interestingly, the ΔBH3 HA-BNIP3 mutant also exhibited increased protein levels and protein stability relative to wild-type in the absence of FLAG-ULK1. Deletion of the “BH3” domain had no observable effect on the binding of HA-BNIP3 to GFP-LC3 after adjusting for increased protein levels due to “BH3” deletion. Combinations of S17 mutation with “BH3” domain deletion behaved similarly to that of S17 mutation alone, suggesting that the effect of S17 status on GFP-LC3 binding was unaffected by “BH3” domain status.

We next sought to determine the domains of FLAG-ULK1 required for interaction with HA-BNIP3. Using domain deletion mutants of FLAG-ULK1, we found that the ULK1 CTD is required for interaction with HA-BNIP3. Consistent with this observation, FLAG-ULK1$^{\Delta CTD}$ was also incapable of stabilizing wild-type HA-BNIP3 protein, suggesting that the interaction between HA-BNIP3 and the FLAG-ULK1 CTD is responsible for HA-BNIP3 stabilization. Interestingly, this domain is known to bind other autophagy-related proteins, including ATG13, and further work is necessary to determine the cellular conditions under which ULK1 binds BNIP3 as opposed to other autophagy-related binding partners.[58] We also observed that FLAG-ULK1 deleted for the final 14 C-

terminal amino acids (Δ1038-1051) increased HA-BNIP3 protein levels greater than that of wild-type FLAG-ULK1, as well as enhanced the interaction of HA-BNIP3 with FLAG-ULK1. This region of ULK1 is believed to be important for the inhibitory dominant negative autophagy function of ULK1, however the proteins responsible for binding this region remain unknown.[58] Our observations suggest that the proteins responsible for binding this region of ULK1 may compete with the ability of BNIP3 to bind the CTD, although further work is necessary to determine the cellular context and significance of this event.

Finally, we sought to determine the domains of HA-BNIP3 required for interaction with FLAG-ULK1. We found that HA-BNIP3 with a S17A mutation exhibited increased interaction with FLAG-ULK1 as compared to wild-type HA-BNIP3, while the S17E mutant bound to FLAG-ULK1 in a manner similar to that of wild-type. This observation is consistent with a hypothesis that kinases detach from their substrates following the phosphorylation event, which would explain the increased binding of the phospho-null S17A mutant and the similarity between the phosphomimetic S17E mutant and the wild-type construct which is able to be phosphorylated by FLAG-ULK1. However, this hypothesis does not explain the similarity between the binding of FLAG-ULK1 to wild-type and S17E mutated HA-BNIP3 in the presence of ULK1 inhibition, which suggests that the interaction between the proteins may involve additional domains of BNIP3. FLAG-ULK1 and HA-BNIP3 sharing multiple binding sites is unsurprising, as we would expect the N-terminal kinase domain of ULK1 to interact with S17 of BNIP3, but we observed that the C-terminal domain of FLAG-ULK1 is critical to HA-BNIP3 binding. Based on its resistance to FLAG-ULK1-indcued protein stabilization, we next tested

whether deletion of the HA-BNIP3 “BH3” domain affected the interaction between FLAG-ULK1 and HA-BNIP3. We found that deletion of the “BH3” domain appeared to slightly decrease the interaction of the two proteins, but more importantly, the combination of S17E with ΔBH3 dramatically decreased the interaction of HA-BNIP3 and FLAG-ULK1, suggesting an additive effect. It is important to note, however, that the interaction was not entirely abolished by this combination of mutants, suggesting that additional domains of BNIP3 may be involved in the interaction with ULK1. Based on the molecular weight disparity between BNIP3 and ULK1, it is entirely feasible that multiple domains of BNIP3 may interact with the ULK1 CTD, and future work must be done to elucidate the identity of these domains.

Our studies have identified a novel function for ULK1 in regulating the stability of BNIP3 by blocking its proteasomal turnover. As will be discussed in Chapter 6, this role may have clinical significance, as ULK1 inhibitors are currently being tested in combination with mTOR inhibition in an attempt to overcome the failure of mTOR inhibitors in clinic.[59,100,216–218] Previous work from our lab has identified a growth-suppressive function of BNIP3 in human cancers.[131] BNIP3 is also known to play a number of important roles in liver homeostasis.[128,172] Our observations in this study indicate that ULK1 inhibition would decrease BNIP3 protein levels, possibly resulting in a loss of liver homeostasis or a growth-promoting phenotype in healthy tissues, however this hypothesis requires additional study. We have also identified the first known function of the poorly conserved BNIP3 “BH3” domain as a regulator of BNIP3 protein stability. How the presence of this domain promotes protein turnover in the absence of ULK1 remains unknown, however we hypothesize that it may be the site of

ubiquitination or SUMOylation events. Indeed, there are two lysine residues present in this domain (at positions 111 and 112), however initial work with these sites has yielded no indication of post-translational events (data not shown).

CHAPTER 5

DEVELOPMENT OF A *Bnip3* CONDITIONAL KNOCKOUT MOUSE MODEL

Introduction

Genetically engineered mouse models are tools commonly used to study human disease due to the pathophysiological similarities between many diseases in mice and humans. In order to assess the role of BNIP3 in cancer progression and metastasis, our lab has utilized mouse models of tumorigenesis crossed with mice carrying a whole-body (constitutive) knockout of *Bnip3*. Crossing *Bnip3* knockout mice with the MMTV-PyMT mouse mammary tumor model revealed that BNIP3-induced mitophagy delays tumor progression by preventing the accumulation of dysfunctional mitochondria and excess production of ROS, further establishing a growth-suppressing role for BNIP3 in cancer[131]. Similar projects have been initiated in other tumor types, including pancreatic ductal adenocarcinoma and hepatocellular carcinoma. While constitutive knockouts are useful for characterizing the effects of a protein in diseases, including cancer, there are drawbacks. Some proteins, including BNIP3, play important roles in specific tissues, and loss of these roles by constitutive knockout may affect phenotypes in the modeling of a disease. For example, BNIP3 is highly expressed in liver tissue, and work from our lab has shown that it plays an important role in lipid metabolism, metabolic homeostasis, and zonation in the liver, especially in response to fasting.[128,172] Constitutive knockout of *Bnip3* to study tumorigenesis in mammary or pancreatic tissue would also result in knockout in the liver. The resulting effect on lipid metabolism or liver function may affect the phenotypes observed in the tumorigenesis model. Constitutive

models are also unable to assess the effects of the loss of a protein at different stages of tumorigenesis, as the gene is knocked out in all tissues at all times.

To solve these problems, methods for conditional knockout models have been developed, including Cre/loxP technology. Cre recombinase, originally derived from the P1 bacteriophage, excises “floxed” regions of DNA, meaning DNA located between two loxP sites.[219] A loxP site is a 34 base pair sequence composed of two palindromic recognition sequences flanking a spacer region.[220] The loxP sites are genetically engineered into murine embryonic stem (ES) cells, which can be injected into a blastocyst to produce a chimeric mouse in which the modified ES cells may be incorporated in the germ line. In order to conditionally knockout the floxed gene in a specific tissue, mice are engineered to express Cre recombinase controlled by cell-specific promoters and enhancers, such as the albumin (Alb) promoter which exclusively expresses Cre recombinase in the liver.[221] In this case, the loxP sites will only be exposed to Cre in liver tissue, leading to tissue-specific excision of the DNA sequence. It is also possible to temporarily induce Cre expression by using an exogenous inducer such as tamoxifen or tetracycline, which allows investigators to knockout floxed genes of interest at a certain age or stage of disease.[221]

In this chapter, we sought to develop a conditional *Bnip3* knockout mouse model for future studies in the lab. This model is now being used in several grant-funded research projects studying metabolic phenotypes and tumor progression.

Developing a Bnip3 conditional knockout mouse model

In order to develop a *Bnip3* conditional knockout mouse model, we collaborated with the Transgenics/ES Cell Technology Mouse Core Facility at the University of Chicago. Through this collaboration with the core, we generated a targeting vector with 5' and 3' homology arms that would allow homologous recombination of a target sequence containing cis placement of loxP sites in the same directional orientation between exons 1 and 2, as well as exons 5 and 6 (Figure 5.1). Therefore, expression of Cre recombinase would result in the excision of *Bnip3* exons 2-5, effectively knocking out expression of the protein (Figure 5.1D). The targeting vector also contained a Neo cassette for selection in murine embryonic stem (ES) cells, which was flanked by FLP recombinase target (FRT) sites for excision by flippase recombinase (FLP) after development of the mouse (Figure 5.1B and Figure 5.1C). Following targeting vector linearization, electroporation into ES cells, and initial screening of 192 clones using PCR, we next performed a Southern blot on 8 positive clones to confirm homologous recombination at the 3' end of the targeted sequence, at the request of our collaborators in the core facility (Figure 5.2). Based on signal intensity in the 3' Southern Blot (Figure 5.2, lanes 2 and 3), clones 19 and 23 were selected for implanting into pseudopregnant females.

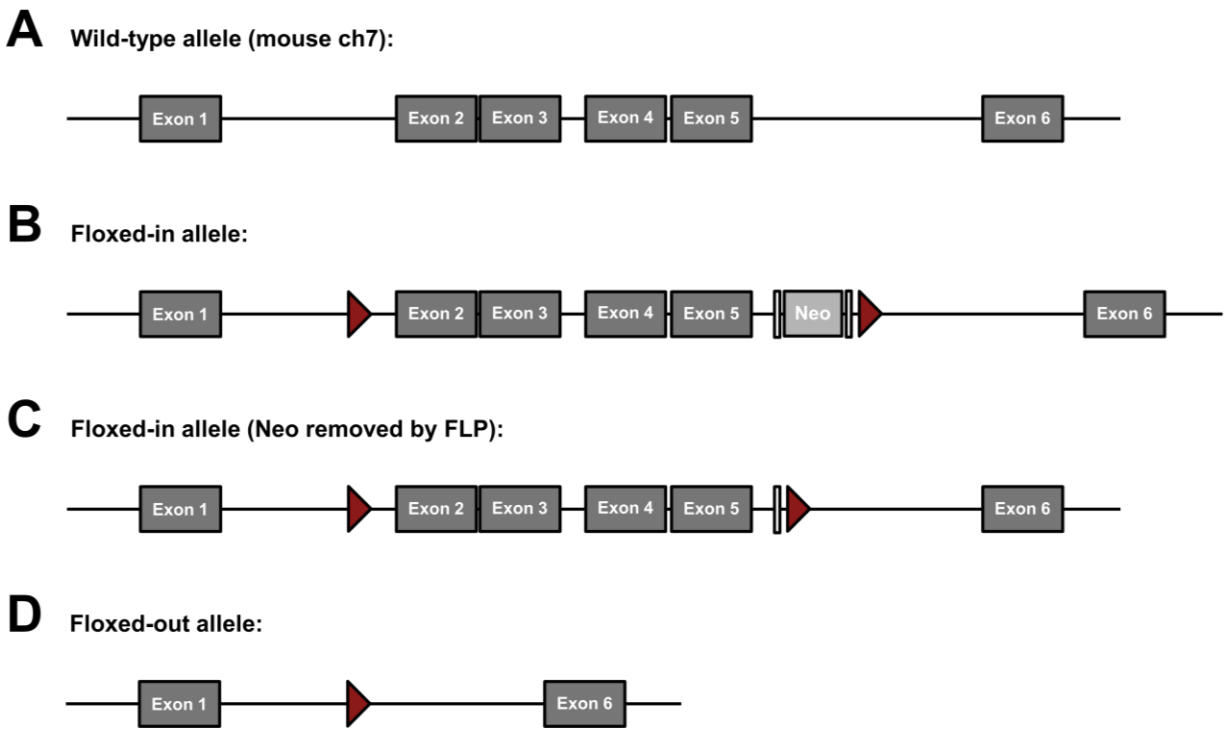

Figure 5.1: Schematic of the wild-type, floxed-in, and floxed-out *Bnip3* alleles. Introns and non-coding sequence are represented by lines. *Bnip3* exons are represented by dark gray boxes. LoxP sites are represented by red triangles. The neomycin cassette is represented by a light gray box. FRT sites are represented by white boxes. A) The wild-type murine *Bnip3* allele on chromosome 7 contains 6 exons. B) LoxP sites and a neomycin cassette (for selection in ES cells) flanked by FRT sites were inserted between exons 1-2 and 5-6 using a targeting construct. C) The neomycin cassette was excised by crossing floxed-in mice with FLP-expressing mice. D) Exons 2-5 of *Bnip3* can be conditionally excised by crossing floxed-in mice with mice expressing cre in specific tissues.

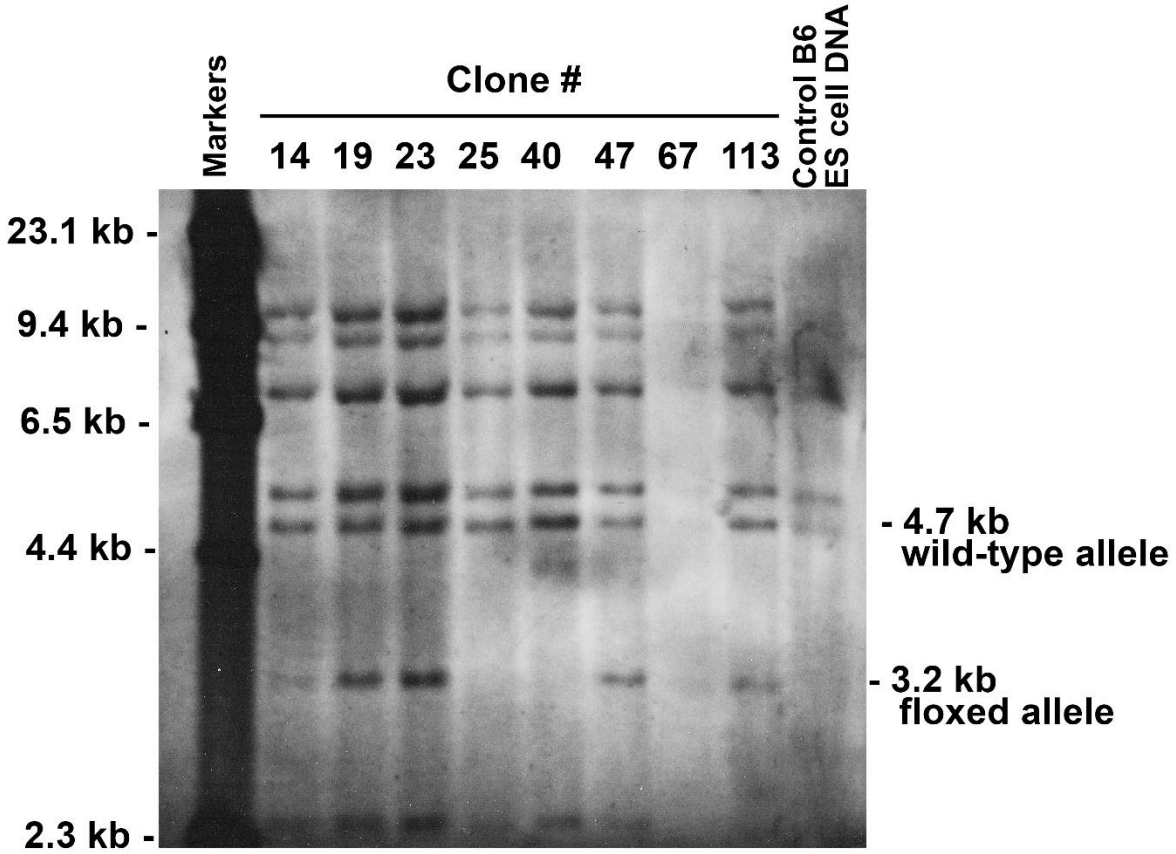

Figure 5.2: Southern blot to detect 3' integration of the targeting construct. A Southern blot was performed to confirm integration of the targeting construct in ES clones following electroporation and selection. The Southern probe was designed to detect integration of the 3' end of the targeting construct. Due to signal strength, clones 19 and 23 were selected for implanting into pseudopregnant females.

The chimeric offspring were bred to achieve *Bnip3* $^{fl/WT}$ mice as genotyped by the presence or absence of the 3' end of the inserted sequence. These mice were then crossed with a number of Cre-expressing mice, including Alb-Cre (liver), Pdx1-Cre (pancreas), and Mox2-Cre (embryonic), in order to test the efficacy of the loxP sites for *Bnip3* deletion in specific tissues. We collected pancreas samples from two *Bnip3* $^{fl/WT}$ mice, one positive and one negative for Pdx1-Cre, as well as tail and spleen samples for negative controls, and performed PCR analysis to detect wild-type and floxed-in alleles. We expected to observe both the wild-type and floxed-in alleles in the tail and spleen samples, and an absence of the floxed-in band in the pancreas sample. Surprisingly, no reduction in the floxed-in allele was observed in the pancreas sample as compared to tail and spleen, suggesting that Cre was unable to excise the sequence between the two loxP sites (Figure 5.3). Similar results were observed in mice expressing Cre in other tissues regardless of age, maternal inheritance of Cre, or tissue site.

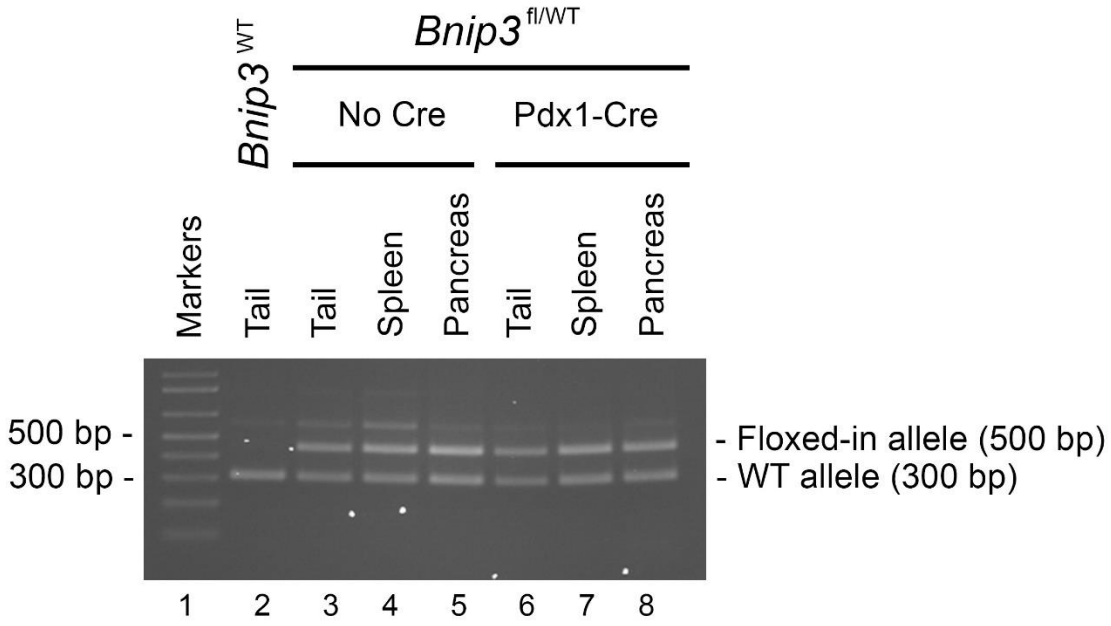

Figure 5.3: Testing of pancreatic deletion of *Bnip3* in *Bnip3* $^{fl/WT}$ mice. *Bnip3* ^{WT} and *Bnip3* $^{fl/WT}$ mice as well as a *Bnip3* $^{fl/WT}$ mouse expressing Pdx1-Cre were sacrificed, and tail, spleen, and pancreas samples were collected for DNA extraction followed by PCR using primers designed to detect wild-type and floxed-in alleles. No *Bnip3* deletion was observed in the pancreas of the Pdx1-Cre-positive mouse, indicating that cre was unable to excise the sequence between the two loxP sites.

To determine why *Bnip3* deletion was not occurring in tissues expressing Cre, we designed PCR primers to amplify the loxP site and surrounding sequence of both the 5' and 3' sites (Figure 5.4). These primers were then utilized in amplifying the aforementioned sequences in the targeting vector, as well as DNA collected from the positive ES cells as previously measured by Southern blot (Figure 5.2). Following amplification, we excised the expected floxed-in and wild-type bands, purified the DNA, and submitted it for sequencing. The 3' primers were designed with one of the primers located within the inserted Neo cassette sequence, so only the presence or absence of a floxed allele could be detected, with no expected wild-type control band (Figure 5.4A). Consistent with the Southern blot and our previous genotyping, the targeting vector and all of the ES clones yielded the expected PCR product and were positive for the 3' loxP site by sequencing. The 5' primers were designed with both primers located in wild-type mouse genomic sequence and therefore both the wild-type and floxed-in alleles could be detected, with the floxed-in allele containing approximately 90 base pairs of inserted sequence (Figure 5.4B). Consistent with our inability to observe a floxed-out allele in Cre-expressing mice from clones 19 and 23, we observed no 5' floxed-in allele in ES clones 19, 23, or 47. To confirm these results, both the wild-type and floxed-in PCR products were sequenced, and as expected, no 5' loxP site was observed in the sequence of ES clones 19, 23, or 47.

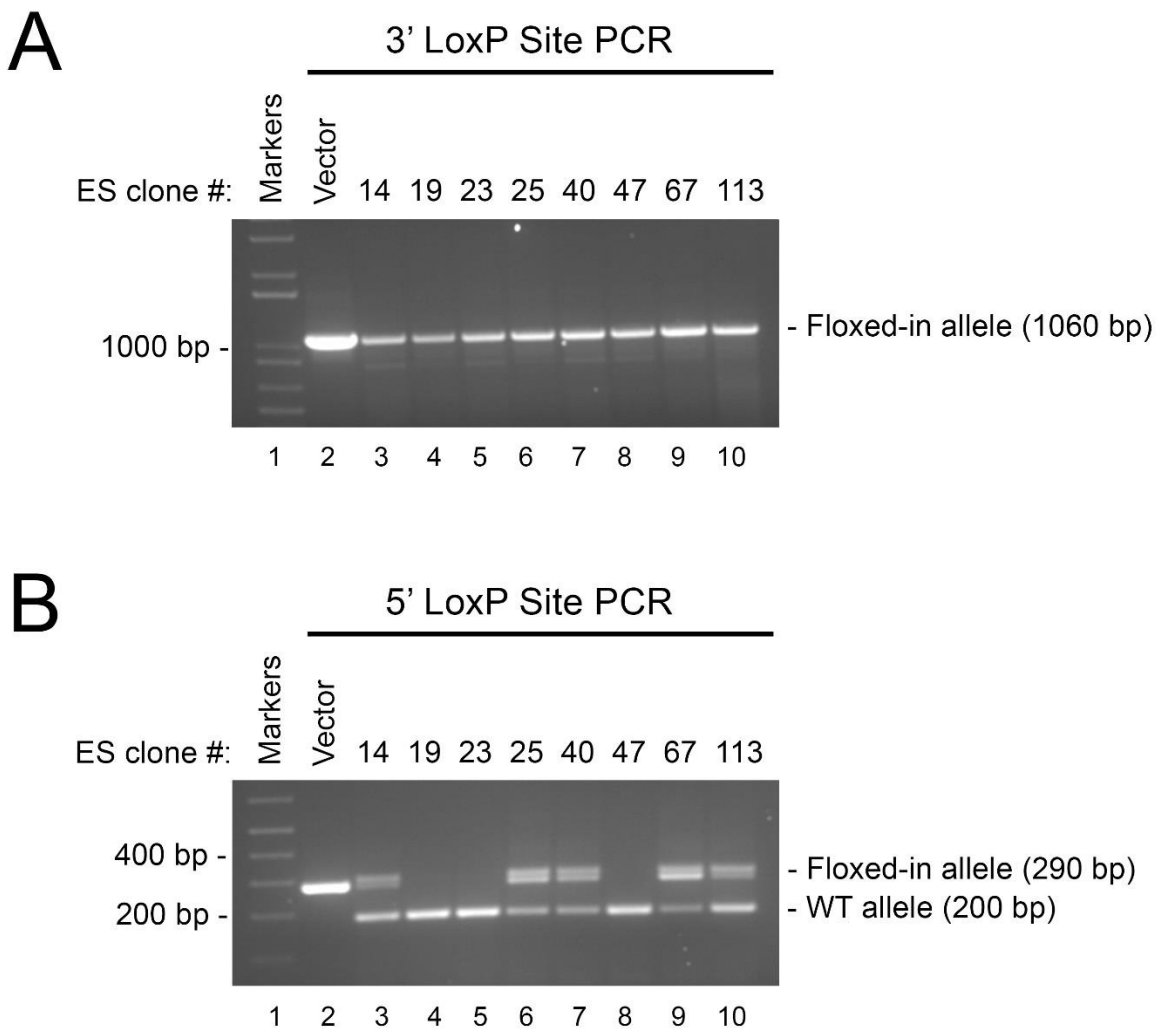

Figure 5.4: PCR amplification of the 5' and 3' loxP sites of selected ES clones for sequencing. Sequences surrounding the 5' and 3' loxP sites in selected ES clones were amplified via PCR and visualized by agarose gel for analysis. Bands were then excised, purified, and submitted for sequencing (data not shown). A) Visualization of the 3' loxP site, which was previously tested via Southern Blot. The targeting vector and all ES clones were positive for presence of the 3' loxP site. Primer design did not allow detection of wild-type alleles. B) Visualization of the 5' loxP site. Primer design allowed the detection of both wild-type (lower band) and loxP-containing (upper band) alleles. ES clones 19, 23, and 47 were not positive for the 5' loxP site, suggesting an error in homologous recombination had occurred.

Based on the PCR and sequencing results, we decided implant ES cell clone 67 into pseudopregnant females. The resulting chimeric mice were then bred to yield mice with a *Bnip3* $^{fl/WT}$ genotype. These mice were then distributed to members of the lab and crossed with a number of Cre-expressing mice, including Alb-Cre (liver), Pdx1-Cre (pancreas), and MCK-Cre (muscle) to eventually achieve *Bnip3* $^{fl/fl}$, Cre-positive mice. The lab then collected tail and pancreas samples from a Pdx1-Cre-negative; *Bnip3* $^{fl/fl}$ mouse, tail and pancreas samples from a Pdx1-Cre-positive; *Bnip3* $^{fl/fl}$ mouse, tail and muscle samples from an MCK-Cre-positive; *Bnip3* $^{fl/fl}$ mouse, and a tail sample from a *Bnip3* wild-type mouse to assess the presence of wild-type, floxed-in, and floxed-out bands via PCR (Figure 5.5). As expected, the wild-type allele was detected in the *Bnip3* wild-type mouse. Only the floxed-in allele was detected in the Cre-negative tissue samples, as well as the tail samples from each *Bnip3* $^{fl/fl}$ mouse. Finally, the floxed-out allele was detected in the pancreatic tissue of the Pdx1-Cre-positive mouse, as well as the muscle tissue of the MCK-Cre-positive mouse. Floxed-in allele was detected in Cre-expressing tissues, but this is likely due to the presence of cells of different lineages residing within the tissue samples, including fibroblasts and immune cells. These PCR results demonstrate that *Bnip3* exons 2-5 are indeed being excised only within the tissues of interest, and that we have successfully developed a conditional *Bnip3* knockout mouse model for future studies. However, the absence of BNIP3 protein will need to be confirmed via western blot and immunohistochemistry for each tissue of interest.

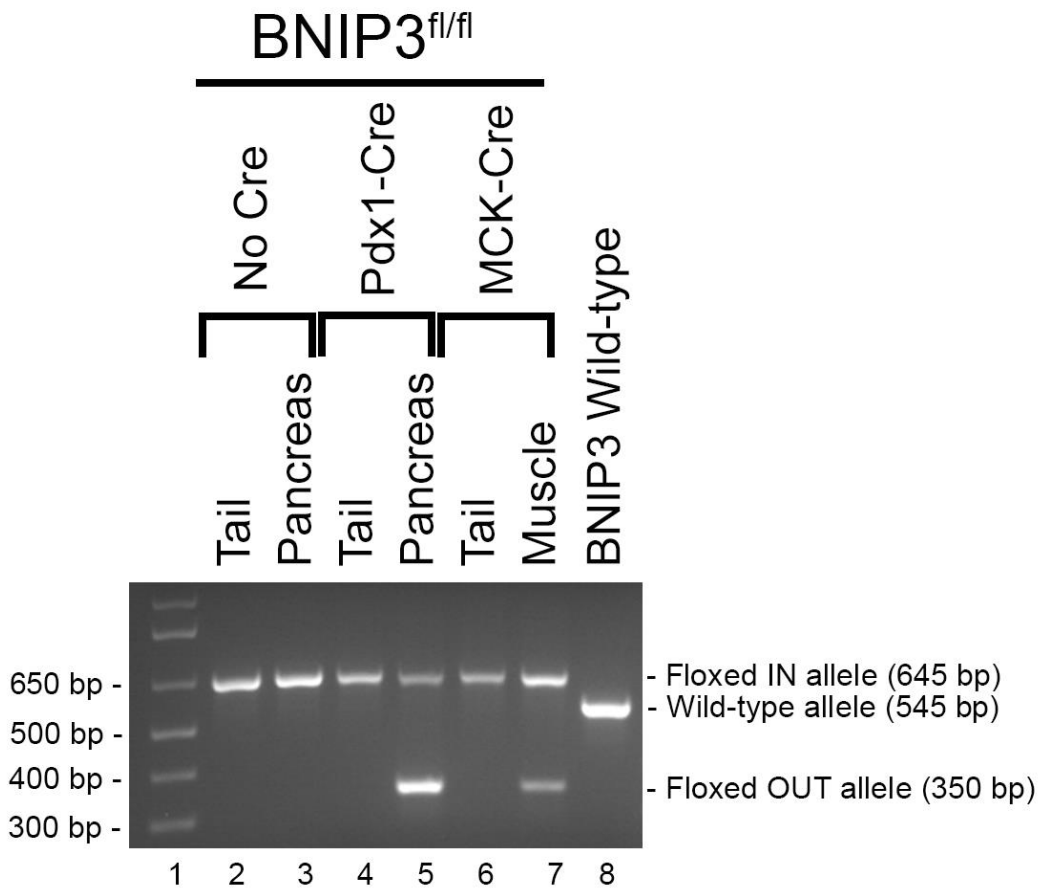

Figure 5.5: Testing of pancreas-specific and muscle-specific deletion of *Bnip3* in *Bnip3* $^{fl/fl}$ mice. *Bnip3* $^{fl/fl}$ mice expressing no cre, Pdx1-Cre (pancreas), or MCK-Cre (muscle) were sacrificed and tail and either pancreas or muscle samples were collected for DNA extraction followed by PCR using primers designed to detect wild-type, floxed-in, and floxed-out alleles. The floxed-in allele was detected in all tissue samples of *Bnip3* $^{fl/fl}$ mice. Detection in cre-expressing tissues was likely due to the presence of cells of different lineages residing within the tissue samples (e.g. fibroblasts). The floxed-out allele was detected in the pancreas sample of the Pdx1-Cre-positive mouse as well as the muscle sample of the MCK-Cre-positive mouse, demonstrating tissue-specific deletion of *Bnip3*. (Done in collaboration with Cara Anderson and Grazyna Bozek)

Conclusions

In this chapter, we collaborated with the Transgenics/ES Cell Technology Mouse Core Facility at the University of Chicago to develop a *Bnip3* conditional knockout mouse model. This model will allow us to specifically delete *Bnip3* in tissues of interest while maintaining normal levels of expression in other tissues. This model has a vast variety of potential uses. First, our lab will utilize his model to create genetically "cleaner" models of a number of human diseases already studied by the lab, including pancreatic and liver cancer, as well as metabolic disorders such as fatty liver disease. Upon crossing the *Bnip3* floxed mouse with tamoxifen-inducible Cre, we can also study the effects of BNIP3 loss at different stages of molecular pathogenesis or tumorigenesis. For example, the molecular pathogenesis of hepatocellular carcinoma, which involves steatosis followed by NASH.[222] Finally, we have also acquired a conditional knockout model of the *Bnip3* homolog *Bnip3l*. Recent work has demonstrated BNIP3L acts as a growth promoter in the progression of pancreatic ductal adenocarcinoma while our unpublished work with a constitutive and conditional knockout of *Bnip3* indicates a growth suppressive role for BNIP3.[210] Crossing a combination of the *Bnip3* and *Bnip3l* conditional knockout models with a pancreas-specific Cre would allow us to determine which effect is dominant in future studies piecing apart the functional differences between these homologous proteins.

CHAPTER 6

DISCUSSION

Summary and significance

The work presented in this dissertation identifies a previously unknown function for ULK1 in regulating mitophagy. We show that ULK1 promotes the interaction of BNIP3 with LC3 by phosphorylating BNIP3 at S17. Mimicking phosphorylation of S17 resulted in increased overlap of LC3 with mitochondria as well as decreased mitochondrial mass as compared to wild-type BNIP3, suggestive of increased rates of mitophagy (Figure 3.12). In addition to BNIP3, our work identifies S35 of BNIP3L (homologous to S17 of BNIP3) as an ULK1 phosphorylation site. Both S17 of BNIP3 and S35 of BNIP3L had previously been reported to be phosphorylated, but the identity of the kinase responsible remained unknown.[133,135] ULK1 has also previously been shown to phosphorylate both FUNDC1 and Bcl2-L-13 to promote their respective interactions with LC3 family proteins thereby increasing rates of mitophagy.[92,223] Taken together, these results further support an emerging role for ULK1 in specifically upregulating mitophagy. Canonically, ULK1 is known to promote general autophagy in response to changes in nutrient status via the phosphorylation of Beclin1 and ATG14, however our work suggests that under specific cellular contexts, ULK1 also specifically upregulates the turnover of mitochondria via mitophagy.[71] Work in this dissertation as well as the literature suggest that hypoxic stress may be one such context. Future studies are required to elucidate the intracellular signaling necessary to specifically promote ULK1 to perform its mitophagy-enhancing function.

In addition to phosphorylating BNIP3 at S17 to promote LC3 interaction, we show that ULK1 also affects BNIP3 protein stability (Figure 4.17). ULK1 inhibition with ULK-101 repressed BNIP3 protein levels in a manner dependent on the proteasome, suggesting that ULK1 acts to block BNIP3 proteasomal turnover. Interestingly, this repressed turnover was not due to changes in mitophagy, as treatment with bafilomycin A_1 was unable to rescue the ULK-101 treatment phenotype. BNIP3 is traditionally believed to act as a stress response protein based on its dramatic transcriptional upregulation in response to a number of cellular stressors, most notably hypoxia.[101] However, in order to rapidly respond to cellular stress, many stress response proteins are continuously expressed at basal levels and ultimately degraded in the absence of stressors. Upon initiation of stress, these existing proteins are stabilized by covalent modification or other rapid mechanisms to block their turnover while the transcriptional machinery upregulates additional expression (Figure 6.1A).[169] Our work with proteasomal inhibitors indicates that like other stress response proteins, BNIP3 is also expressed in the absence of stress and turned over at the proteasome. Further, treatment with ULK-101 resulted in proteasomal turnover of BNIP3 in hypoxia-treated cells, suggesting that the stabilization of BNIP3 protein under hypoxic stress is dependent on the covalent modification or binding of BNIP3 by ULK1 (Figure 6.1B).

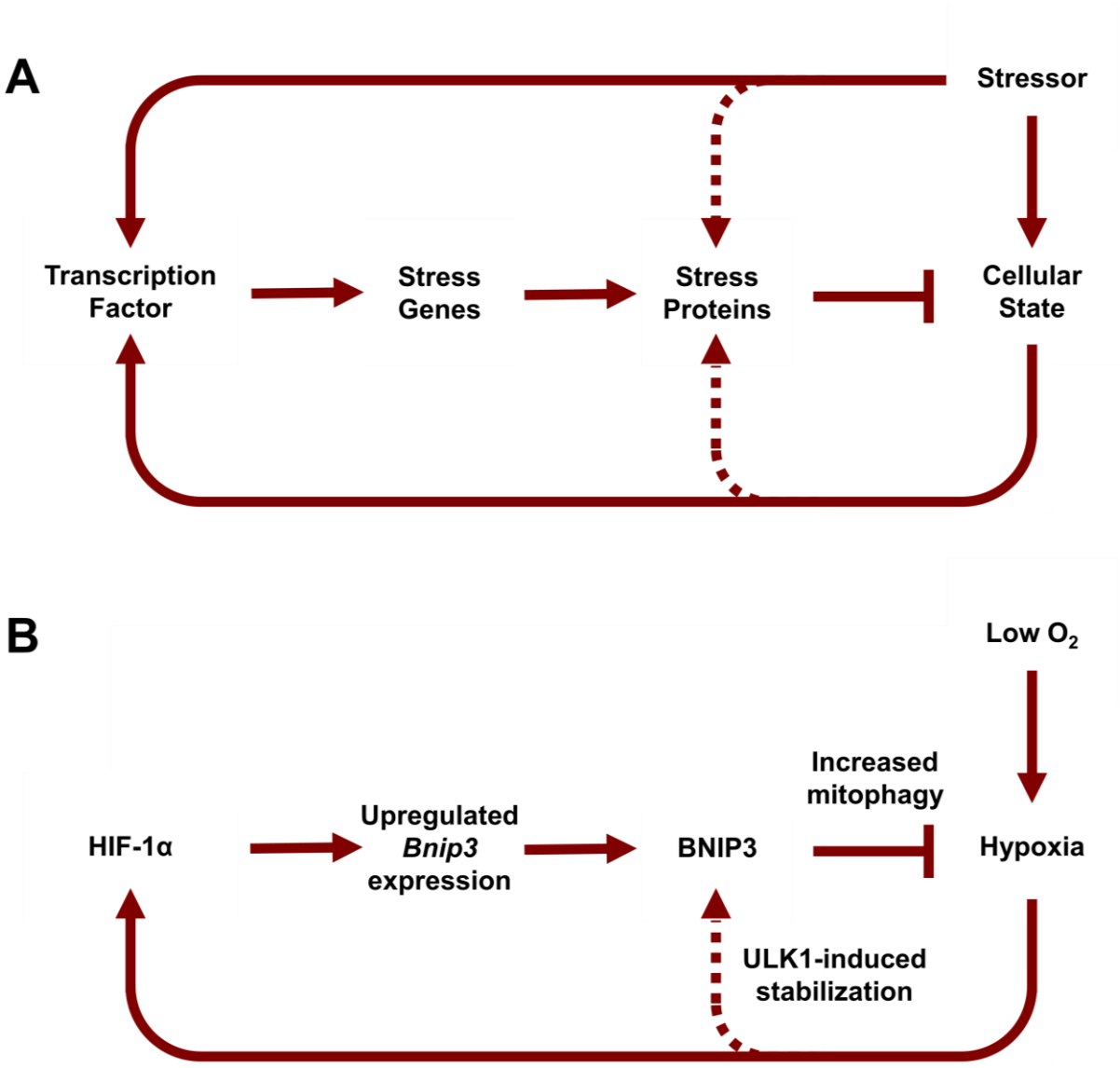

Figure 6.1: Model of the epigenetic and post-translational regulation of stress response proteins. A) Cellular response to external stressors often involves both transcriptional (solid outer lines) and post-translational (dotted inner lines) mechanisms. Transcription factors are activated by the stressor or cellular state, leading to the upregulation of stress-response genes. However, existing stress-response proteins may be stabilized through post-translational modification or other rapid mechanisms in order to increase the rate of response. Adapted from Zhang *et al.*[169] B) *Bnip3* is transcriptionally upregulated by HIF-1α in response to hypoxic stress. Our work demonstrates that in addition to this transcriptional control, BNIP3 protein is also stabilized by ULK1. Stabilization of BNIP3 protein results in increased rates of mitophagy to limit O_2 consumption and ROS generation in response to hypoxia.

Conversely, we demonstrated that overexpression of ULK1 leads to a stabilization of BNIP3 protein, resulting in increased BNIP3 protein levels. Stabilization of BNIP3 occurred independently of S17 phosphorylation, as both S17A and S17E mutant forms of BNIP3 were stabilized to the same degree as wild-type. Following the test of several point- and domain deletion mutants of BNIP3, we identified two domain deletion mutants with resistance to ULK1-induced BNIP3 protein stabilization. First, BNIP3 protein harboring a deletion of the transmembrane domain (ΔTM), which is required for integration of BNIP3 into the OMM, was relatively unaffected by ULK1 overexpression. This suggests that ULK1 may be stabilizing BNIP3 at the mitochondria following its integration into the OMM. Second, BNIP3 protein with a deleted "BH3" domain (ΔBH3) appeared resistant to the effects of ULK1 overexpression. Interestingly, the ΔBH3 form of BNIP3 exhibited increased protein levels relative to wild-type, as well as increased protein stability in the absence of ULK1. These results suggest that ULK1-induced stabilization of BNIP3 protein may rely on the BNIP3 "BH3" domain.

To further understand how the interaction of BNIP3 and ULK1 affected BNIP3 protein levels, we sought to determine which domain of ULK1 was required for the interaction. We found that the ULK1 C-terminal domain was required for the interaction of ULK1 with BNIP3. The ULK1 CTD is known to bind autophagy related proteins, including ATG13, suggesting that BNIP3 is yet another autophagy-related protein known to interact with ULK1.[58] Interestingly, overexpression of a CTD-null form of ULK1 (ΔCTD) failed to increase levels of BNIP3 protein, suggesting that the ability of ULK1 to bind BNIP3 is critical for its effect on BNIP3 stability.

Uncovering the domains of BNIP3 necessary for ULK1 binding requires additional study. We found that blocking S17 phosphorylation (S17A) resulted in increased binding to ULK1, while a phosphomimetic mutant of BNIP3 (S17E) interacted with ULK1 to a similar extent as wild-type. This interaction between S17 of BNIP3 and ULK1 almost certainly occurs at the N-terminal ULK1 kinase domain. Meanwhile, the ULK1 C-terminal domain appears to act as a docking domain to aid in substrate anchoring and specificity.[215] Preliminary results from our work suggest that the ULK1 CTD may, in part, interact with the BNIP3 “BH3” domain, as “BH3” deletion led to a slight decrease in BNIP3 and ULK1 interaction relative to wild-type. Importantly, combination of ΔBH3 and S17E mutation dramatically decreased the interaction of BNIP3 with ULK1, suggesting an additive effect. However, it is important to note that the combination of mutations did not fully ablate the interaction, and that additional BNIP3 domains may play a role in the interaction of BNIP3 with ULK1. To hypothesis that the ULK1 CTD may interact with multiple domains of BNIP3 is not unreasonable considering the size disparity between the ULK1 CTD and the cytosolic N-terminus of BNIP3 following integration into the OMM. Further work combining domain deletions of BNIP3 is necessary in order to fully understand the domains required for interaction with ULK1.

Under what cellular contexts does ULK1 phosphorylate and/or stabilize BNIP3?

Our study into the post-translational regulation of BNIP3 has uncovered two modes of BNIP3 regulation by the kinase ULK1. We show that ULK1 phosphorylates BNIP3 on S17, adjacent to its LIR motif, to promote its interaction with LC3 at the autophagosome. Additionally, ULK1 stabilizes BNIP3 protein by blocking its

proteasomal turnover, leading to increased BNIP3 protein levels. Taken together, we find that ULK1 has a dual effect on promoting BNIP3-induced mitophagy in response to hypoxia. While our endogenous studies were done in the context of hypoxia, the scope of cellular contexts under which ULK1 regulates BNIP3 remains unknown.

In addition to hypoxia, BNIP3 is known to be transcriptionally regulated by several other stress-related proteins including NF-κB, PPARα, FoxO3, and p53.[130,162–168] For many stress response proteins, transcriptional upregulation is accompanied by post-translational stabilization to increase the rapidity of stress response.[169] While performing our study, we sought to determine the contexts under which S17 is phosphorylated, which would also suggest ULK1 binding. To do so, we worked with a company to design a pS17-BNIP3 phospho-specific antibody, however this process has high rates of error and the final antibody did not recognize its epitope (data not shown). Therefore, we focused our attention on studying the effects of ULK1 inhibition on endogenous BNIP3 in response to the best characterized context of BNIP3 induction, hypoxia. We found that BNIP3 protein is stabilized by ULK1 binding, however whether and how BNIP3 stabilization occurs under additional cellular contexts has yet to be determined. Interestingly, ULK1 is also known to be regulated by a number of the same stress-related proteins as BNIP3. For example, PPARα and FoxO3 are known to transcriptionally upregulate both BNIP3 and ULK1.[224–226] Understanding the mechanisms of BNIP3 stabilization concurrent with transcriptional upregulation is critical to understanding its function as a stress response protein. Future studies will focus on whether ULK1 stabilizes BNIP3 under each of these contexts, or if other proteins perform similar roles under different contexts.

It also remains unclear whether BNIP3 competes with other autophagy-related proteins to bind the ULK1 CTD. Further study of ULK1 CTD interactors and their potential competition with BNIP3 may shed additional light onto the contexts in which ULK1 regulates BNIP3 stability. For example, the CTD is known to bind ATG13, which is a critical component of the ULK1 complex responsible for autophagy initiation. Whether both ATG13 and BNIP3 can interact with ULK1 simultaneously or if the interaction with either ATG13 or BNIP3 promotes general autophagy versus mitophagy, respectively, remains unknown. Simultaneous binding or separate pools of ULK1 binding either protein may be the most likely outcome, as ATG13 interaction with ULK1 is required for the clearance of depolarized mitochondria by autophagy.[81]

In addition to finding that the CTD is required for BNIP3 interaction, our work demonstrated an effect of the 14-most C-terminal amino acids (amino acids 1038-1051) of ULK1 on BNIP3 binding. Deletion of amino acids 1038-1051 of ULK1 resulted in an increase in the stabilization of BNIP3 as compared to wild-type ULK1, as well as an enhancement in the interaction of ULK1 and BNIP3 that could not be fully explained by the increase in BNIP3 protein levels. The final 14 amino acids of the ULK1 protein sequence are believed to be required for the inhibitory dominant negative autophagy function of ULK1 via the binding of an unknown protein.[58] These results suggest that this unknown protein competes with BNIP3 for ULK1 binding, as the presence of the unknown protein binding site decreases the interaction of BNIP3 with ULK1 (Figure 6.2). It is possible that this unknown protein interaction and the subsequent dominant negative function not only helps to decrease rates of autophagy following cessation of stress, but may also inhibit the interaction of ULK1 with BNIP3 in order to block BNIP3

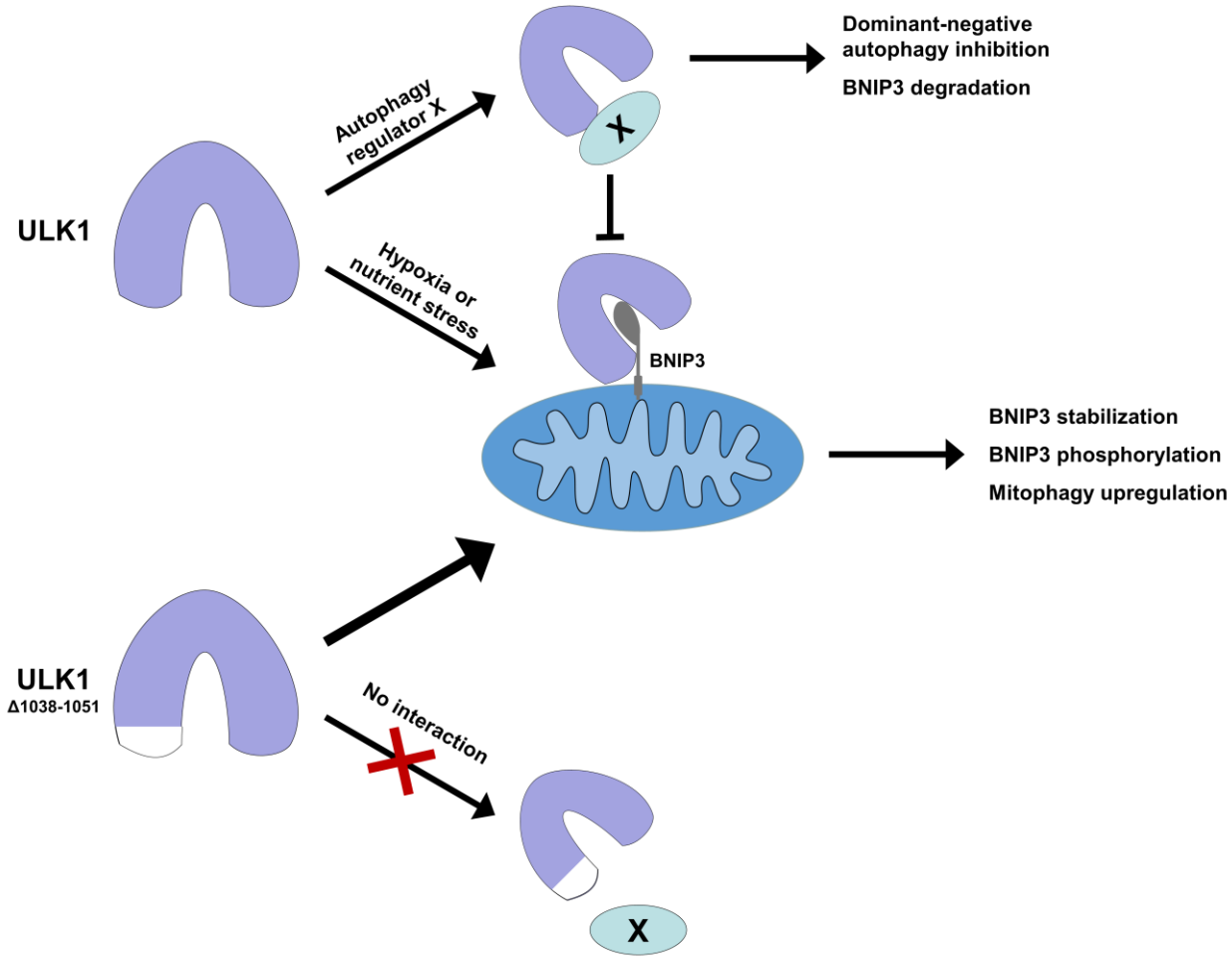

Figure 6.2: Model of competitive binding of ULK1 with either BNIP3 or unknown autophagy regulator protein X. Our work demonstrated that deletion of the last 14 amino acids of ULK1 (1038-1051) resulted in an increase in HA-BNIP3 protein levels relative to wild-type ULK1, as well as an increase in ULK1 and BNIP3 interaction beyond the increase in protein levels. 1038-1051 is thought to be the binding site for an unknown autophagy-regulating protein (X) which is responsible for the dominant-negative autophagy inhibitory function of ULK1. Our results suggest that BNIP3 and protein X may compete for ULK1 binding, and that the binding of ULK1 to protein X promotes BNIP3 protein degradation, possibly in the absence of stress.

stabilization and decrease protein levels in the absence of stress. Although outside of the scope of our current study, identifying the unknown protein that interacts with ULK1 amino acids 1038-1051 through a proteomics approach may shed additional light onto the contexts under which ULK1 stabilizes BNIP3 protein.

How is BNIP3 turned over at the proteasome?

Our work with proteasomal inhibitors indicates that like other stress response proteins, BNIP3 is constantly expressed at low levels in the absence of stress, followed by degradation at the proteasome. Upon hypoxic stress, BNIP3 protein is stabilized, likely via a mechanism dependent on the binding of the ULK1 CTD to BNIP3. However, the mechanism by which ULK1 blocks BNIP3 proteasomal turnover remains unknown.

BNIP3 and its homolog BNIP3L are tail-anchored proteins that do not possess N-terminal mitochondrial-targeting signal peptides. Instead, these proteins are post-translationally integrated into the OMM via a mechanism reliant on the positively charged residues flanking their moderately hydrophobic C-terminal transmembrane domains.[155,157,227] Many tail-anchored OMM proteins are known to be regulated by the ubiquitin proteasome system.[228] Parkin is one of several mitochondrial-associated E3 ubiquitin ligases, well known for its role in targeting depolarized mitochondria to the autophagosome.[101] However, studies have also demonstrated a role for parkin in stimulating the retrotranslocation, and subsequent proteasomal degradation, of mitochondrial proteins by the AAA-ATPase p97, through a process termed the mitochondrial-associated degradation system.[228–230]

Based on the evidence presented in this dissertation, we hypothesize that the binding of ULK1 to BNIP3 is blocking the retrotranslocation and subsequent degradation

of BNIP3 by limiting the access of p97 and E3 ubiquitin ligases to BNIP3 at the OMM. In addition to our evidence of ULK1 inhibition enhancing the proteasomal turnover of endogenous BNIP3 under hypoxia, we found that transmembrane domain-null (ΔTM) BNIP3, which is unable to integrate into the OMM, was relatively unaffected by ULK1-induced BNIP3 stabilization as compared to wild-type. These results suggest that ULK1-induced stabilization takes place at the surface of the OMM. Additionally, the large size of ULK1 (112 kDa) as compared to BNIP3 (21.4 kDa) would allow ULK1 binding to effectively hinder the interaction of BNIP3 with other binding partners, possibly including E3 ubiquitin ligases. Assessing potential interactions between BNIP3 and p97 or E3 ubiquitin ligases, and how these interactions regulate BNIP3 turnover will be the subject of future investigation.

In addition to understanding how ULK1 blocks the proteasomal turnover of BNIP3, future work must also determine the mechanism by which BNIP3 is targeted to the proteasome in the absence of ULK1. Our work suggests a novel function for the BNIP3 “BH3” domain in regulating this process. BNIP3 was originally identified as a “BH3-only” protein, however the purported BH3 domain of BNIP3 is poorly conserved.[137,141] The domain was originally believed to play a role in the interaction of BNIP3 with Bcl-2 and Bcl-XL, however these interactions instead rely on the BNIP3 N-terminus.[127] Our work demonstrates that deletion of the BNIP3 “BH3” domain increases BNIP3 protein levels and enhances BNIP3 stability. While “BH3” deletion appeared to increase the binding of BNIP3 to LC3, this observation was simply the result of increased protein levels, meaning loss of the “BH3” domain did not affect the affinity of BNIP3 to bind LC3. These observations set forth a model in which the BH3 domain

limits mitophagy by promoting the proteasomal turnover of BNIP3. Consistent with a role in proteasomal turnover, BNIP3 lacking a “BH3” domain was also resistant to ULK1-induced BNIP3 stabilization. At this time, it is not clear how the “BH3” domain promotes the proteasomal degradation of BNIP3, however there are two lysine residues (at positions 111 and 112) located within the domain. It is possible that these residues may be subject to ubiquitination or SUMOylation to promote BNIP3 turnover, however preliminary results have yielded no supporting evidence (data not shown). Dissecting the mechanism of BNIP3 targeting to the proteasome, and which E3 ligases are responsible will be the focus of future studies.

Do effects on mitophagy and BNIP3 protein levels impact the clinical success of co-treatment with mTORC1 and ULK1 inhibitors?

The mechanistic target of rapamycin complex 1 (mTORC1) is considered a principal regulator of cell metabolism and growth, coordinating signals from a variety of upstream pathways in response to changes in nutrient-, oxygen-, and growth factor status.[231] Due to its importance in cell growth and proliferation, aberrant expression of upstream regulators leading to the constitutive activation of mTORC1 has been reported in a wide variety of solid tumors.[216] Therefore, drugs that selectively bind to and inhibit mTORC1 were anticipated to elicit an anti-tumor effect by hindering cell metabolism and lipid and protein synthesis. Sadly, first-generation mTORC1 allosteric inhibitors, broadly called “rapalogs”, were generally cytostatic instead of cytotoxic, and tumors often regrew upon cessation of treatment.[232] This was believed to be due to their inability to completely inhibit mTOR signaling, which led to the development of ATP-competitive inhibitors of mTOR. These drugs are often called PI3K/mTOR inhibitors, as they are

also known to inhibit PI3K due to high sequence homology in the hinge region of each kinase.[233] A number of PI3K/mTOR inhibitors appeared promising in pre-clinical studies, however clinical trial results have been mixed.[216] For example, a phase I/II trial of the PI3K/mTOR inhibitor BEZ235 was ended early due to toxicity and lack of clinical efficacy. In fact, patients had shorter progression-free survival and trended toward shorter overall survival as compared to patients treated with the rapalog Everolimus.[218] The PI3K/mTOR inhibitor PF-0469152 also demonstrated limitations when tested in a variety of solid tumors. While PI3K was down-regulated, no objective tumor response was observed.[217]

Some groups have hypothesized that the failure of ATP-competitive mTOR inhibitors in the clinic may actually be due to the upregulation of autophagy in response to mTOR inhibition. Autophagy plays a paradoxical role in the stages of tumorigenesis. During transformation and tumor initiation, autophagy is upregulated in response to oxidative stress, which limits genomic instability and suppresses transformation.[234] However, during malignant progression, autophagy is utilized to meet the metabolic demands of the cell, as well as support anoikis resistance and dormancy.[234] mTOR regulates autophagy via the phosphorylation of ULK1 (at S757) and ATG13, which represses the activity of the ULK1 complex responsible for autophagy initiation.[3,86] At least seven ULK1 inhibitors have been developed since 2015, including ULK-101 and SBI-0206965.[59,100] Recent work has demonstrated that treatment of nutrient-deprived cells with mTOR inhibitors resulted the upregulation of autophagy, leading to cell survival.[59] However, co-treatment of the same nutrient-deprived cells with both mTOR

and ULK1 selective inhibitors blocked the upregulation of autophagy, inducing cell death.[59]

While these early co-treatment results appear promising, the extent to which the cell death-inducing effects of ULK1 inhibition are due to specific effects on mitophagy as opposed to general autophagy remains unknown. Our work, in combination with work on FUNDC1 and Bcl2-L-13, support an emerging role for ULK1 in specifically upregulating mitophagy as opposed to general autophagy in nutrient stressed cells. Further work should be done to determine if the survival of cells treated with mTOR inhibitors alone is due to the specific upregulation of mitophagy by ULK1 as opposed to upregulation of general autophagy. Understanding the importance of mitochondrial mass, mitochondrial function, and mitophagy to the survival of mTOR inhibitor-treated cells may yield additional drug targets for co-treatment in the event that co-treatment with mTOR and ULK1 inhibitors is toxic or fails to induce cell death in the context of specific tumor types.

Finally, it is also important to note that our findings indicate that ULK1 inhibition results in increased turnover of BNIP3. Initial work studying co-treatment with mTOR and ULK1 inhibitors has focused on the apparent synthetic lethality observed in nutrient-deprived cells. The effects of BNIP3 loss in healthy cells co-treated with mTOR and ULK1 inhibitors remains unknown. Work from our lab and others has demonstrated that BNIP3 acts as a growth-suppressor, and loss of BNIP3 promotes tumor growth and metastasis.[131] BNIP3 expression is commonly disrupted in a number of human malignancies, including liver, gastric, and pancreatic cancer.[201,205,206] BNIP3 is also known to play important roles in the liver, and how downregulation of BNIP3 via

inhibition of ULK1 will affect liver homeostasis remains unknown.[128,172] Additionally, unpublished work from our lab has indicated that BNIP3 may have mitophagy-independent functions and that these functions may play a role in the growth-suppressive phenotype of BNIP3-expressing cells. Therefore, due to the potential of metabolic or tumorigenic effects of BNIP3 loss following treatment with ULK1 inhibitors, future investigation should focus on the effects of co-treatment with mTOR and ULK1 inhibitors on healthy, nutrient abundant tissues, with a particular focus on the liver.

REFERENCES

1. Galluzzi, L. *et al.* Molecular definitions of autophagy and related processes. *EMBO J.* **36**, 1811–1836 (2017).
2. Dikic, I. & Elazar, Z. Mechanism and medical implications of mammalian autophagy. *Nat. Rev. Mol. Cell Biol.* **19**, 349–364 (2018).
3. Kim, J., Kundu, M., Viollet, B. & Guan, K.-L. AMPK and mTOR regulate autophagy through direct phosphorylation of Ulk1. *Nat. Cell Biol.* **13**, 132–141 (2011).
4. Lee, J. W., Park, S., Takahashi, Y. & Wang, H.-G. The Association of AMPK with ULK1 Regulates Autophagy. *PLOS ONE* **5**, e15394 (2010).
5. Hurley, J. H. & Young, L. N. Mechanisms of Autophagy Initiation. *Annu. Rev. Biochem.* **86**, 225–244 (2017).
6. Hamasaki, M. *et al.* Autophagosomes form at ER–mitochondria contact sites. *Nature* **495**, 389–393 (2013).
7. Nascimbeni, A. C. *et al.* ER–plasma membrane contact sites contribute to autophagosome biogenesis by regulation of local PI3P synthesis. *EMBO J.* **36**, 2018–2033 (2017).
8. Abada, A. & Elazar, Z. Getting ready for building: signaling and autophagosome biogenesis. *EMBO Rep.* **15**, 839–852 (2014).
9. Kohler, V., Aufschnaiter, A. & Büttner, S. Closing the Gap: Membrane Contact Sites in the Regulation of Autophagy. *Cells* **9**, (2020).
10. Russell, R. C. *et al.* ULK1 induces autophagy by phosphorylating Beclin-1 and activating VPS34 lipid kinase. *Nat. Cell Biol.* **15**, 741–750 (2013).
11. Wold, M. S., Lim, J., Lachance, V., Deng, Z. & Yue, Z. ULK1-mediated phosphorylation of ATG14 promotes autophagy and is impaired in Huntington's disease models. *Mol. Neurodegener.* **11**, (2016).

12. Kihara, A., Noda, T., Ishihara, N. & Ohsumi, Y. Two Distinct Vps34 Phosphatidylinositol 3–Kinase Complexes Function in Autophagy and Carboxypeptidase Y Sorting inSaccharomyces cerevisiae. *J. Cell Biol.* **152**, 519–530 (2001).

13. Polson, H. E. J. *et al.* Mammalian Atg18 (WIPI2) localizes to omegasome-anchored phagophores and positively regulates LC3 lipidation. *Autophagy* **6**, 506–522 (2010).

14. Kaiser, S. E. *et al.* Noncanonical E2 recruitment by the autophagy E1 revealed by Atg7–Atg3 and Atg7–Atg10 structures. *Nat. Struct. Mol. Biol.* **19**, 1242–1249 (2012).

15. Kuma, A., Mizushima, N., Ishihara, N. & Ohsumi, Y. Formation of the ~350-kDa Apg12-Apg5·Apg16 Multimeric Complex, Mediated by Apg16 Oligomerization, Is Essential for Autophagy in Yeast *. *J. Biol. Chem.* **277**, 18619–18625 (2002).

16. Shpilka, T., Weidberg, H., Pietrokovski, S. & Elazar, Z. Atg8: an autophagy-related ubiquitin-like protein family. *Genome Biol.* **12**, 226 (2011).

17. Weidberg, H., Shvets, E. & Elazar, Z. Biogenesis and Cargo Selectivity of Autophagosomes. *Annu. Rev. Biochem.* **80**, 125–156 (2011).

18. Yang, A., Li, Y., Pantoom, S., Triola, G. & Wu, Y.-W. Semisynthetic Lipidated LC3 Protein Mediates Membrane Fusion. *ChemBioChem* **14**, 1296–1300 (2013).

19. Xie, Z., Nair, U. & Klionsky, D. J. Atg8 Controls Phagophore Expansion during Autophagosome Formation. *Mol. Biol. Cell* **19**, 3290–3298 (2008).

20. Orsi, A. *et al.* Dynamic and transient interactions of Atg9 with autophagosomes, but not membrane integration, are required for autophagy. *Mol. Biol. Cell* **23**, 1860–1873 (2012).

21. Manil-Ségalen, M. *et al.* The C. elegans LC3 Acts Downstream of GABARAP to Degrade Autophagosomes by Interacting with the HOPS Subunit VPS39. *Dev. Cell* **28**, 43–55 (2014).

22. Olsvik, H. L. *et al.* FYCO1 Contains a C-terminally Extended, LC3A/B-preferring LC3-interacting Region (LIR) Motif Required for Efficient Maturation of Autophagosomes during Basal Autophagy. *J. Biol. Chem.* **290**, 29361–29374 (2015).

23. Nakatogawa, H., Ishii, J., Asai, E. & Ohsumi, Y. Atg4 recycles inappropriately lipidated Atg8 to promote autophagosome biogenesis. *Autophagy* **8**, 177–186 (2012).

24. Diao, J. *et al.* ATG14 promotes membrane tethering and fusion of autophagosomes to endolysosomes. *Nature* **520**, 563–566 (2015).

25. Itakura, E., Kishi-Itakura, C. & Mizushima, N. The Hairpin-type Tail-Anchored SNARE Syntaxin 17 Targets to Autophagosomes for Fusion with Endosomes/Lysosomes. *Cell* **151**, 1256–1269 (2012).

26. Bowman, E. J., Siebers, A. & Altendorf, K. Bafilomycins: a class of inhibitors of membrane ATPases from microorganisms, animal cells, and plant cells. *Proc. Natl. Acad. Sci. U. S. A.* **85**, 7972–7976 (1988).

27. Liang, X. H. *et al.* Induction of autophagy and inhibition of tumorigenesis by beclin 1. *Nature* **402**, 672–676 (1999).

28. Goldsmith, J., Levine, B. & Debnath, J. Autophagy and Cancer Metabolism. *Methods Enzymol.* **542**, 25–57 (2014).

29. Tam, S. Y., Wu, V. W. C. & Law, H. K. W. Hypoxia-Induced Epithelial-Mesenchymal Transition in Cancers: HIF-1α and Beyond. *Front. Oncol.* **10**, (2020).

30. Catalano, M. *et al.* Autophagy induction impairs migration and invasion by reversing EMT in glioblastoma cells. *Mol. Oncol.* **9**, 1612–1625 (2015).

31. Lv, Q. *et al.* DEDD Interacts with PI3KC3 to Activate Autophagy and Attenuate Epithelial–Mesenchymal Transition in Human Breast Cancer. *Cancer Res.* **72**, 3238–3250 (2012).

32. Qiang, L. *et al.* Regulation of cell proliferation and migration by p62 through stabilization of Twist1. *Proc. Natl. Acad. Sci. U. S. A.* **111**, 9241–9246 (2014).

33. Peng, Y.-F. *et al.* Autophagy inhibition suppresses pulmonary metastasis of HCC in mice via impairing anoikis resistance and colonization of HCC cells. *Autophagy* **9**, 2056–2068 (2013).

34. Cai, Q., Yan, L. & Xu, Y. Anoikis resistance is a critical feature of highly aggressive ovarian cancer cells. *Oncogene* **34**, 3315–3324 (2015).

35. Sharifi, M. N. *et al.* Autophagy Promotes Focal Adhesion Disassembly and Cell Motility of Metastatic Tumor Cells through the Direct Interaction of Paxillin with LC3. *Cell Rep.* **15**, 1660–1672 (2016).

36. Sandilands, E. *et al.* Autophagic targeting of Src promotes cancer cell survival following reduced FAK signalling. *Nat. Cell Biol.* **14**, 51–60 (2012).

37. Guo, J. Y. *et al.* Activated Ras requires autophagy to maintain oxidative metabolism and tumorigenesis. *Genes Dev.* **25**, 460–470 (2011).

38. Zou, Z. *et al.* Aurora kinase A inhibition-induced autophagy triggers drug resistance in breast cancer cells. *Autophagy* **8**, 1798–1810 (2012).

39. Galluzzi, L., Bravo-San Pedro, J. M., Demaria, S., Formenti, S. C. & Kroemer, G. Activating autophagy to potentiate immunogenic chemotherapy and radiation therapy. *Nat. Rev. Clin. Oncol.* **14**, 247–258 (2017).

40. Hu, Y.-L., Jahangiri, A., DeLay, M. & Aghi, M. K. Tumor cell autophagy as an adaptive response mediating resistance to treatments like anti-angiogenic therapy. *Cancer Res.* **72**, 4294–4299 (2012).

41. Michaud, M. *et al.* Autophagy-Dependent Anticancer Immune Responses Induced by Chemotherapeutic Agents in Mice. *Science* **334**, 1573–1577 (2011).

42. Martins, I. *et al.* Premortem autophagy determines the immunogenicity of chemotherapy-induced cancer cell death. *Autophagy* **8**, 413–415 (2012).

43. Michaud, M. *et al.* An autophagy-dependent anticancer immune response determines the efficacy of melanoma chemotherapy. *Oncoimmunology* **3**, (2014).

44. Wong, P.-M., Puente, C., Ganley, I. G. & Jiang, X. The ULK1 complex. *Autophagy* **9**, 124–137 (2013).

45. Tsukada, M. & Ohsumi, Y. Isolation and characterization of autophagy-defective mutants of Saccharomyces cerevisiae. *FEBS Lett.* **333**, 169–174 (1993).

46. Thumm, M. *et al.* Isolation of autophagocytosis mutants of Saccharomyces cerevisiae. *FEBS Lett.* **349**, 275–280 (1994).

47. Harding, T. M., Morano, K. A., Scott, S. V. & Klionsky, D. J. Isolation and characterization of yeast mutants in the cytoplasm to vacuole protein targeting pathway. *J. Cell Biol.* **131**, 591–602 (1995).

48. Hara, T. *et al.* FIP200, a ULK-interacting protein, is required for autophagosome formation in mammalian cells. *J. Cell Biol.* **181**, 497–510 (2008).

49. Yorimitsu, T. & Klionsky, D. J. Atg11 Links Cargo to the Vesicle-forming Machinery in the Cytoplasm to Vacuole Targeting Pathway. *Mol. Biol. Cell* **16**, 1593–1605 (2005).

50. Cheong, H. *et al.* Atg17 Regulates the Magnitude of the Autophagic Response. *Mol. Biol. Cell* **16**, 3438–3453 (2005).

51. Kabeya, Y. *et al.* Atg17 Functions in Cooperation with Atg1 and Atg13 in Yeast Autophagy. *Mol. Biol. Cell* **16**, 2544–2553 (2005).

52. Kabeya, Y. *et al.* Characterization of the Atg17–Atg29–Atg31 complex specifically required for starvation-induced autophagy in Saccharomyces cerevisiae. *Biochem. Biophys. Res. Commun.* **389**, 612–615 (2009).

53. Jao, C. C., Ragusa, M. J., Stanley, R. E. & Hurley, J. H. A HORMA domain in Atg13 mediates PI 3-kinase recruitment in autophagy. *Proc. Natl. Acad. Sci.* **110**, 5486–5491 (2013).

54. Suzuki, H., Kaizuka, T., Mizushima, N. & Noda, N. N. Structure of the Atg101–Atg13 complex reveals essential roles of Atg101 in autophagy initiation. *Nat. Struct. Mol. Biol.* **22**, 572–580 (2015).

55. Michel, M. *et al.* The mammalian autophagy initiator complex contains 2 HORMA domain proteins. *Autophagy* **11**, 2300–2308 (2015).

56. Qi, S., Kim, D. J., Stjepanovic, G. & Hurley, J. H. Structure of the Human Atg13-Atg101 HORMA Heterodimer: an Interaction Hub within the ULK1 Complex. *Structure* **23**, 1848–1857 (2015).

57. Yan, J. *et al.* Identification of Mouse ULK1, a Novel Protein Kinase Structurally Related toC. elegansUNC-51. *Biochem. Biophys. Res. Commun.* **246**, 222–227 (1998).

58. Chan, E. Y. W., Longatti, A., McKnight, N. C. & Tooze, S. A. Kinase-Inactivated ULK Proteins Inhibit Autophagy via Their Conserved C-Terminal Domains Using an Atg13-Independent Mechanism. *Mol. Cell. Biol.* **29**, 157–171 (2009).

59. Egan, D. F. *et al.* Small Molecule Inhibition of the Autophagy Kinase ULK1 and Identification of ULK1 Substrates. *Mol. Cell* **59**, 285–297 (2015).

60. Miller, M. L. *et al.* Linear Motif Atlas for Phosphorylation-Dependent Signaling. *Sci. Signal.* **1**, ra2–ra2 (2008).

61. Turk, B. E. Understanding and exploiting substrate recognition by protein kinases. *Curr. Opin. Chem. Biol.* **12**, 4–10 (2008).

62. Zachari, M. & Ganley, I. G. The mammalian ULK1 complex and autophagy initiation. *Essays Biochem.* **61**, 585–596 (2017).

63. Shang, L. *et al.* Nutrient starvation elicits an acute autophagic response mediated by Ulk1 dephosphorylation and its subsequent dissociation from AMPK. *Proc. Natl. Acad. Sci.* **108**, 4788–4793 (2011).

64. Alemu, E. A. *et al.* ATG8 Family Proteins Act as Scaffolds for Assembly of the ULK Complex. *J. Biol. Chem.* **287**, 39275–39290 (2012).

65. Kraft, C. *et al.* Binding of the Atg1/ULK1 kinase to the ubiquitin-like protein Atg8 regulates autophagy. *EMBO J.* **31**, 3691–3703 (2012).

66. Okazaki, N. *et al.* Interaction of the Unc-51-like kinase and microtubule-associated protein light chain 3 related proteins in the brain: possible role of vesicular transport in axonal elongation. *Mol. Brain Res.* **85**, 1–12 (2000).

67. Ragusa, M. J., Stanley, R. E. & Hurley, J. H. Architecture of the Atg17 Complex as a Scaffold for Autophagosome Biogenesis. *Cell* **151**, 1501–1512 (2012).

68. Fujioka, Y. *et al.* Structural basis of starvation-induced assembly of the autophagy initiation complex. *Nat. Struct. Mol. Biol.* **21**, 513–521 (2014).

69. Stjepanovic, G. *et al.* Assembly and dynamics of the autophagy-initiating Atg1 complex. *Proc. Natl. Acad. Sci.* **111**, 12793–12798 (2014).

70. Herzig, S. & Shaw, R. J. AMPK: guardian of metabolism and mitochondrial homeostasis. *Nat. Rev. Mol. Cell Biol.* **19**, 121–135 (2018).

71. Lin, M. G. & Hurley, J. H. Structure and Function of the ULK1 Complex in Autophagy. *Curr. Opin. Cell Biol.* **39**, 61–68 (2016).

72. Egan, D. F. *et al.* Phosphorylation of ULK1 (hATG1) by AMP-Activated Protein Kinase Connects Energy Sensing to Mitophagy. *Science* **331**, 456–461 (2011).

73. Mack, H. I. D., Zheng, B., Asara, J. M. & Thomas, S. M. AMPK-dependent phosphorylation of ULK1 regulates ATG9 localization. *Autophagy* **8**, 1197–1214 (2012).

74. Condon, K. J. & Sabatini, D. M. Nutrient regulation of mTORC1 at a glance. *J. Cell Sci.* **132**, (2019).

75. Yeh, Y.-Y., Wrasman, K. & Herman, P. K. Autophosphorylation Within the Atg1 Activation Loop Is Required for Both Kinase Activity and the Induction of Autophagy in Saccharomyces cerevisiae. *Genetics* **185**, 871–882 (2010).

76. Kijanska, M. *et al.* Activation of Atg1 kinase in autophagy by regulated phosphorylation. *Autophagy* **6**, 1168–1178 (2010).

77. Lazarus, M. B., Novotny, C. J. & Shokat, K. M. Structure of the Human Autophagy Initiating Kinase ULK1 in Complex with Potent Inhibitors. *ACS Chem. Biol.* **10**, 257–261 (2015).

78. Bach, M., Larance, M., James, D. E. & Ramm, G. The serine/threonine kinase ULK1 is a target of multiple phosphorylation events. *Biochem. J.* **440**, 283–291 (2011).

79. Lin, S.-Y. *et al.* GSK3-TIP60-ULK1 Signaling Pathway Links Growth Factor Deprivation to Autophagy. *Science* **336**, 477–481 (2012).

80. Zhou, X. *et al.* Unc-51-like kinase 1/2-mediated endocytic processes regulate filopodia extension and branching of sensory axons. *Proc. Natl. Acad. Sci.* **104**, 5842–5847 (2007).

81. Joo, J. H. *et al.* Hsp90-Cdc37 Chaperone Complex Regulates Ulk1- and Atg13-Mediated Mitophagy. *Mol. Cell* **43**, 572–585 (2011).

82. Liu, C.-C. *et al.* Cul3-KLHL20 Ubiquitin Ligase Governs the Turnover of ULK1 and VPS34 Complexes to Control Autophagy Termination. *Mol. Cell* **61**, 84–97 (2016).

83. Nazio, F. *et al.* Fine-tuning of ULK1 mRNA and protein levels is required for autophagy oscillation. *J. Cell Biol.* **215**, 841–856 (2016).

84. Ganley, I. G. *et al.* ULK1·ATG13·FIP200 Complex Mediates mTOR Signaling and Is Essential for Autophagy. *J. Biol. Chem.* **284**, 12297–12305 (2009).

85. Jung, C. H. *et al.* ULK-Atg13-FIP200 Complexes Mediate mTOR Signaling to the Autophagy Machinery. *Mol. Biol. Cell* **20**, 1992–2003 (2009).

86. Hosokawa, N. *et al.* Nutrient-dependent mTORC1 Association with the ULK1–Atg13–FIP200 Complex Required for Autophagy. *Mol. Biol. Cell* **20**, 1981–1991 (2009).

87. Di Bartolomeo, S. *et al.* The dynamic interaction of AMBRA1 with the dynein motor complex regulates mammalian autophagy. *J. Cell Biol.* **191**, 155–168 (2010).

88. Young, A. R. J. *et al.* Starvation and ULK1-dependent cycling of mammalian Atg9 between the TGN and endosomes. *J. Cell Sci.* **119**, 3888–3900 (2006).

89. Pengo, N., Agrotis, A., Prak, K., Jones, J. & Ketteler, R. A reversible phospho-switch mediated by ULK1 regulates the activity of autophagy protease ATG4B. *Nat. Commun.* **8**, 294 (2017).

90. Petherick, K. J. *et al.* Pharmacological Inhibition of ULK1 Kinase Blocks Mammalian Target of Rapamycin (mTOR)-dependent Autophagy. *J. Biol. Chem.* **290**, 11376–11383 (2015).

91. Honda, S. *et al.* Ulk1-mediated Atg5-independent macroautophagy mediates elimination of mitochondria from embryonic reticulocytes. *Nat. Commun.* **5**, 4004 (2014).

92. Wu, W. *et al.* ULK1 translocates to mitochondria and phosphorylates FUNDC1 to regulate mitophagy. *EMBO Rep.* **15**, 566–575 (2014).

93. Lazarou, M. *et al.* The ubiquitin kinase PINK1 recruits autophagy receptors to induce mitophagy. *Nature* **524**, 309–314 (2015).

94. Henckaerts, L. *et al.* Genetic variation in the autophagy gene ULK1 and risk of Crohn's disease. *Inflamm. Bowel Dis.* **17**, 1392–1397 (2011).

95. Pike, L. R. G. *et al.* Transcriptional up-regulation of ULK1 by ATF4 contributes to cancer cell survival. *Biochem. J.* **449**, 389–400 (2012).

96. ZOU, Y. *et al.* High expression levels of unc-51-like kinase 1 as a predictor of poor prognosis in colorectal cancer. *Oncol. Lett.* **10**, 1583–1588 (2015).

97. Yun, M. *et al.* ULK1: A Promising Biomarker in Predicting Poor Prognosis and Therapeutic Response in Human Nasopharygeal Carcinoma. *PLOS ONE* **10**, e0117375 (2015).

98. Chen, M.-B. *et al.* Ulk1 over-expression in human gastric cancer is correlated with patients' T classification and cancer relapse. *Oncotarget* **8**, 33704–33712 (2017).

99. Tang, J. *et al.* Low expression of ULK1 is associated with operable breast cancer progression and is an adverse prognostic marker of survival for patients. *Breast Cancer Res. Treat.* **134**, 549–560 (2012).

100. Martin, K. R. *et al.* A Potent and Selective ULK1 Inhibitor Suppresses Autophagy and Sensitizes Cancer Cells to Nutrient Stress. *iScience* **8**, 74–84 (2018).

101. Poole, L. P. & Macleod, K. F. Mitophagy in tumorigenesis and metastasis. *Cell. Mol. Life Sci.* **78**, 3817–3851 (2021).

102. Harper, J. W., Ordureau, A. & Heo, J.-M. Building and decoding ubiquitin chains for mitophagy. *Nat. Rev. Mol. Cell Biol.* **19**, 93–108 (2018).

103. Villa, E. *et al.* Parkin-Independent Mitophagy Controls Chemotherapeutic Response in Cancer Cells. *Cell Rep.* **20**, 2846–2859 (2017).

104. Yun, J. *et al.* MUL1 acts in parallel to the PINK1/parkin pathway in regulating mitofusin and compensates for loss of PINK1/parkin. *eLife* **3**, e01958 (2014).

105. Rojansky, R., Cha, M.-Y. & Chan, D. C. Elimination of paternal mitochondria in mouse embryos occurs through autophagic degradation dependent on PARKIN and MUL1. *eLife* **5**, e17896 (2016).

106. Chen, Z. *et al.* Mitochondrial E3 ligase MARCH5 regulates FUNDC1 to fine-tune hypoxic mitophagy. *EMBO Rep.* **18**, 495–509 (2017).

107. Geisler, S. *et al.* PINK1/Parkin-mediated mitophagy is dependent on VDAC1 and p62/SQSTM1. *Nat. Cell Biol.* **12**, 119–131 (2010).

108. Chen, Y. & Dorn, G. W. PINK1- Phosphorylated Mitofusin 2 is a Parkin Receptor for Culling Damaged Mitochondria. *Science* **340**, 471–475 (2013).

109. Sarraf, S. A. *et al.* Landscape of the PARKIN-dependent ubiquitylome in response to mitochondrial depolarization. *Nature* **496**, 372–376 (2013).

110. Jin, S. M. & Youle, R. J. The accumulation of misfolded proteins in the mitochondrial matrix is sensed by PINK1 to induce PARK2/Parkin-mediated mitophagy of polarized mitochondria. *Autophagy* **9**, 1750–1757 (2013).

111. Fiesel, F. C., James, E. D., Hudec, R. & Springer, W. Mitochondrial targeted HSP90 inhibitor Gamitrinib-TPP (G-TPP) induces PINK1/Parkin-dependent mitophagy. *Oncotarget* **8**, 106233–106248 (2017).

112. Schwarten, M. *et al.* Nix directly binds to GABARAP: a possible crosstalk between apoptosis and autophagy. *Autophagy* **5**, 690–698 (2009).

113. Novak, I. *et al.* Nix is a selective autophagy receptor for mitochondrial clearance. *EMBO Rep.* **11**, 45–51 (2010).

114. Hanna, R. A. *et al.* Microtubule-associated Protein 1 Light Chain 3 (LC3) Interacts with Bnip3 Protein to Selectively Remove Endoplasmic Reticulum and Mitochondria via Autophagy. *J. Biol. Chem.* **287**, 19094–19104 (2012).

115. Marinković, M., Šprung, M. & Novak, I. Dimerization of mitophagy receptor BNIP3L/NIX is essential for recruitment of autophagic machinery. *Autophagy* **0**, 1–12 (2020).

116. Ohi, N. *et al.* A novel adenovirus E1B19K-binding protein B5 inhibits apoptosis induced by Nip3 by forming a heterodimer through the C-terminal hydrophobic region. *Cell Death Differ.* **6**, 314–325 (1999).

117. Guo, K. *et al.* Hypoxia induces the expression of the pro-apoptotic gene BNIP3. *Cell Death Differ.* **8**, 367–376 (2001).

118. Dayan, F., Roux, D., Brahimi-Horn, M. C., Pouyssegur, J. & Mazure, N. M. The oxygen sensor factor-inhibiting hypoxia-inducible factor-1 controls expression of distinct genes through the bifunctional transcriptional character of hypoxia-inducible factor-1alpha. *Cancer Res.* **66**, 3688–3698 (2006).

119. Zhang, T. *et al.* BNIP3 Protein Suppresses PINK1 Kinase Proteolytic Cleavage to Promote Mitophagy. *J. Biol. Chem.* **291**, 21616–21629 (2016).

120. Ding, W.-X. *et al.* Nix Is Critical to Two Distinct Phases of Mitophagy, Reactive Oxygen Species-mediated Autophagy Induction and Parkin-Ubiquitin-p62-mediated Mitochondrial Priming. *J. Biol. Chem.* **285**, 27879–27890 (2010).

121. Gao, F. *et al.* The mitochondrial protein BNIP3L is the substrate of PARK2 and mediates mitophagy in PINK1/PARK2 pathway. *Hum. Mol. Genet.* **24**, 2528–2538 (2015).

122. Liu, J. *et al.* Parkin targets HIF-1α for ubiquitination and degradation to inhibit breast tumor progression. *Nat. Commun.* **8**, 1823 (2017).

123. Li, C. *et al.* PINK1 and PARK2 Suppress Pancreatic Tumorigenesis through Control of Mitochondrial Iron-Mediated Immunometabolism. *Dev. Cell* **46**, 441-455.e8 (2018).

124. Liu, L. *et al.* Mitochondrial outer-membrane protein FUNDC1 mediates hypoxia-induced mitophagy in mammalian cells. *Nat. Cell Biol.* **14**, 177–185 (2012).

125. Chen, G. *et al.* A regulatory signaling loop comprising the PGAM5 phosphatase and CK2 controls receptor-mediated mitophagy. *Mol. Cell* **54**, 362–377 (2014).

126. Wu, W. *et al.* FUNDC1 regulates mitochondrial dynamics at the ER–mitochondrial contact site under hypoxic conditions. *EMBO J.* **35**, 1368–1384 (2016).

127. Boyd, J. M. *et al.* Adenovirus E1B 19 kDa and Bcl-2 proteins interact with a common set of cellular proteins. *Cell* **79**, 341–351 (1994).

128. Glick, D. *et al.* BNip3 Regulates Mitochondrial Function and Lipid Metabolism in the Liver. *Mol. Cell. Biol.* **32**, 2570–2584 (2012).

129. Rikka, S. *et al.* Bnip3 impairs mitochondrial bioenergetics and stimulates mitochondrial turnover. *Cell Death Differ.* **18**, 721–731 (2011).

130. Tracy, K. *et al.* BNIP3 Is an RB/E2F Target Gene Required for Hypoxia-Induced Autophagy. *Mol. Cell. Biol.* **27**, 6229–6242 (2007).

131. Chourasia, A. H. *et al.* Mitophagy defects arising from BNip3 loss promote mammary tumor progression to metastasis. *EMBO Rep.* **16**, 1145–1163 (2015).

132. Ray, R. *et al.* BNIP3 heterodimerizes with Bcl-2/Bcl-X(L) and induces cell death independent of a Bcl-2 homology 3 (BH3) domain at both mitochondrial and nonmitochondrial sites. *J. Biol. Chem.* **275**, 1439–1448 (2000).

133. Zhu, Y. *et al.* Modulation of Serines 17 and 24 in the LC3-interacting Region of Bnip3 Determines Pro-survival Mitophagy versus Apoptosis. *J. Biol. Chem.* **288**, 1099–1113 (2013).

134. Birgisdottir, Å. B., Lamark, T. & Johansen, T. The LIR motif – crucial for selective autophagy. *J. Cell Sci.* **126**, 3237–3247 (2013).

135. Rogov, V. V. *et al.* Phosphorylation of the mitochondrial autophagy receptor Nix enhances its interaction with LC3 proteins. *Sci. Rep.* **7**, 1131 (2017).

136. Kuang, Y. *et al.* Structural basis for the phosphorylation of FUNDC1 LIR as a molecular switch of mitophagy. *Autophagy* **12**, 2363–2373 (2016).

137. Chen, G. *et al.* The E1B 19K/Bcl-2–binding Protein Nip3 is a Dimeric Mitochondrial Protein that Activates Apoptosis. *J. Exp. Med.* **186**, 1975–1983 (1997).

138. Rogers, S., Wells, R. & Rechsteiner, M. Amino acid sequences common to rapidly degraded proteins: the PEST hypothesis. *Science* **234**, 364–368 (1986).

139. Rechsteiner, M. & Rogers, S. W. PEST sequences and regulation by proteolysis. *Trends Biochem. Sci.* **21**, 267–271 (1996).

140. Park, C. W. *et al.* BNIP3 is degraded by ULK1-dependent autophagy via MTORC1 and AMPK. *Autophagy* **9**, 345–360 (2013).

141. Lomonosova, E. & Chinnadurai, G. BH3-only proteins in apoptosis and beyond: an overview. *Oncogene* **27**, S2-19 (2008).

142. Day, C. L. *et al.* Structure of the BH3 Domains from the p53-Inducible BH3-Only Proteins Noxa and Puma in Complex with Mcl-1. *J. Mol. Biol.* **380**, 958–971 (2008).

143. Giam, M., Huang, D. C. S. & Bouillet, P. BH3-only proteins and their roles in programmed cell death. *Oncogene* **27**, S128–S136 (2008).

144. Cizeau, J., Ray, R., Chen, G., Gietz, R. D. & Greenberg, A. H. The C. elegans orthologue ceBNIP3 interacts with CED-9 and CED-3 but kills through a BH3- and caspase-independent mechanism. *Oncogene* **19**, 5453–5463 (2000).

145. Yasuda, M., Theodorakis, P., Subramanian, T. & Chinnadurai, G. Adenovirus E1B-19K/BCL-2 Interacting Protein BNIP3 Contains a BH3 Domain and a Mitochondrial Targeting Sequence*. *J. Biol. Chem.* **273**, 12415–12421 (1998).

146. Egan, B. *et al.* Targeting of tail-anchored proteins to yeast mitochondria in vivo. *FEBS Lett.* **451**, 243–248 (1999).

147. Masaki, R., Kameyama, K. & Yamamoto, A. Post-Translational Targeting of a Tail-Anchored Green Fluorescent Protein to the Endolpasmic Reticulum. *J. Biochem. (Tokyo)* **134**, 415–426 (2003).

148. Mullen, R. T. & Trelease, R. N. The Sorting Signals for Peroxisomal Membrane-bound Ascorbate Peroxidase Are within Its C-terminal Tail*. *J. Biol. Chem.* **275**, 16337–16344 (2000).

149. Chio, U. S., Cho, H. & Shan, S. Mechanisms of Tail-Anchored Membrane Protein Targeting and Insertion. *Annu. Rev. Cell Dev. Biol.* **33**, 417–438 (2017).

150. Landes, T. *et al.* The BH3-only Bnip3 binds to the dynamin Opa1 to promote mitochondrial fragmentation and apoptosis by distinct mechanisms. *EMBO Rep.* **11**, 459–465 (2010).

151. Liu, K. E. & Frazier, W. A. Phosphorylation of the BNIP3 C-Terminus Inhibits Mitochondrial Damage and Cell Death without Blocking Autophagy. *PLoS ONE* **10**, (2015).

152. Sulistijo, E. S., Jaszewski, T. M. & MacKenzie, K. R. Sequence-specific Dimerization of the Transmembrane Domain of the “BH3-only” Protein BNIP3 in Membranes and Detergent *. *J. Biol. Chem.* **278**, 51950–51956 (2003).

153. Sulistijo, E. S. & MacKenzie, K. R. Sequence Dependence of BNIP3 Transmembrane Domain Dimerization Implicates Side-chain Hydrogen Bonding and a Tandem GxxxG Motif in Specific Helix–Helix Interactions. *J. Mol. Biol.* **364**, 974–990 (2006).

154. Zhang, J. & Ney, P. A. Role of BNIP3 and NIX in cell death, autophagy, and mitophagy. *Cell Death Differ.* **16**, 939–946 (2009).

155. Sulistijo, E. S. & MacKenzie, K. R. Structural Basis for Dimerization of the BNIP3 Transmembrane Domain,. *Biochemistry* **48**, 5106–5120 (2009).

156. Kim, S. *et al.* Transmembrane glycine zippers: Physiological and pathological roles in membrane proteins. *Proc. Natl. Acad. Sci.* **102**, 14278–14283 (2005).

157. Bocharov, E. V. *et al.* Unique Dimeric Structure of BNip3 Transmembrane Domain Suggests Membrane Permeabilization as a Cell Death Trigger *. *J. Biol. Chem.* **282**, 16256–16266 (2007).

158. Frazier, D. P. *et al.* Acidosis Regulates the Stability, Hydrophobicity, and Activity of the BH3-Only Protein Bnip3. *Antioxid. Redox Signal.* **8**, 1625–1634 (2006).

159. Kubli, D. A., Quinsay, M. N., Huang, C., Lee, Y. & Gustafsson, Å. B. Bnip3 functions as a mitochondrial sensor of oxidative stress during myocardial ischemia and reperfusion. *Am. J. Physiol.-Heart Circ. Physiol.* **295**, H2025–H2031 (2008).

160. Youle, R. J. & Narendra, D. P. Mechanisms of mitophagy. *Nat. Rev. Mol. Cell Biol.* **12**, 9–14 (2011).

161. Bruick, R. K. Expression of the gene encoding the proapoptotic Nip3 protein is induced by hypoxia. *Proc. Natl. Acad. Sci.* **97**, 9082–9087 (2000).

162. Shaw, J. *et al.* Antagonism of E2F-1 regulated Bnip3 transcription by NF-κB is essential for basal cell survival. *Proc. Natl. Acad. Sci.* **105**, 20734–20739 (2008).

163. Gang, H. *et al.* Epigenetic Regulation of E2F-1-Dependent Bnip3 Transcription and Cell Death by Nuclear Factor-κB and Histone Deacetylase-1. *Pediatr. Cardiol.* **32**, 263–266 (2011).

164. Lee, J. M. *et al.* Nutrient-sensing nuclear receptors coordinate autophagy. *Nature* **516**, 112–115 (2014).

165. Mammucari, C. *et al.* FoxO3 Controls Autophagy in Skeletal Muscle In Vivo. *Cell Metab.* **6**, 458–471 (2007).

166. Kalas, W. *et al.* H-ras Up-regulates Expression of BNIP3. *Anticancer Res.* **31**, 2869–2875 (2011).

167. Wu, S.-Y. *et al.* Ras-related tumorigenesis is suppressed by BNIP3-mediated autophagy through inhibition of cell proliferation. *Neoplasia N. Y. N* **13**, 1171–1182 (2011).

168. Shimizu, N. *et al.* A muscle-liver-fat signalling axis is essential for central control of adaptive adipose remodelling. *Nat. Commun.* **6**, 6693 (2015).

169. Zhang, Q. *et al.* Adaptive Posttranslational Control in Cellular Stress Response Pathways and Its Relationship to Toxicity Testing and Safety Assessment. *Toxicol. Sci.* **147**, 302–316 (2015).

170. Graham, R. M., Thompson, J. W., Wei, J., Bishopric, N. H. & Webster, K. A. Regulation of Bnip3 Death Pathways by Calcium, Phosphorylation, and Hypoxia–Reoxygenation. *Antioxid. Redox Signal.* **9**, 1309–1316 (2007).

171. Mellor, H. R., Rouschop, K. M., Wigfield, S. M., Wouters, B. G. & Harris, A. L. Synchronised phosphorylation of BNIP3, Bcl-2 and Bcl-xL in response to microtubule-active drugs is JNK-independent and requires a mitotic kinase. *Biochem. Pharmacol.* **79**, 1562–1572 (2010).

172. Springer, M. Z. *et al.* BNIP3-dependent mitophagy promotes cytosolic localization of LC3B and metabolic homeostasis in the liver. *Autophagy* **0**, 1–17 (2021).

173. Ben-Moshe, S. & Itzkovitz, S. Spatial heterogeneity in the mammalian liver. *Nat. Rev. Gastroenterol. Hepatol.* **16**, 395–410 (2019).

174. Matsushima, M. *et al.* Isolation, mapping, and functional analysis of a novel human cDNA (BNIP3L) encoding a protein homologous to human NIP3. *Genes. Chromosomes Cancer* **21**, 230–235 (1998).

175. Imazu, T. *et al.* Bcl-2/E1B 19 kDa-interacting protein 3-like protein (Bnip3L) interacts with Bcl-2/Bcl-x L and induces apoptosis by altering mitochondrial membrane permeability. *Oncogene* **18**, 4523–4529 (1999).

176. Sandoval, H. *et al.* Essential role for Nix in autophagic maturation of erythroid cells. *Nature* **454**, 232–235 (2008).

177. Esteban-Martínez, L. & Boya, P. BNIP3L/NIX-dependent mitophagy regulates cell differentiation via metabolic reprogramming. *Autophagy* **14**, 915–917 (2018).

178. Xiang, G. *et al.* BNIP3L-dependent mitophagy accounts for mitochondrial clearance during 3 factors-induced somatic cell reprogramming. *Autophagy* **13**, 1543–1555 (2017).

179. O'Sullivan, T. E., Johnson, L. R., Kang, H. H. & Sun, J. C. BNIP3- and BNIP3L-Mediated Mitophagy Promotes the Generation of Natural Killer Cell Memory. *Immunity* **43**, 331–342 (2015).

180. Wu, X. *et al.* BNIP3L/NIX degradation leads to mitophagy deficiency in ischemic brains. *Autophagy* **0**, 1–13 (2020).

181. Chinnadurai, G., Vijayalingam, S. & Gibson, S. B. BNIP3 subfamily BH3-only proteins - mitochondrial stress sensors in normal and pathological functions. *Oncogene* **27**, S114–S127 (2008).

182. Feng, X., Liu, X., Zhang, W. & Xiao, W. p53 directly suppresses BNIP3 expression to protect against hypoxia-induced cell death. *EMBO J.* **30**, 3397–3415 (2011).

183. Fei, P. *et al.* Bnip3L is induced by p53 under hypoxia, and its knockdown promotes tumor growth. *Cancer Cell* **6**, 597–609 (2004).

184. Yuan, Y. *et al.* BNIP3L/NIX-mediated mitophagy protects against ischemic brain injury independent of PARK2. *Autophagy* **13**, 1754–1766 (2017).

185. Rosa, S. C. da S. *et al.* BNIP3L/Nix-induced mitochondrial fission, mitophagy, and impaired myocyte glucose uptake are abrogated by PRKA/PKA phosphorylation. *Autophagy* **0**, 1–16 (2020).

186. Fader, C. & Colombo, M. I. Multivesicular Bodies and Autophagy in Erythrocyte Maturation. *Autophagy* **2**, 122–125 (2006).

187. Schweers, R. L. *et al.* NIX is required for programmed mitochondrial clearance during reticulocyte maturation. *Proc. Natl. Acad. Sci. U. S. A.* **104**, 19500–19505 (2007).

188. Diwan, A. *et al.* Unrestrained erythroblast development in Nix−/− mice reveals a mechanism for apoptotic modulation of erythropoiesis. *Proc. Natl. Acad. Sci. U. S. A.* **104**, 6794–6799 (2007).

189. Esteban-Martínez, L. *et al.* Programmed mitophagy is essential for the glycolytic switch during cell differentiation. *EMBO J.* **36**, 1688–1706 (2017).

190. Li, Y. *et al.* Bnip3 mediates the hypoxia-induced inhibition on mammalian target of rapamycin by interacting with Rheb. *J. Biol. Chem.* **282**, 35803–35813 (2007).

191. Melser, S. *et al.* Rheb Regulates Mitophagy Induced by Mitochondrial Energetic Status. *Cell Metab.* **17**, 719–730 (2013).

192. Vara-Perez, M., Felipe-Abrio, B. & Agostinis, P. Mitophagy in Cancer: A Tale of Adaptation. *Cells* **8**, (2019).

193. Cesari, R. *et al.* Parkin, a gene implicated in autosomal recessive juvenile parkinsonism, is a candidate tumor suppressor gene on chromosome 6q25-q27. *Proc. Natl. Acad. Sci. U. S. A.* **100**, 5956–5961 (2003).

194. Veeriah, S. *et al.* Somatic mutations of the Parkinson's disease-associated gene PARK2 in glioblastoma and other human malignancies. *Nat. Genet.* **42**, 77–82 (2010).

195. Agnihotri, S. *et al.* PINK1 Is a Negative Regulator of Growth and the Warburg Effect in Glioblastoma. *Cancer Res.* **76**, 4708–4719 (2016).

196. Bernardini, J. P., Lazarou, M. & Dewson, G. Parkin and mitophagy in cancer. *Oncogene* **36**, 1315–1327 (2017).

197. Fujiwara, M. *et al.* Parkin as a tumor suppressor gene for hepatocellular carcinoma. *Oncogene* **27**, 6002–6011 (2008).

198. Zhang, C. *et al.* Parkin, a p53 target gene, mediates the role of p53 in glucose metabolism and the Warburg effect. *Proc. Natl. Acad. Sci. U. S. A.* **108**, 16259–16264 (2011).

199. Kim, K.-Y. *et al.* Parkin is a lipid-responsive regulator of fat uptake in mice and mutant human cells. *J. Clin. Invest.* **121**, 3701–3712 (2011).

200. Villa, E., Marchetti, S. & Ricci, J.-E. No Parkin Zone: Mitophagy without Parkin. *Trends Cell Biol.* **28**, 882–895 (2018).

201. Okami, J., Simeone, D. M. & Logsdon, C. D. Silencing of the Hypoxia-Inducible Cell Death Protein BNIP3 in Pancreatic Cancer. *Cancer Res.* **64**, 5338–5346 (2004).

202. Sowter, H. M. *et al.* Expression of the cell death genes BNip3 and NIX in ductal carcinoma in situ of the breast; correlation of BNip3 levels with necrosis and grade. *J. Pathol.* **201**, 573–580 (2003).

203. Erkan, M. *et al.* Loss of BNIP3 expression is a late event in pancreatic cancer contributing to chemoresistance and worsened prognosis. *Oncogene* **24**, 4421–4432 (2005).

204. Murai, M. *et al.* Aberrant DNA methylation associated with silencing BNIP3 gene expression in haematopoietic tumours. *Br. J. Cancer* **92**, 1165–1172 (2005).

205. Murai, M. *et al.* Aberrant Methylation and Silencing of the BNIP3 Gene in Colorectal and Gastric Cancer. *Clin. Cancer Res.* **11**, 1021–1027 (2005).

206. Calvisi, D. F. *et al.* Mechanistic and prognostic significance of aberrant methylation in the molecular pathogenesis of human hepatocellular carcinoma. *J. Clin. Invest.* **117**, 2713–2722 (2007).

207. Koop, E. A. *et al.* Expression of BNIP3 in invasive breast cancer: correlations with the hypoxic response and clinicopathological features. *BMC Cancer* **9**, 175 (2009).

208. Lyons, A. *et al.* Insulin-like growth factor 1 signaling is essential for mitochondrial biogenesis and mitophagy in cancer cells. *J. Biol. Chem.* **292**, 16983–16998 (2017).

209. Labuschagne, C. F., Cheung, E. C., Blagih, J., Domart, M.-C. & Vousden, K. H. Cell Clustering Promotes a Metabolic Switch that Supports Metastatic Colonization. *Cell Metab.* **30**, 720-734.e5 (2019).

210. Humpton, T. J. *et al.* Oncogenic KRAS Induces NIX-Mediated Mitophagy to Promote Pancreatic Cancer. *Cancer Discov.* **9**, 1268–1287 (2019).

211. Li, J. *et al.* The mitophagy effector FUNDC1 controls mitochondrial reprogramming and cellular plasticity in cancer cells. *Sci. Signal.* **13**, (2020).

212. Wu, L. *et al.* FUN14 domain-containing 1 promotes breast cancer proliferation and migration by activating calcium-NFATC1-BMI1 axis. *EBioMedicine* **41**, 384–394 (2019).

213. Li, Y. *et al.* A mitochondrial FUNDC1/HSC70 interaction organizes the proteostatic stress response at the risk of cell morbidity. *EMBO J.* **38**, (2019).

214. Stepanenko, A. A. & Dmitrenko, V. V. HEK293 in cell biology and cancer research: phenotype, karyotype, tumorigenicity, and stress-induced genome-phenotype evolution. *Gene* **569**, 182–190 (2015).

215. Oliveira, P. S. L. de *et al.* Revisiting protein kinase–substrate interactions: Toward therapeutic development. *Sci. Signal.* **9**, re3–re3 (2016).

216. Bhaoighill, M. N. & Dunlop, E. A. Mechanistic target of rapamycin inhibitors: successes and challenges as cancer therapeutics. *Cancer Drug Resist.* **2**, 1069–1085 (2019).

217. Britten, C. D. *et al.* Phase I study of PF-04691502, a small-molecule, oral, dual inhibitor of PI3K and mTOR, in patients with advanced cancer. *Invest. New Drugs* **32**, 510–517 (2014).

218. Salazar, R. *et al.* Phase II Study of BEZ235 versus Everolimus in Patients with Mammalian Target of Rapamycin Inhibitor-Naïve Advanced Pancreatic Neuroendocrine Tumors. *The Oncologist* **23**, 766-e90 (2018).

219. Hall, B., Limaye, A. & Kulkarni, A. B. Overview: Generation of Gene Knockout Mice. *Curr. Protoc. Cell Biol. Editor. Board Juan Bonifacino Al* **CHAPTER**, Unit-19.1217 (2009).

220. Bouabe, H. & Okkenhaug, K. Gene Targeting in Mice: a Review. *Methods Mol. Biol. Clifton NJ* **1064**, 315–336 (2013).

221. Kim, H., Kim, M., Im, S.-K. & Fang, S. Mouse Cre-LoxP system: general principles to determine tissue-specific roles of target genes. *Lab. Anim. Res.* **34**, 147–159 (2018).

222. Villanueva, A. Hepatocellular Carcinoma. *N. Engl. J. Med.* **380**, 1450–1462 (2019).

223. Murakawa, T. *et al.* A Mammalian Mitophagy Receptor, Bcl2-L-13, Recruits the ULK1 Complex to Induce Mitophagy. *Cell Rep.* **26**, 338-345.e6 (2019).

224. Liu, Z. *et al.* Ciliogenesis is reciprocally regulated by PPARA and NR1H4/FXR through controlling autophagy in vitro and in vivo. *Autophagy* **14**, 1011–1027 (2018).

225. Chaanine, A. H. *et al.* FOXO3a regulates BNIP3 and modulates mitochondrial calcium, dynamics, and function in cardiac stress. *Am. J. Physiol. - Heart Circ. Physiol.* **311**, H1540–H1559 (2016).

226. Audesse, A. J. *et al.* FOXO3 directly regulates an autophagy network to functionally regulate proteostasis in adult neural stem cells. *PLOS Genet.* **15**, e1008097 (2019).

227. Borgese, N., Brambillasca, S. & Colombo, S. How tails guide tail-anchored proteins to their destinations. *Curr. Opin. Cell Biol.* **19**, 368–375 (2007).

228. Taylor, E. B. & Rutter, J. Mitochondrial quality control by the ubiquitin–proteasome system. *Biochem. Soc. Trans.* **39**, 1509–1513 (2011).

229. Xu, S., Peng, G., Wang, Y., Fang, S. & Karbowski, M. The AAA-ATPase p97 is essential for outer mitochondrial membrane protein turnover. *Mol. Biol. Cell* **22**, 291–300 (2010).

230. Heo, J.-M. *et al.* A stress-responsive system for mitochondrial protein degradation. *Mol. Cell* **40**, 465–480 (2010).

231. Saxton, R. A. & Sabatini, D. M. mTOR Signaling in Growth, Metabolism, and Disease. *Cell* **168**, 960–976 (2017).

232. Zhavoronkov, A. Inhibitors of mTOR in aging and cancer. *Oncotarget* **6**, 45010–45011 (2015).

233. Schenone, S., Brullo, C., Musumeci, F., Radi, M. & Botta, M. ATP-competitive inhibitors of mTOR: an update. *Curr. Med. Chem.* **18**, 2995–3014 (2011).

234. Sun, K. *et al.* Paradoxical roles of autophagy in different stages of tumorigenesis: protector for normal or cancer cells. *Cell Biosci.* **3**, 35 (2013).